AMERICAN UNIVERSITY OF BEIRUT

PREPARATION OF CURCUMIN CONJUGATED ZINC
OXIDE NANOPARTICLES AND THEIR APPLICATIONS

by
CELINE ANTOINE ARAB

A thesis
submitted in partial fulfillment of the requirements
for the degree of Master of Science
to the Department of Chemistry
of the Faculty of Arts and Sciences
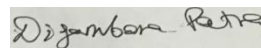at the American University of Beirut

Beirut, Lebanon
January 2021

AMERICAN UNIVERSITY OF BEIRUT

PREPARATION OF CURCUMIN CONJUGATED ZINC OXIDE NANOPARTICLES AND THEIR APPLICATIONS

by
CELINE ANTOINE ARAB

Approved by:

_____
[Dr. Digambara Patra, Professor]   Advisor
[Chemistry]

_____
[Dr. Tarek Ghaddar, Professor]   Member of Committee
[Chemistry]

_____
[Dr. Elias Baydoun, Associate Professor]   Member of Committee
[Biology]

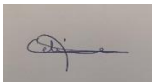Date of thesis defense: January 27, 2021

AMERICAN UNIVERSITY OF BEIRUT

THESIS RELEASE FORM

Student Name: Celine Antoine Arab

I authorize the American University of Beirut, to: (a) reproduce hard or electronic copies of my thesis; (b) include such copies in the archives and digital repositories of the University; and (c) make freely available such copies to third parties for research or educational purposes:

☐ As of the date of submission

☐ One year from the date of submission of my thesis.

☒ Two years from the date of submission of my thesis.

☐ Three years from the date of submission of my thesis.

5/2/2021

_____

Signature   Date

ACKNOWLEDGMENTS

ABSTRACT

OF THE THESIS OF

Celine Antoine Arab   for   <u>Master of Science</u>
<u>Major</u>: Chemistry

Title: <u>Preparation of Conjugated Curcumin Zinc Oxide Nanoparticles and their Application</u>

Nanoparticles have been widely prepared and used in different domains, due to their unique optical properties, small sizes and relative structure. Among these nanoparticles, zinc oxide nanoparticles (ZnO NPs) have been developed and investigated to be applicable in various field. In this work, the synthesis of zinc oxide nanoparticles was carried out based on simple green method with optimization of the reaction parameters by taking into consideration the best flow rate of potassium hydroxide (KOH) for the formation of ZnO, under the appropriate pH, and at the proper temperature. Curcumin was used as a selective conjugated reagent to increase the solubility and to enhance the activity of ZnO NPs. The obtained nanoparticles were coated with chitosan polymer in order to increase their stability.

The formed nanoparticles were characterized via UV-Visible, Fluorescence, XRD, TGA and SEM. The purpose of this study is to establish the creation of the best nanoparticles and utilize them in numerous applications.

First, their anticancer activity was monitored with MCF-7 breast cancer cells and Capan-1 pancreatic cancer cells. These nanoparticles were remarked to hinder up to 90% cancer cells proliferation after 72 hours.

Second, zinc curcumin oxide nanoparticles coated with chitosan polymer (Zn(Cur)O-Chi) played the role of outstanding nanosensors for the detection of ascorbic acid (AA) in a fast, easy, stable, and selective way. As the concentration of AA increases (0-10 mM), the emission intensity was noticed to increase as well. The LOD attained was equal to 36 μM. The recovery range was between 94-100.6%.

Third, the adsorption of different anionic and cationic organic dyes onto the surface of Zn(Cur)O NPs was tested with kinetic and isothermal studies. In a first place a full study of the adsorption of congo red using Zn(Cur)O NPs as adsorbent was established. The impact of the adsorbent dose, the concentration of the organic dye, and the pH of the solution were varied and adjusted in a specific range. It was detected that the adsorption improves with increasing the quantity of the nanoparticles and with reducing the concentration of the organic dye. Therefore, the various adsorption sites will reach saturation. Moreover, an acidic medium enhanced the adsorption process of congo red.

In a second place, the adsorption of different anionic and cationic dyes was developed and the effect of the pH was validated. The kinetics study was monitored and it was found that the adsorption process follows a pseudo 2nd order kinetic model.

TABLE OF CONTENTS

ILLUSTRATIONS

Figure

TABLES

Table

17

ABBREVIATIONS

AA   Ascorbic Acid

CR   Congo Red

DDW   Double Distilled Water

HCl   Hydrochloric Acid

KOH   Potassium Hydroxide

MB   Methylene Blue

MO   Methyl Orange

NaOH   Sodium Hydroxide

Rh6G   Rhodamine 6G

RhB   Rhodamine B

SEM   Scanning Electron Microscopy

TGA   Thermogravimetric Analysis

XRD   X-Ray Diffraction

ZnO   Zinc Oxide Nanoparticles

Zn(Cur)O   Zinc Curcumin Oxide Nanoparticles

Zn(Cur)O-Chi   Zinc Curcumin Oxide Nanoparticles Coated With Chitosan

CHAPTER I

INTRODUCTION

A. Nanotechnology and nanoparticles

1. *Definition of nanotechnology and nanoparticles*

Nanoparticle science has gained an increased importance worldwide, especially during the past 10 years. It was encouraged by the Presidential Nanoscience Initiative supported by Bush and Clinton administrations. The interest in nanoscience has improved due to the utility of nanoparticles in a wide range of applications [1].

Moreover, nanotechnology was estimated by the National Science Foundation to reach in the upcoming future an industry of one trillion US dollars [2], [3]. Usually, nanoparticles possess a spherical shape with a diameter of 100 nm or less, on an order of around 10 nm.

2. *Properties of nanoparticles*

Solid particles with their unique scales have outstanding properties allowing them to be used in different fields [1]. Most importantly, they are highly stable, highly reactive, and have notable optical features. Furthermore, the size of those nanoparticles allows them to penetrate into the human body through lungs and skin.

Thus, nanoparticles can be also harmful by simply passing through the cell membranes. Consequently, many researchers are currently studying the toxicity of

nanoparticles, and the governments are funding these types of studies in order to determine their characteristics and toxicity effects [3].

3. *Type of nanoparticles*

There are numerous types of nanoparticles. Among them, we can find the carbon nanotubes, magnetic, metal oxide, liposome and polymeric nanoparticles.

Magnetic nanoparticles own special crystal symmetry structure with ramifications. The creation of those nanoparticles is based on their atomic, surface, and magnetic structures. In other words, symmetry and spin dynamics should be understood.

Their importance is related to the broad range of applications as [1]:

- Power generation: used as powder compacts.

- Biosensing: used as surface functionalized particles.

- Magnetic resonance imaging: used as contrasting agents.

- Magnetic storage media: used as particle arrays.

- Audio speakers: used as ferrofluids in solutions.

- Medical treatment: anti-cancer, anti-inflammatory, anti-oxidant, etc.

As for metal oxide nanoparticles, they are very essential and are used in different sectors. The distinctive chemical and physical properties of those transition metals grabbed the attention of the scientists due to their limited size and the sites present on their surface area. In consequence; their synthesis was spread all over the world especially because of the variety of their identities [4].

Among these nanoparticles, zinc oxide nanoparticles have been recently developed and widely investigated in different field.

B. Zinc oxide nanoparticles

1. Crystal structure of zinc oxide nanoparticles

Zinc oxide nanoparticles could be found in three different forms (See Figure 1). First, ZnO NPs can exist in the wurtzite crystal structure. It is characterized by a hexagonal shape with the presence of 2 lattice parameters. Every O^{2-} anion is surrounded by four Zn^{2+} cations in a tetrahedral structural shape. This will generate sp3 covalent bonding [5]. The other two structures are the zinc blende cubic structure and the rocksalt [6]. At ambient conditions, the most stable one is the wurtzite crystal structure [7].

Rocksalt   **Zinc blende**   **Wurtzite**

(a)   (b)   (c)
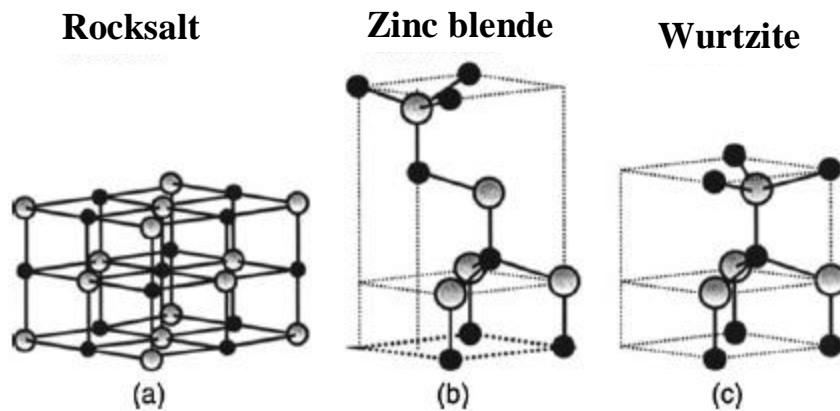
Figure 1 Crystal structure of ZnO NPs.

2. *Properties of zinc oxide nanoparticles*

Zinc oxide nanoparticles (ZnO NPs) have gained much importance as n-type semiconductor sensors. They hold a wide band gap as well as a great exciton binding energy of 3.37 eV and 60 mV respectively. This will enhance the electron mobility in those transition metal oxide nanoparticles.

Moreover, the surface and volume of these nanoparticles could be controlled due to their varied shapes and forms such as nanorods, wires, disks, ellipsoids and so on. They could be produced at low cost in a simple and harmless method. They are as well thermally stable.

Furthermore, ZnO NPs are highly sensitive and selective towards biological and chemical toxins. Additionally, ZnO nanoparticles are naturally chemo-resistant. Their sensing ability is primarily controlled by the variation in the chemical response obtained when the specific analyte molecules get in contact with the external surface of those particles [8].

They are also photo-chemically reactive and can be used for the production of gas sensors, photodetectors, solar cells, field effect transistors, ultraviolet lasers, light emitting diodes, etc.

The main two advantages of those nanostructures are their quantum confinement and high surface area, enhancing their importance and usage in different domain [9].

3. *Application of zinc oxide nanoparticles*

The importance of zinc oxide nanoparticles was revealed in several studies.

a.   <u>Adsorption activity</u>

The increase in the number of industry was conducted with a rise of the water pollution. This is due to the high release of different heavy metals and dyes. For this purpose, researchers have investigated the importance of zinc oxide nanoparticles as adsorbent for the removal of toxic chemicals.

For example, Mittal et al. have synthesized zinc oxide nanoparticles using hydrogels. The generated ZnO NPs were utilized as adsorbents for the removal of malachite green organic dye from aqueous solutions with a high adsorption capacity of 766.52 mg/g [10].

In addition, Zafar et al. have produced spherical zinc oxide nanoparticles. These nanoparticles have shown great adsorption capacity for the removal of azo dyes as methyl orange and amaranth. The results have exposed that 0.3 g pf ZnO NPs displayed maximum removal efficiency equal to 40 ppm for each dye [11].

Yuvaraja et al. have prepared ZnO nanorods and applied them as adsorbent material for the removal of Arsenic (As (III)) from aqueous solution. They have found that the maximum As (III) sorption capacity of ZnO nanorods was equal to 52.36 mg/g at pH 7, with 0.4 g of adsorbent [12].

Another study conducted by Nalwa et al. have confirmed the role of ZnO NPs as adsorbent for the removal of copper II metals. Hence, a high percentage removal was obtained at initial concentration of 300 mg/L. The percentage removal was equal to 98.71% of Cu (II) from its aqueous solution at pH 5 [13].

Another adsorption application refers to the adsorption of Cr(VI) and Cd(II) heavy metals. Ghiloufi et al. studied the capability of Ga-doped ZnO nanoparticles in adsorbing heavy metals from aqueous media with an adsorption capacity q_e equal to 66.36 mg/g and 220.7 mg/g for Cd(II) and Cr(VI) respectively [14].

b.   <u>Sensing application</u>

Furthermore, zinc oxide nanoparticles have shown unique performance as a biosensor. This activity is related to the distinct properties of ZnO NPs, presenting a high isoelectric point, great biocompatibility and numerous multifunctional characteristics [15].

In recent times, Dayakar et al. have developed a non-enzymatic glucose biosensor using ZnO NPs. In this study, a glassy carbon electrode glucose sensor was fabricated by coating the electrode with the ZnO NPs. The detection of glucose was reproducible with sensitivity equal to 631.30 $\mu A.mM^{-1}.cm^{-2}$ and a linear dynamic range from 1 to 8.6 mM, coupled with a very low detection limit equal to 0.043 μM [16].

Additional study was directed by Zheng et al. were they have produced ZnO NPs synthesized by a Corymbia citriodora leaf extract. These nanoparticles were employed for the construction of an electrochemical hydrogen peroxide (H_2O_2) biosensor. Hence, a linear relationship was obtained between the ZnO NPs electrode and H_2O_2 concentration (0.1-150 μM), with a detection limit equal to 0.07 μM [17].

On the other hand, small ZnO NPs in the range of 4-8 nm have shown an excellent biosensor for the detection of silymarin. The study done by Sharma et al. has shown a good

linear relationship with ZnO NPs and silymarin in a concentration range between 0.014 and 0.152 mg/L, with a lower limit of detection equal to 0.08 mg/L [18].

In addition, Cao et al. have used zinc oxide/reduced graphene oxide (ZnO/rGO) heterostructure for the detection of NO_2 gas with a detection range of 5 ppb to 5 ppm and a detection limit of 5 ppb [19].

c.   Anti-cancer activity

Another application for zinc oxide nanoparticles is their anticancer activity. Several biomedical studies have relied on nanoparticles as anticancer agent.

For example, Javed Akhtar et al. have tested the effect of ZnO NPs on three types of cancer cells: human hepatocellular carcinoma HepG2 (human liver cancer cells), human lung adenocarcinoma A549, and human bronchial epithelial BEAS-2B. The results obtained highlight the importance of ZnO NPs on killing the three kinds of cancer cells with no influence on normal cells. The remarkable difference between the normal cells and the cancer cells in cytotoxicity studies and results indicates the utility of ZnO NPs in cancer treatment and their ability to become a new substitute in the biomedical field [20].

d.   Optical and magnetic application

It was found out that zinc oxide nanoparticles could be used for example as UV absorbers like in the research conducted by Becheri et al. in order to shield this type of light and test the effectiveness of the sunscreen activity [21]. Likewise, they are important to improve biomedical applications [22], in optoelectronics devices and as infrared biomarkers [23].

Furthermore, Zinc oxide nanoparticles were also applied as magnetic semiconductor. This was investigated by Zargar et al., where copper-doped zinc oxide nanoparticles were used as magnetic semiconductors for spintronic device applications [24].

To end up, ZnO NPs were used for polymer solar cells as cathode interfacial layers. The choice of those NPs was due to their stability in the environment, low cost, visible region transparency, crystallinity and mobility of their electrons [25].

e.   Anti-bacterial application

The growing concern about resistant microorganisms encourages the study of new and more effective antimicrobial agents. Efficient antimicrobial effects have been obtained from metal oxide nanoparticles as zinc oxide nanoparticles [26].

Sivakumar et al. pointed out the role of ZnO NPs as antibacterial agent due to their photocatalytic activity. The antibacterial effect was tested against Gram-negative *E. coli* and Gram-positive *S. aureus* bacteria. When ROS were generated after irradiation, the bacterial growth was inhibited for *E. coli* with 99.99% antibacterial activity, and for *S. aureus* with 99.87% [27].

f.   Anti-Diabetes agent

Another application was done by Dhobale et al. where zinc oxide nanoparticles were used as fresh and novel alpha-amylase inhibitors. Their role relies on the prevention of the absorption of dietary starches by the body by way of hindering the decomposition of

complex sugars into simple sugars. As a result, those nanoparticles could play an interesting role in diabetes control [28].

So on, these various applications of zinc oxide nanoparticles is related also to the different available routes present to produce ZnO NPs.

4. *Synthesis of zinc oxide nanoparticles*

Different procedures could be applied to produce ZnO NPs such as co-precipitation, sol–gel, microemulsion, hydrothermal and methods that require the presence of a microwave in order to generate zinc oxide nanoparticles having diverse properties.

a. Co-precipitation method

Co-precipitation technique is the carrying down by a precipitate of substances normally soluble under the conditions employed. In a classic co-precipitation synthesis, a salt precursor is dissolved in aqueous solution and then the corresponding hydroxides are precipitated by the addition of a specific base such as ammonium hydroxide or sodium hydroxide. After washing the produced ammonium or sodium salt, the hydroxides are calcined resulting in metal oxide powders [29]. Co-precipitation method is a simple, low-cost, and efficient technique for the production of nanoparticles.

Zinc curcumin oxides are commonly created following this procedure. Devi et al. have produced pure ZnO NPs and cobalt doped ZnO NPs using co-precipitation method. They have used zinc nitrate as salt precursor, polyethylene glycol as surfactant and sodium

hydroxide to achieve the formation of the precipitate. After reflux for 24 hours, the precipitate was dried at 120℃ [30].

In another study, they were synthesized using zinc nitrate $Zn(NO_3)_2$ along with sodium hydroxide (NaOH). The latter was added to the former that was heated, drop by drop with stirring. After cooling and precipitation for 24 hours, the product was washed and dried before annealing [31].

b.   Sol-gel method

This method is usually practiced in wet chemistry. Sol-gel method is one of the most used synthetic routes for the formation of metal oxide nanoparticles. This technique is highly recommended due the outstanding control over the texture and the surface properties of the materials. Basically, sol-gel method consists of 5 essential steps; starting with the hydrolysis, poly-condensation, aging, drying and ending with thermal decomposition [32], [33].

Ong et al. used this technique to form ZnO NPs. In a simple way, the sol was prepared by zinc nitrate and oxalic acid dehydrate, while the solvent was represented by ethyl alcohol, methyl alcohol and ultrapure water. Oxalic acid was added drop by drop in a slow manner to zinc nitrate at room temperature that itself dissolved in the different solvents under stirring. After sonication, drying and calcination, zinc oxide nanoparticles were obtained [34].

Another study was established by Hasnidawani et al. presenting the synthesis of ZnO NPs using the sol-gel method. In this study, the authors have mixed. Zinc Acetate

Dihydrate with Sodium Hydroxide in double distilled water. The solution was stirred continuously with the addition of ethanol drop wise in order to get a white precipitate [35].

c. Micro-emulsion method

Moving on to another technique, micro-emulsion could be taken into consideration. The synthesis of nanoparticles based on micro-emulsion technique has attained a significant interest in both basic research and industrial fields [36].

In a study elaborated by Lin et al., zinc oxide nanoparticles were produced via a micro-emulsion technique. This was done by mixing equal amount of zinc acetate solution and triethanolamine powder, in the presence of butanol and toluene as surfactant [37].

Kumar et al. have successfully generated zinc oxide nanoparticles via microemulsion where $ZnSO_4.6H_2O$ solution was added dropwise to the microemulsion (non-ionic surfactant, PVP, 1:9 cyclohexane and triple distilled water) with stirring [38].

d. Hydrothermal method

Hydrothermal technique is one of the common methods used for the preparation of nanoparticles. It is fundamentally a solution reaction-based approach. In this method, the formation of nanoparticles can occur at different temperatures, from room temperature to very high temperatures [39].

Zinc oxide nanoparticles can be synthesized at low-cost with high quality and efficiently by the hydrothermal technique.

In a study done by Wasly et al., a mixture of zinc acetate and sodium hydroxide was maintained under stirring for 2 hours. Later on, it was transferred to a Teflon-lined

stainless steel autoclave and kept for 8 hours at 150℃. After cooling, the white product was centrifuged and washed, then dried for 6 hours using an oven at a temperature of 75℃ [40].

e. Green synthesis

Green synthesis of nanomaterials is flattering one of the most central methodologies in nanotechnology. This technique is based on the consumption of natural entities that help decreasing the use of hazardous substances leading to the diminishing of the synthesis of toxic products [41].

Nowadays, green synthesis is the most common technique to be taken into consideration for the preparation of ZnO nanoparticles.

Plant leaf extracts are mostly used as reducing agents as well as stabilizing agents for the production of the nanoparticles due to numerous advantages like the easiness and facile ways, the economic aspect, and most importantly the nontoxic ecofriendly results over the other techniques [9]. For example. Lingaraju et al. have green synthesized zinc oxide nanoparticles by the usage of aqueous stem extract of *Ruta graveolens*, a herb that belongs to the family *Rutaceae*, as reducing agent [42].

Lately, plant leaf extracts are being replaced by curcumin, due to the easy manipulation and the minimization of the extraction steps. Curcumin was being used as a reducing agent and conjugated agent to produce curcumin conjugated zinc oxide nanoparticles.

Perera et al. have produced curcumin loaded zinc oxide nanoparticles using aqueous solution of zinc nitrate hexahydrate and sodium hydroxide. The aqueous solution

was mixed with curcumin and kept under stirring for 24 hours to ensure a complete graphing of curcumin molecule on the surface of the zinc oxide nanoparticles [43].

Another study directed by Moussawi et al. have established the synthesis of curcumin conjugated zinc oxide nanoparticles. In this study, the authors have synthesized the NPs by mixing curcumin with zinc nitrate in double distilled water and refluxed for 1 hour at 90 degree Celsius. The solution was centrifuged and the precipitate was washed and freeze dried for environmental application [44].

The use of curcumin in the synthesis of ZnO NPs has enhanced the activity of the nanoparticles. This allows curcumin to be considered as an essential reagent in the production.

C. Curcumin

1. Definition

Curcumin $C_{21}H_{20}O_6$, (1,7-bis(4-hydroxy-3-methoxyphenyl)-1,6-heptadiene-3,5-dione), also called diferuloylmethane, and extracted from the ground rhizome of an East Indian plant named *Curcuma Longa* commonly known as turmeric, is a hydrophobic bright yellow polyphenolic pigment [45]–[47].

It is a member of the curcuminoids and it has been used for centuries in Ayurveda, the traditional Indian medicine, in order to cure diabetic wounds, jaundice, skin and eye infections, and to treat sinusitis, flatulence, acnes, ulcers, rheumatism, arthritis, sprains, and as a therapy for hepatic disorders, dysentery, and upset stomach [48]–[50].

The largest market and consumption of curcumin is found in North America, followed by Europe and Asia-Pacific countries. Furthermore, the market of curcumin is predicted to reach around 94.3 million dollars probably by the year 2022 [51]. India is the largest stock and source of turmeric production [52]. Other derivatives than curcumin from *Curcuma Longa* plant include dimethoxy curcumin, ar-turmerone, bisdemethoxycurcumin, methyl curcumin, and sodium curcuminate [53]. Curcumin is the most abundant and consists of around 75% of the turmeric plant. The following two major components are dimethoxy curcumin (~20%) and bisdemethoxycurcumin (~5%) [54].

2. *History of curcumin*

It was isolated first by Vogel in 1842. Initially, curcumin was isolated from turmeric by solvent extraction, followed by column chromatography [55]. Among solvent extraction, soxhlet, ultrasonic and microwave extraction were useful in the purpose of extracting curcumin [56].

Later on, it was characterized by Milobedeska in 1910, where he found that curcumin is a diferuloylmethane compound, where it's IUPAC name is (1,7-bis (4-hydroxy-3-methoxyphenyl)-1,6-hepadiene-3,5-dione).

Finally it was synthesized and proved by Lamp in 1913 [57], [58].

The synthesis of curcumin involves five consecutive steps. The raw materials are carbomethoxyferuloyl chloride and ethyl acetoacetate.

Pabon et al. have developed a new method to prepare curcumin using acetyl acetone in the presence of boron trioxide, with different substituted aromatic aldehydes, trialkyl borate and n-butylamine (See Figure 2) [59].
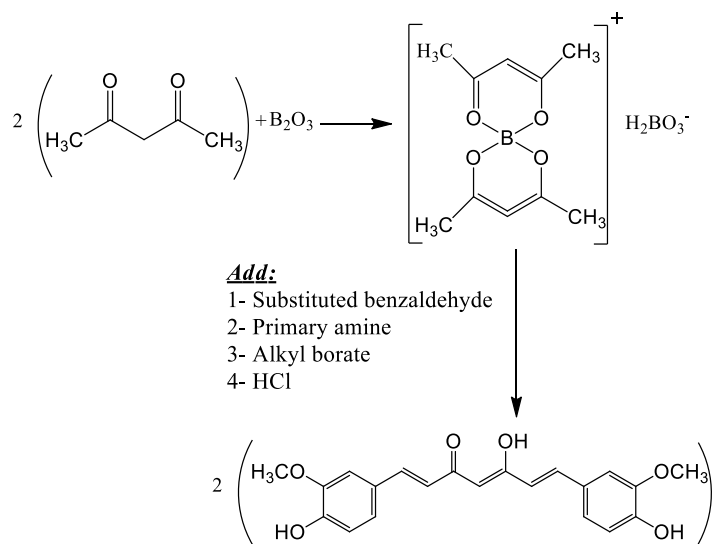
Figure 2 Synthesis of curcumin based on Pabon et al. mechanism.

3. *Tautomerization of curcumin*

The common name of curcumin is diferuloylmethane as mentioned earlier. It is chemically called a bis-α,β-unsaturated β-diketone. It exhibits a keto-enol tautomerism, where the enolic form dominates in alkaline solutions so that the phenolic part of curcumin act as an electron donor, whereas the keto form is more stable and dominant in acidic and neutral media hence curcumin will act as a proton donor (See Figure 3). Under physiological conditions, both forms co-exist in equilibrium [52], [60].

Keto form

Enol form
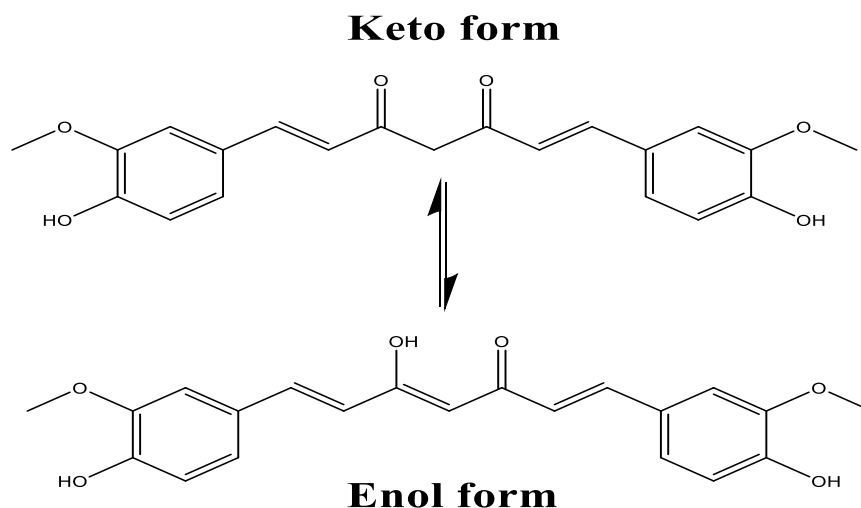
Figure 3 keto-enol tautomerism of curcumin.

4. *Chemical properties of curcumin*

In nature, curcumin is crystalline and soluble in extremely acidic and alkaline solvents [61]. It is an oil-soluble compound that dissolves easily in dimethylsulfoxide (DMSO), methanol, ethanol, chloroform, or acetone, but it is slightly soluble in neutral or acidic aqueous solutions since it is hydrophobic especially due to the diketone part of the molecule [49], [51], [52].

The vivid and intense yellow color of turmeric is mostly due to the existence of the various polyphenolic curcuminoids. Curcumin's yellow color changes into dark red at highly basic pH due to its degradation into feruloyl methane, ferulic acid and vanillin since it is unstable under alkaline conditions.

To sum up, curcumin has low solubility in acidic and neutral solutions, while it is unstable and undergoes a hydrolytic degradation under basic conditions [46], [51]

5. *Toxicity of curcumin*

Food and Drug Administration (FDA) identified curcumin as a safe molecule for human consumption. Several studies, preclinical as well as clinical, measured the safety of this compound. Healthy subjects were tested in a clinical study.

Some of them took up to 8000 mg/day of curcumin where no levels were detected in their serum, while the others took around 10000 mg/day and 12000 mg/day where only traces of curcumin were spotted. No harmful effects were observed in the healthy patients meaning that curcumin is safe and not toxic.

Likewise, a good safety profile of this compound was experimentally detected for unhealthy subjects having high-risk conditions or cancer, and taking doses up to 8000 mg/day of curcumin. Only few side effects and slight toxicity were remarked such as headache, nausea, diarrhea, and yellow stool by patients affected by primary sclerosing cholangitis, and they are considered as grade 1 toxicity, while intractable abdominal pain was reported by patients affected by advanced pancreatic cancer and taking gemcitabine medication.

Finally, curcumin was established to be, due to several studies, low-cost, effective, safe, and well-tolerated in healthy as well as high-risk conditions patients [47], [62], [63].

6. *Limitation of curcumin*

Moving on to the disadvantages of curcumin, it has poor gastrointestinal absorption and systematic bioavailability in addition to low solubility as mentioned earlier [64]. Furthermore, metabolism plays an important role in reducing the oral bioavailability and bioactivity of curcumin compound.

The parent molecule, curcumin, will undergo a series of complex metabolic reactions in the gastrointestinal tract generating a variety of metabolites having diverse properties [65].

Despite having numerous benefits and a good safety profile, studies showed that around 75% of curcumin were eliminated out of the body in feces, while insignificant quantities of that compound were detected in the urine when they were ingested by rats at a dose of 1 g/kg.

To overcome these drawbacks and limitations, the combination of curcumin molecule with adjuvant substances like piperine, or formulation in nanoparticles, micelles, liposomes, or encapsulation with cyclodextrin (CD) or polylactic-co-glycolic acid (PLGA) for example, or dispersion with colloidal sub-micron particles, showed an enhancement in therapeutic possibilities and an increase in bioavailability through different studies [62].

7. Curcumin's application

Curcumin presents a wide band of application. Its usage in bile duct problems, meaning biliary diseases, was recognized by the treatment of 67 patients first in 1937. Next, its antibacterial activity was documented in 1949. Moreover, its capability to reduce blood sugar levels in humans, in other words its usage as an antidiabetic treatment, was detected in 1972 [50].

According to several studies, in vitro and in vivo, the safe low-cost and effective curcumin drug has anticancer [52], [66], anti-inflammatory such as anti-rheumatoid arthritis [61] and psoriasis [62], antimicrobial [67], antioxidant [62], anti-Alzheimer [63], anti-

Parkinson [61], anti-cardiovascular diseases, anti-depression and anti-anxiety pharmacological effects [61].

a. Curcumin as conjugated and reducing agent

Lately, researchers started to elaborate the role of curcumin as a reducing/stabilizing agent in chemical preparation of nanoparticles. Mainly, curcumin was used as reducing agent in the synthesis of metallic nanoparticles. Hence, the electrons in province from curcumin provide the reduction of the metal from M^{x+} to M^0. Meaning that, the transformation of the metallic species from its bulk composition to its electric state occurs [68].

For example, El-Kurdi et al. have synthesized gold nanoparticles in neutral media using Chloroauric acid and curcumin, in the presence of surfactant only, without the need to use toxic reagent like sodium borohydride [69], [70].

Another explanation was adopted by Khan et al. in order to evaluate the role of curcumin as reducing agent to produce Ag NPs [71]. Briefly, Khan et al. have dissolved a specific amount of curcumin in NaOH. According to the authors, when adding NaOH to curcumin, curcumin oxide is formed.

Hence, when curcumin was added to $AgNO_3$ in the first place, a complex was formed (equation 1). This complex reacted with curcumin oxide in order to produce Ag^0 (equation 2).

$Ag^+ + Cur \longrightarrow [Ag(Cur)]^+$ 	Equation (1)

$[Ag(Cur)]^+ + R\text{-}COH \longrightarrow [Ag(Cur)]^+ R\text{-}COOH$ 	Equation (2)
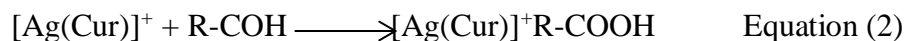
Moreover, curcumin is also used to reduce copper, and iron ions respectively [72].

In addition, curcumin was conjugated to zinc oxide nanoparticles [43], [44] and copper oxide nanoparticles in order to increase their efficiency and their activity [73], [74].

b. Anti-cancer activity

Starting with anticancer activities, this yellow compound could participate in the therapy of different cancer sorts like colorectal (colon), breast, familial adenomatous polyposis [63], lung [75], and pancreatic cancer types [76].

In a study conducted for several months, patients were administrated orally 180 mg of curcumin in order to examine its efficiency in the treatment of colon cancer. This dose seemed to be safe. Its concentration in the tissues of the colon mucosa was found to be between 0.2 and 1.8 mmol/g. In another study carried out for 7 days, twelve patients aged between 47 and 72 years old and affected by colorectal cancer were administrated 3.6 g, 1.8 g, or 0.45 g of curcumin. Measurements of its concentration in the colorectum of humans were done and found to be 7.7±1.8 nmol/g which is efficacious. Consequently, curcumin could achieve the effective therapeutic concentration by accumulating in the colorectum, and by doing that, having the potential to treat and cure colon cancer patients [63].

c. Anti-inflammatory activity

Moving further to the anti-inflammatory activities of curcumin, *Yang et al.* studied the effect of curcumin on the inflammatory bowel disease (IBD). It is a chain of inflammations taking place in the small intestine and the colon. There are two main forms of it: Crohn's disease and ulcerative colitis. Patients were treated with curcumin. At the

beginning, all the patients had sigmoidoscopies and biopsies. At the end of the treatment, the indexes of inflammation decreased making by that curcumin a promising agent against inflammations [63].

Another important role for this bright yellow compound is its antioxidant as well as pro-oxidant features.

d. Anti-oxidant activity

In a study, curcumin inhibited the generation of reactive oxygen species (ROS) in addition to the removal of OH· radicals and O_2^-. In other studies, curcumin showed pro-oxidant effects too. Consequently, it was found that antioxidant and pro-oxidant effects are dependent on the dose of curcumin used and on the chemical environment as well. Therefore, a balance between these two activities should be taken into consideration [52]. Besides its antioxidant and pro-oxidant activities, curcumin inhibits beta-amyloid (Aβ) neurotoxicity in the brain and is recognized to reduce the Alzheimer's pathology due to its anti-aggregation activity against Aβ. The overall dysfunction of the memory in Alzheimer's disease has improved [61].

D. Aims

After illustrating the information regarding nanoparticles, metal oxide nanoparticles and curcumin, we will focus in our work on the synthesis of zinc curcumin oxide nanoparticles.

The formation of zinc oxide nanoparticles will be achieved using curcumin as conjugated agent.

The synthesis of zinc curcumin oxide nanoparticles is performed based on a simple, green, low-cost and efficient method. In Chapter III, we will highlight the mechanism of the synthesis in addition to the optimization of the reaction parameters, in order to obtain the most suitable zinc curcumin oxide nanoparticles. The reaction parameters that are optimized are as follows: the flow rate of KOH, pH of the medium, reflux temperature and effect of polymer addition.

Moreover, as said earlier, ZnO NPs were found to be nontoxic to normal cells. Hence, curcumin reacts as anti-cancer reagent but it has poor bioavailability. For this reason the conjugation of zinc oxide nanoparticles with curcumin will be elaborated. In Chapter IV the formed nanoparticles will be applied as anticancer agents against MCF-7 breast and Capan-1 pancreatic cancer cells.

Ascorbic acid or Vitamin C is an indispensable nutrient found mostly in fruits and vegetables. The body needs ascorbic acid in order to form and preserve bones, blood vessels, and skin. Ascorbic acid likewise encourages the healing of cuts, abrasions and wounds; aids in fighting infections; prevents conversion of irritants in smog, tobacco smoke, and certain foods into cancer-causing substances. For this reason, it is quiet good to find a simple, low cost and effective method to detect it. In Chapter V, zinc curcumin oxide nanoparticles coated with chitosan will be designed as effective nanoprobes to detect ascorbic acid. The detection of ascorbic acid was done using fluorescence emission technique. The selectivity and the accuracy of the method are also investigated.

Azo dyes are organic compounds presenting the functional group R−N=N−R′, in which R and R′ are usually aryl. Azo dyes are extensively used to treat textiles, leather articles, and some foods. Azo dyes are presented in water, increasing thereby its pollution. So far, it is important to form an adsorbent in order to remove the azo dyes form water. An important azo dye is congo red. In Chapter VI, zinc curcumin oxide nanoparticles will be elaborated as new complex in the removal of congo red from aqueous solution. The efficiency of zinc curcumin oxide nanoparticles will be compared with zinc oxide nanoparticles in order to prove the role of curcumin in enhancing the activity of ZnO NPs.

As organic azo dyes are found in huge amounts in waste water, different dyes as methyl orange, methylene blue, rhodamine 6G and rhodamine B will be also evaluated. In Chapter VII, zinc curcumin oxide will be used as adsorbent for the removal of these dyes. Since, they are divided into cationic and anionic dyes; the effect of pH will be investigated.
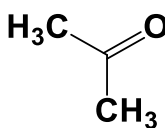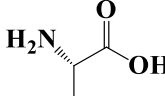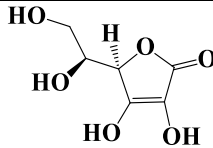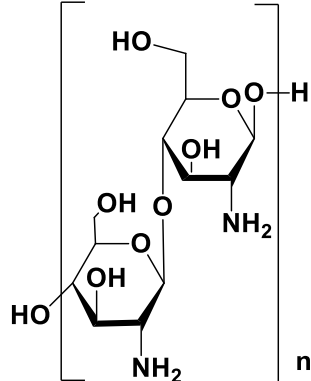
In Chapter VI and VII the adsorption study will be achieved by measuring the absorbance of the solution mixture within time.
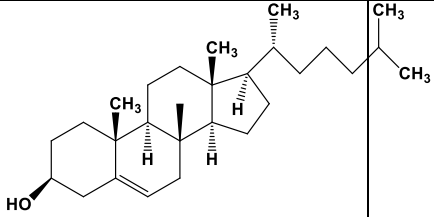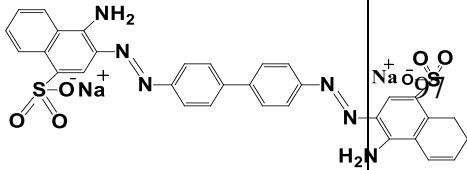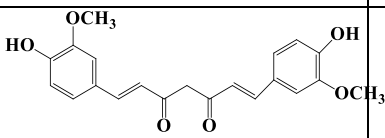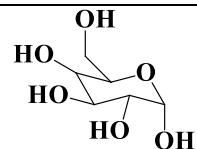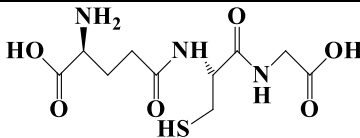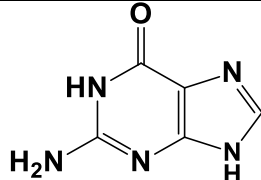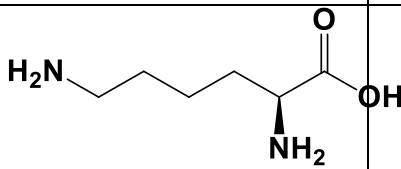
CHAPTER II
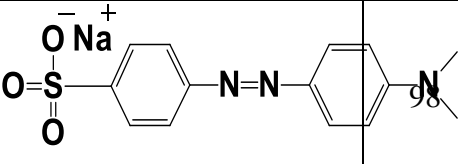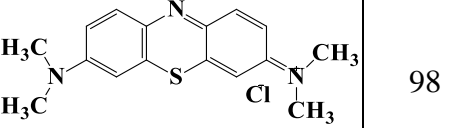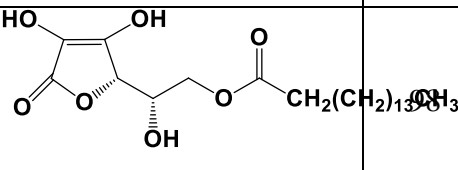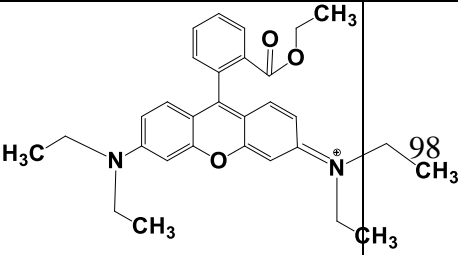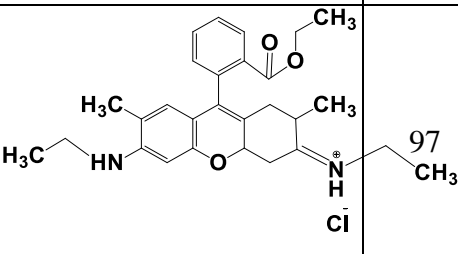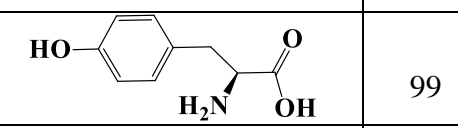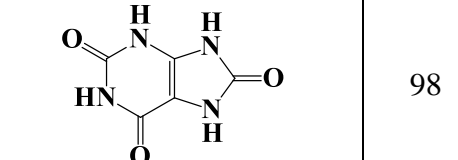
MATERIALS AND METHODS

A. Materials

All the chemicals that were used in our research work are presented in Table 1 with their respective chemical formula, chemical structure, purity and source.

Nomenclature	Chemical formula	Chemical structure	Purity (%)	Source
Acetone	CH_3COCH_3		99	Sigma Aldrich
Alanine	$C_3H_7NO_2$		98	Merck
Ascorbic acid	$C_6H_8O_6$		99	Acros
Chitosan oligosaccharide lactate	$C_{12}H_{24}N_2O_9$		98	Sigma Aldrich
Cholesterol	$C_{27}H_{46}O$		98	Sigma Aldrich

Congo red	$C_{32}H_{22}N_6Na_2O_6S_2$		97	Acros
Curcumin	$C_{21}H_{20}O_6$		99	Sigma Aldrich
Glucose	$C_6H_{12}O_6$		98	Sigma Aldrich
Glutathione	$C_{10}H_{17}N_3O_6S$		98	Fluka
Guanine	$C_5H_5N_5O$		99	Acros
Hydrochloric acid 32%	HCl	H—Cl	-	Sigma Aldrich
Lysine	$C_6H_{14}N_2O_2$		98	Merck

Methyl Orange	$C_{14}H_{14}N_3NaO_3S$		98	Acros
Methylene blue	$C_{16}H_{18}ClN_3S$		98	Acros
6-O-Palmitoyl-L-ascorbic acid	$C_{22}H_{38}O_7$		98	Sigma Aldrich
Potassium Hydroxide	KOH	K—OH	98	Acros
Rhodamine B	$C_{32}H_{30}N_2O_3$		98	Sigma Aldrich
Rhodamine 6G	$C_{32}H_{30}N_2O_3$		97	Sigma Aldrich
Sodium hydroxide	NaOH	Na—OH	98	Sigma Aldrich
Tyrosine	$C_9H_{11}NO_3$		99	Acros
Uric acid	$C_5H_4N_4O_3$		98	Sigma Aldrich

Zinc nitrate hexahydrate	Zn(NO₃)₂.6H₂O	Zn^{2+} (structure) $[H_2O]_6$	99	Acros

Table 1 List of chemicals used.

B. Sample Preparation

Zinc curcumin oxide nanoparticles were prepared as follow (See Figure 4).
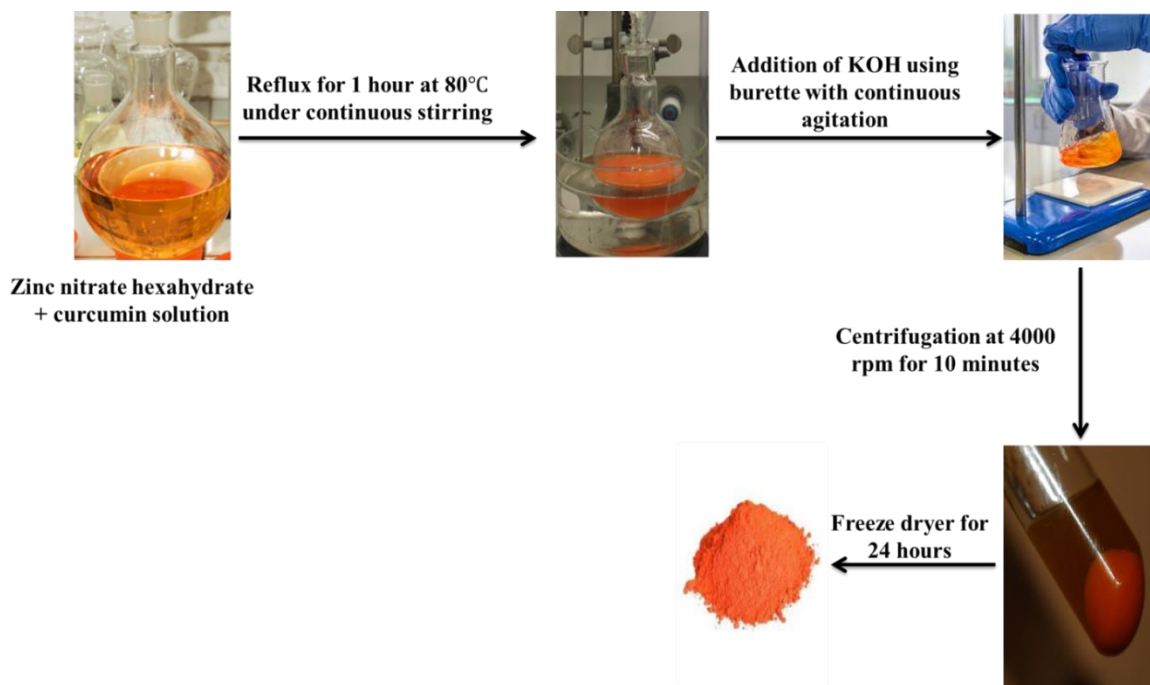
Figure 4 scheme illustrating the synthesis of zinc curcumin oxide nanoparticles.

In a first step 1.48 g of zinc nitrate hexahydrate (C=0.1 M) in 50 mL of a pH=13 solution heated at 80℃. In a second step, 0.18 g of curcumin (C=0.1 M) dissolved in 5 mL of acetone were mixed with the zinc nitrate solution. Later on, the mixture was kept under reflux for one hour at 80℃ with constant stirring. After that, 0.11 g of KOH (C=0.2 M)

dissolved in 10 mL pH=13 solution heated at 80°C was added dropwise using a burette to the mixture while stirring. Subsequently, the final solution was centrifuged at 4000 rpm and the precipitate was washed with double distilled water DDW 3 times. Finally, the washed precipitate was kept 24 hours under freeze dryer to obtain a washed solid precipitate of Zn(Cur)O NPs.

C. Instrumentation

Scanning electron microscopy (SEM) analysis was done using a Tescan, Vega 3 LMU with an Oxford EDX detector (Inca XmaW20). The accelerating voltage was 5 kV with a magnification of 500 nm. In short, few powder of zinc curcumin oxide nanoparticles solution were deposited on an aluminum stub and coated with carbon conductive adhesive tape.

Zeta potential and dynamic light scattering value were measured using Particulate systems, NanoPlus Zeta Potential/Nano Particle analyzer.

The absorption spectra were recorded at room temperature using a JASCO V-570 UV-VIS–NIR spectrophotometer in the wavelength range of 200–800 nm in a 3 mL cuvette.

Fluorescence spectrum was measured using a Jobin-Yvon-Horiba Fluorolog III fluorometer and the FluorEssence program. The excitation source was a 100 W Xenon lamp, and the detector used was R-928 instrument operating at a voltage of 950 V by keeping the excitation and emission slits width at 5 nm. For all spectroscopic measurements, 1 mg of Zn(Cur)O nanoparticles were mixed with 5 mL of DDW and

stored. From this solution 0,1 mL was transferred and diluted to 3 mL with DDW and the measurement was carried out in a 3 mL cuvette.

The X-ray diffraction (XRD) data were collected using a Bruker d8 discover X-ray diffractometer equipped with Cu-Ka radiation ($\lambda = 1.5405$ Å). The monochromator used was a Johansson type monochromator.

Thermo gravimetric analysis (TGA) was performed using a Netzsch TGA 209 in the temperature range of 30 to 1000 °C with an increase of 10 °C. min^{-1} under N_2 atmosphere.

D. Optimization of the reaction parameters

Different size and shape of zinc oxide nanoparticles can be produced based on the reaction parameters. In this context several modifications were done during the preparation to test their effect on the formed NPs. The parameters that were modified are:

a) Flow rate of KOH

b) pH

c) Reflux temperature

d) Addition of polymer

The synthesized nanoparticles were characterized using spectroscopic and microscopic techniques to check the difference between the obtained shape and size.

E. Application of Zinc Curcumin Oxide Nanoparticles

Zinc oxide nanoparticles have taken much importance in different fields. These nanoparticles have been used as catalyst, anti-oxidant, anti-cancer, quenching agent, and in many sensing applications, etc. In our research work, different applications were carried out to examine the efficiency and suitability of these nanoparticles. Among those applications, we had focused on:

a) Anti-cancer activity of Zn(Cur)O-NPs coated with chitosan.

b) The use of Zn(Cur)O coated with chitosan as nanoprobes.

c) The efficiency of Zn(Cur)O NPs as adsorbent for organic dyes.

It is important to mention that for each application, the sample preparation is developed in its specific chapter.

CHAPTER III

CHARACTERIZATION AND OPTIMIZATION OF THE REACTION PARAMETERS IN THE SYNTHESIS OF ZINC CURCUMIN OXIDE NANOPARTICLES

A. Introduction

Nanoparticles can be found in different structures; as different shapes and sizes. They can also have different crystallinity and variable stability that can make them applicable in different fields [77]. Nanoparticles are classified in two grand categories as organic and inorganic nanoparticles. Mainly organic nanoparticles are used in drug delivery. Besides, metal and metal oxide based nanoparticles are considered as inorganic nanoparticles. Among these metal oxide nanoparticles, zinc oxide nanoparticles (ZnO NPs) are widely investigated and developed [77], [78]. The synthesis of zinc oxide nanoparticles could be done through several chemical, physical and biological reactions [79]. Zinc oxide nanoparticles have superior catalytic properties, resulting from the large ratio of the nanoparticle surface to its volume [78]. The structure, morphology and the size of ZnO NPs depend strongly on the synthesis process, salt precursor used, additive reagents, pH, temperature and surface modification [80]. Zinc oxide may be formed in nanorods shape [81], nanoplates [82], nanospheres and nanosheets [83], nanowires [84], etc.

Recently, the activity of zinc oxide nanoparticles is enhanced when modifying its surface. Hence, since 2014, curcumin was being used as a non-toxic reagent that can be easily added to the ZnO NPs to form zinc curcumin oxide nanoparticles (Zn(Cur)O NPs).

Recently, curcumin is being developed to be used as a reducing agent for metal nanoparticles [85], [86], and as a conjugating agent for metal oxide nanoparticles [87], [88]. The combination of curcumin and zinc oxide nanoparticles decreases on the first hand its toxicity and enhances on the other hand its bioavailability and efficiency on a different level.

As said earlier, the shape, stability and crystallinity of zinc oxide nanoparticles depend on the reaction factors. For this purpose, our work was based on the development and the optimization of the synthesis parameters in order to get the most suitable and efficient zinc curcumin oxide nanoparticles.

B. Methods of preparation

The size, shape, crystallinity, etc. depend strongly on the reaction parameters. For this purpose, the reaction parameters were optimized in order to prepare the suitable Zn(Cur)O NPs.

Among these parameters, the ones that were tested are the following: flow rate of KOH, pH of the reaction, variation in temperature and addition of a chitosan polymer.

1. Effect of the flow rate of KOH

A solution of KOH (C=0.2 M) was prepared by dissolving 0.11 g of KOH in 10 mL double distilled water. It was added to the final solution obtained after reflux by 4 different ways. Accordingly, 4 final solutions were prepared. The first way was the addition of 10 mL KOH directly. In the second solution, this quantity was divided into two part: 5 mL were added using a graduated pipet and the solution was kept under stirring for 2 to 3 minutes, then the other 5 mL were added and stirred for the same time interval. The third way was similar to the second one but with the division of the 10 mL into 3 parts (3.33 mL in each step, separated with 30 seconds of stirring). The last one refers to the addition of the 10 mL KOH drop by drop using a burette while stirring the solution.

2. Effect of pH

The preparations are similar to the previous ones mentioned above with slightly small changes. After choosing the best way to add KOH, the study of the variation in pH was done to investigate its role in the production of Zn(Cur)O NPs. In this case, the zinc nitrate and the KOH solutions were both prepared in different solutions of pH equal to 4, 7, 10, and 13 consecutively instead of using double distilled water.

3. Effect of temperature

After the adoption of the suitable pH, Zn(Cur)O NPs were prepared similarly with variation in temperature, since this parameter is essential and could affect the results in a considerable way. The temperatures used were 40, 60, 80, and 95°C.

4. *Effect of polymer addition*

Moreover, coating with a polymer was necessary since it improves the results significantly. Chitosan polymer was used for this purpose. Hence, 10 mg of it was added in 3 ways. The first one was its addition directly before reflux. The second way refers to its addition before KOH and the last one was adding chitosan at the end, meaning after KOH.

C. Results and discussion

The preparation of Zn(Cur)O NPs was carried out through one simple route under reflux. Different shapes and properties could be achieved when varying the reactions parameters. For this purpose, different optimizations were established and the obtained Zn(Cur)O were compared and characterized through UV-Visible absorption spectroscopy, fluorescence spectroscopy, TGA and XRD.

1. *Effect of the flow rate of KOH*

These experiments were done as follows. In the first place, curcumin was dissolved in acetone, and zinc nitrate was dissolved in double distilled water heated at 80 degrees Celsius. The two solutions were mixed and kept under reflux for 1 hour at 80 degrees Celsius. 10 mL of KOH were added in four different ways.

In this experiment, KOH is used as supporting reducing agent, where it increases the yield of the nanoparticles formation. UV-Visible absorption spectroscopy was used initially in order to characterize the obtained products from the four different trials. As shown in Figure 5, curcumin peak is usually found to be around 425 nm. This peak was red

shifted to higher wavelength when Zn(Cur)O nanoparticles were formed after the addition of KOH solution in 2 steps, 5 mL each, or 3 steps, 3.33 mL each.
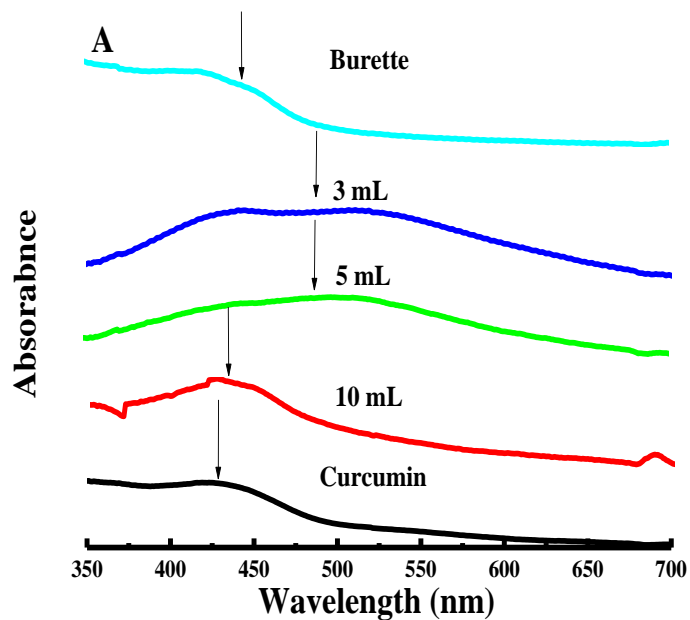
Figure 5 UV-Visible of curcumin and Zn(Cur)O prepared at different flow rates of KOH.

No remarkable change was observed when adding KOH in one step, 10 mL directly using a pipet. However the addition of KOH solution drop by drop using a burette caused the occurrence of a slight blue shift indicating the formation of smaller NPs. As for the fluorescence study, free curcumin exhibits an emission wavelength around 500 nm (Figure 6).
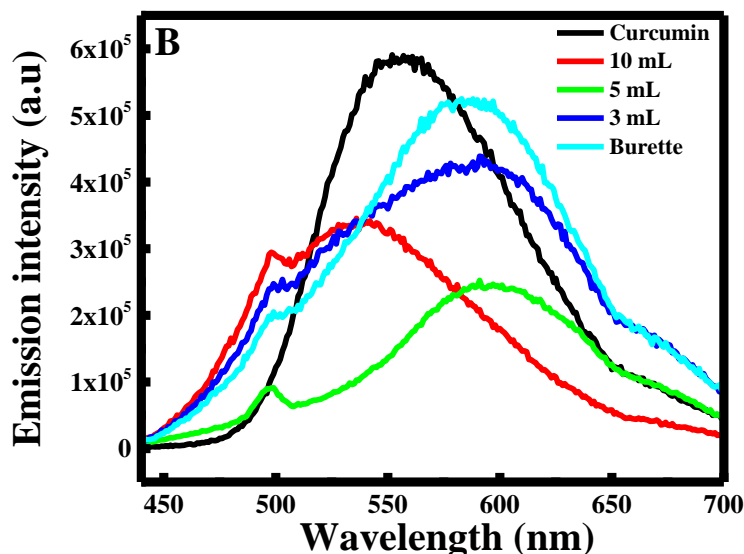
Figure 6 Fluorescence of curcumin and Zn(Cur)O prepared at different flow rates of KOH.

This wavelength is red shifted to higher wavelength when complexed to ZnO NPs. However, when adding directly 10 mL of KOH, the peak was slightly shifted to 540 nm with a decrease in the emission intensity. Also, this peak is red shifted to 600 nm when adding the KOH in several steps. Thus, the highest emission intensity was observed when adding KOH dropwise using a burette, revealing the most efficient formation of nanoparticles.

The X-Ray Diffraction (XRD) analysis was also done and the results are depicted in Figure 7. The characteristic peaks of curcumin alone appeared at diffraction angles of 2θ equal to 8.06°, 9.14°, 12.37°, 15.06° and 17.75°, etc. indicating that curcumin is present in the crystalline form.
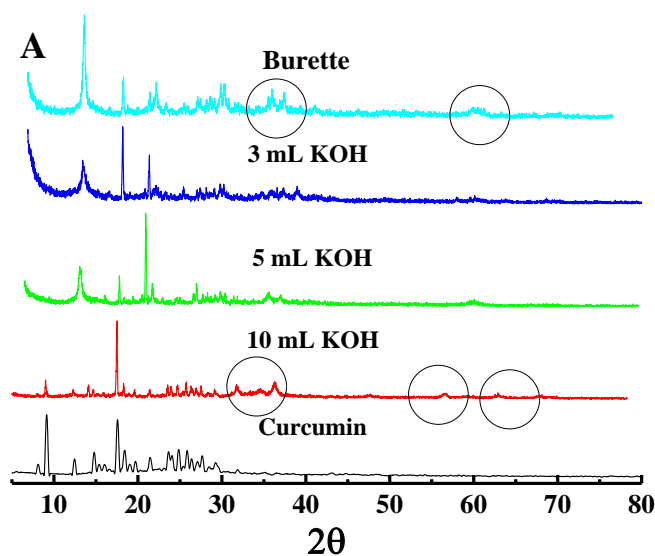
Figure 7 X-Ray diffractogram of curcumin and Zn(Cur)O prepared at different flow rates of KOH.

Curcumin characteristic peaks were slightly present in the Zn(Cur)O NPs X-Ray pattern in the four different cases, meaning that curcumin is being complexed with ZnO nanoparticles inducing their crystallinity. As for the experiments where the flow rate of KOH was added using burette or in direct way 10 mL, Zn(Cur)O peaks were somehow observed better than the other two cases. To sum up, curcumin peaks were slightly absent in all cases, therefore new peaks were noticed at 2θ equal to 33° and 34.9° and 58° when adding KOH drop by drop. These new peaks correspond then to the generated Zn(Cur)O nanoparticles.

In addition, based on the thermogravimetric analysis TGA, the percentage of the mass loss with increasing temperature was found lesser for the NPs formed when the burette was used than the other experiments (Figure 8). The TGA analysis showed a weight loss in two steps at 210 ℃ and 430℃. The weight loss is attributed to the decomposition of

curcumin. Approximately, Zn(Cur)O NPs prepared in all cases undergo the same

degradation.
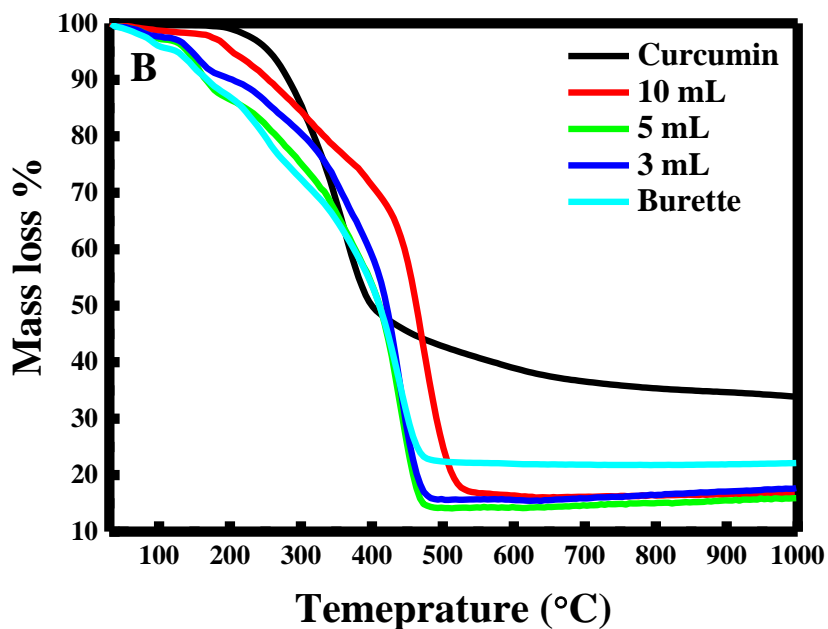
Figure 8 Thermogravimetric analysis of curcumin and Zn(Cur)O prepared at different flow
rates of KOH.

The TGA results indicate that a mass loss of ~80% happened during the thermal

breakdown of Zn(Cur)O NPs prepared using a burette for the addition of KOH, and a mass

loss of ~85% occurred during the thermal decomposition of the other nanoparticles.

Therefore, the lowest mass loss occurred when using the burette.

Consequently, the flow rate of KOH that will be used throughout the experiments

is the one where KOH will be added drop by drop using a burette since the nanoparticles

obtained using this flow rate were the most stable and crystalline.

2. *Effect of pH*

It is known that curcumin is slightly soluble in water and acidic media. Hence, it is highly soluble in basic media, at high pH. Earlier studies have shown that curcumin complexation to ZnO NPs is more stable at higher pH, in alkaline solution, where less than 6% of curcumin was lost after incubation [89]. For this reason, zinc nitrate was dissolved in different solutions of different pH (4, 7, 10 and 13) and heated at 80℃. The solutions were kept under reflux for 1 hour at 80℃ and 10 mL of KOH were added drop by drop using a burette. As it is shown in Figure 9, the highest absorbance was obtained at pH=10 and pH=13 with a slight red shift of the wavelength. However, at pH=4 and pH=7, the maximum wavelength remains fix compared to the curcumin peak.
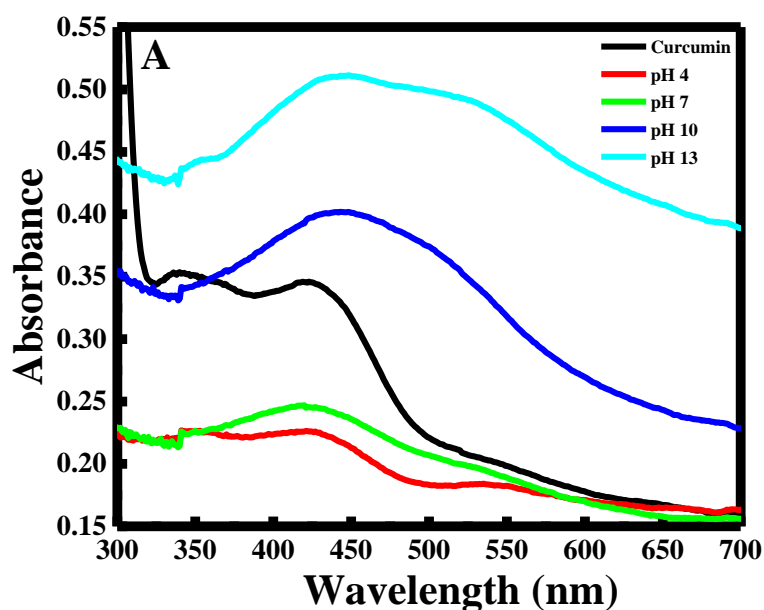
Figure 9 UV-Visible spectrum of curcumin and Zn(Cur)O NPs prepared at different pH.

Moreover, the emission spectrum was recorded and illustrated in Figure 10. As it is shown, Zn(Cur)O NPs prepared at pH=4 have the lowest emission intensity. This is due

to the fact that curcumin is insoluble in acidic media. However, the emission intensity increases with the increase of the pH, conducted with a blue shift to 500 nm at pH=13. This difference in the intensity is mainly due to the fact that curcumin strongly interacts with zinc oxide nanoparticles at basic media.
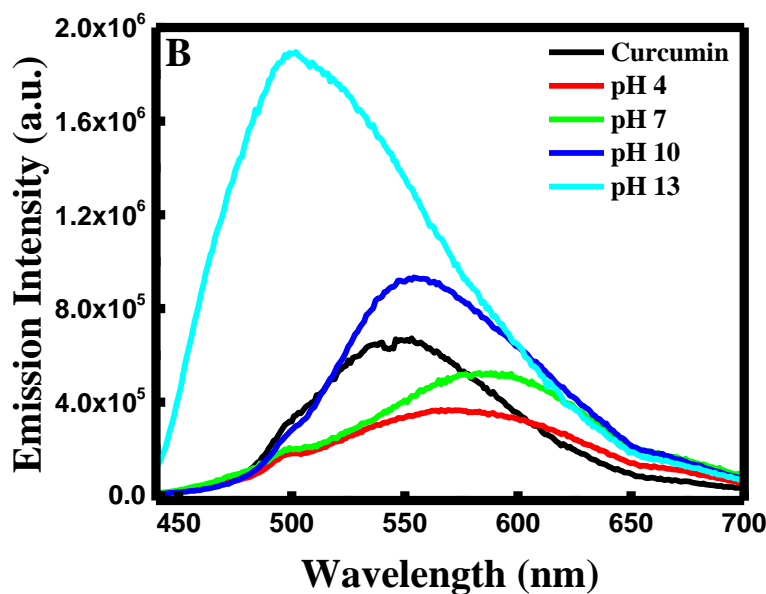
Figure 10 Fluorescence emission spectrum of curcumin and Zn(Cur)O NPs prepared at different pH.

These results were verified by XRD diffractogram, where the characteristic peaks of Zn(Cur)O NPs were remarkably observed only at pH=13 at 2θ values equal to 31.63° (hkl, 100), 34.45° (hkl, 002), 36.32° (hkl, 101), 47.45° (hkl, 102), 56.66° (hkl, 110), 63.02° (hkl, 103), 67.87° (hkl, 112) and 69.25° (hkl, 201). These diffraction peaks indicate the formation of a hexagonal wurtzite structure.
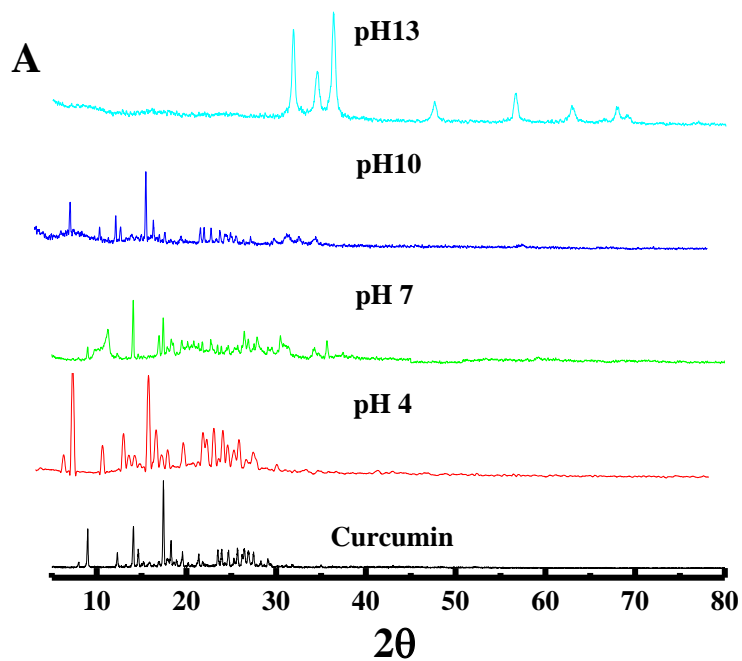
Figure 11 X-Ray diffractrogram of curcumin and Zn(Cur)O NPs prepared at different pH.

These results were similarly obtained with Nasrallah et al. and Soumya et al. [46], [90]. Interestingly, curcumin diffraction peaks were totally disappeared indicating that curcumin has been complexed to ZnO completely (Figure 11). In contrast, curcumin peaks were obtained at pH equal to 4, 7 and 10, meaning that curcumin did not react totally and thereby inhibiting the formation of Zn(Cur)O NPs.

Finally, looking at the results of the TGA illustrated in Figure 12, no degradation of curcumin was observed and a high stability for the Zn(Cur)O was obtained with <20% loss in mass at pH=13. The highest percentage of mass loss was observed for pH=4 (the most acidic) and it is approximately equal to 70%. In addition, Zn(Cur)O NPs prepared at pH=7 and pH=10 had a mass loss of about 45%.
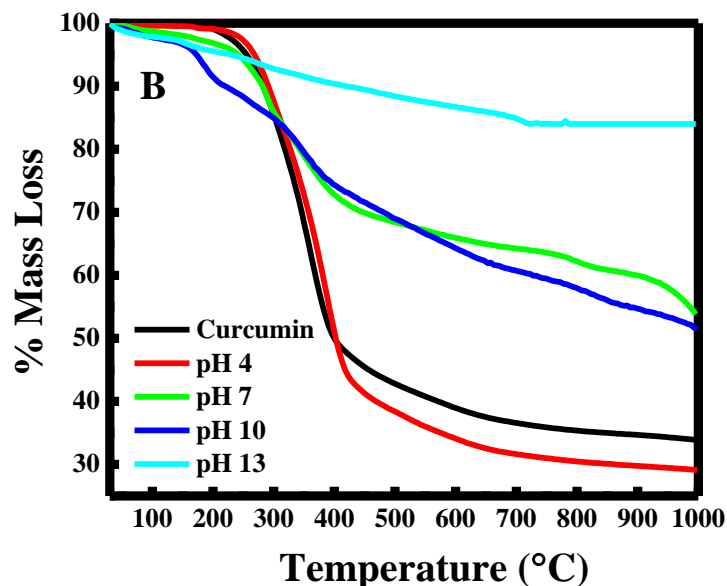
Figure 12 Thermogravimetric analysis of curcumin and Zn(Cur)O NPs prepared at different pH.

In conclusion, based on the analysis done above, pH=13 was found to be the most suitable for the formation of zinc curcumin oxide nanoparticles.

3. *Effect of temperature*

The reaction temperature was varied from 40 to 95℃. When the temperature was increased from 40 to 80℃, more curcumin has reacted allowing the formation of more Zn(Cur)O NPs. as shown in Figure 13A where the absorbance increases. The same applies for the emission intensity that increases with the temperature as well (See Figure 13B), except for the highest temperature, 95℃, where both the absorbance and emission intensities decreased with slight red shift in the UV-Visible absorption peak, this small

change could be new defect site at higher temperature due to less amount of curcumin conjugation.
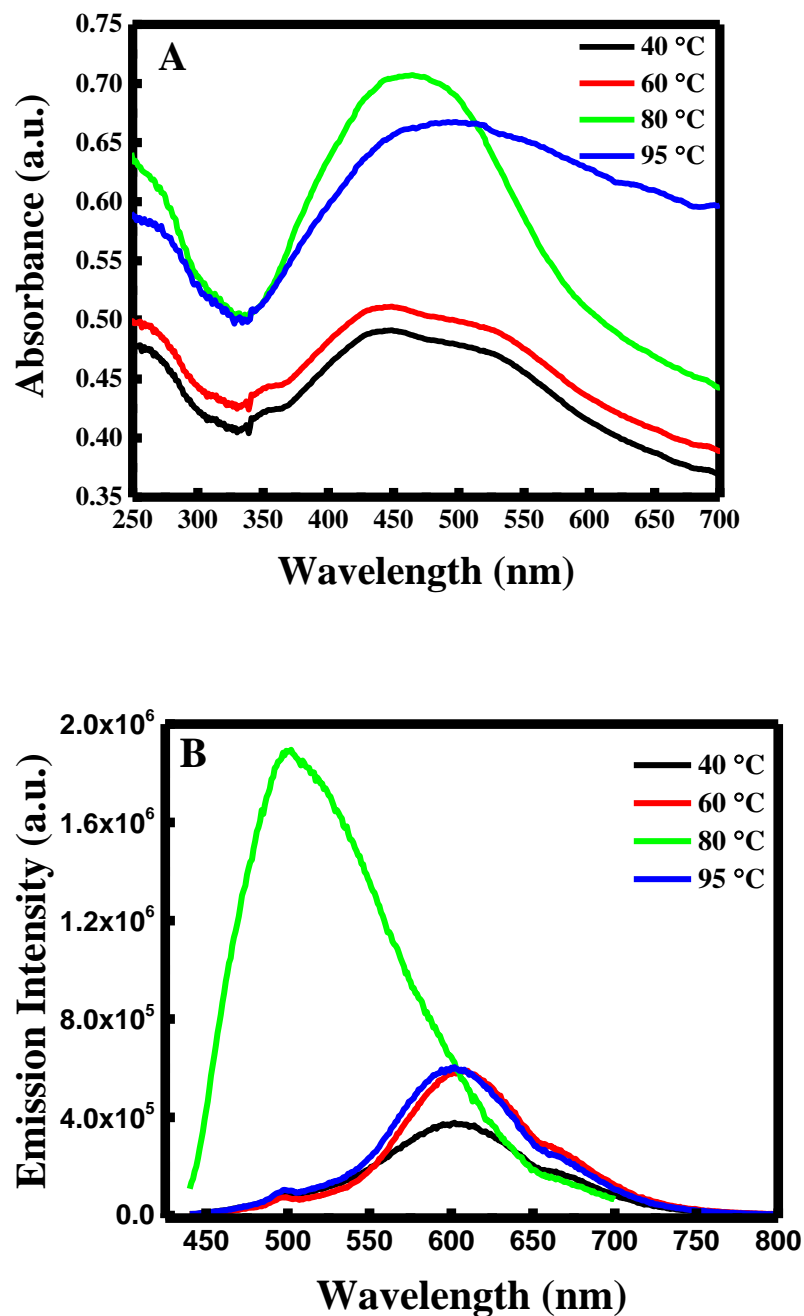
Figure 13 (A) UV-Visible and (B) Fluorescence of Zn(Cur)O prepared at different temperature.

As for the X-Ray Diffraction analysis (Figure 14), the patterns for the lowest two temperatures 40 and 60℃ indicate the presence of only two characteristic peaks for Zn(Cur)O NPs implying the occurrence of an incomplete reaction inhibiting the formation of Zn(Cur)O NPs. However, the XRD patterns of 80 and 95℃ represent the characteristic peaks of Zn(Cur)O nanoparticles, meaning that at high temperature curcumin can be easily complexed to ZnO NPs.
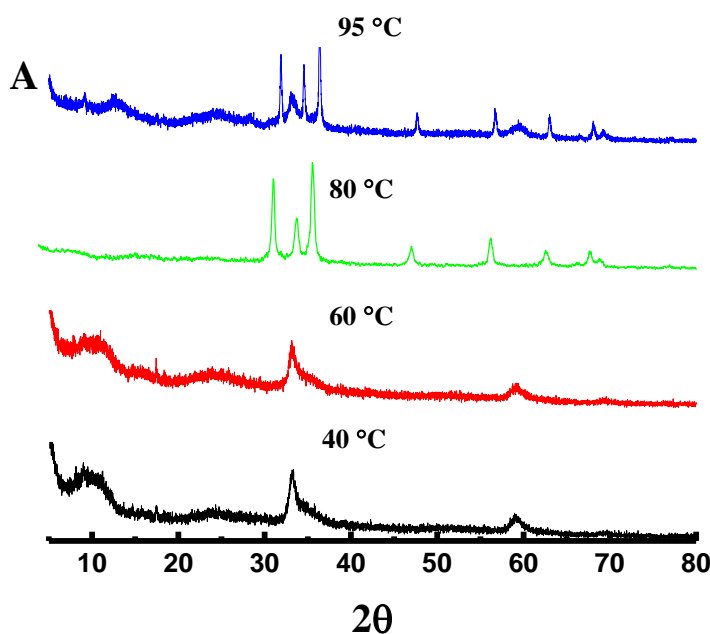
Figure 14 X-Ray diffractogram of curcumin and Zn(Cur)O NPs prepared at different reflux temperatures.

TGA results (see Figure 15) indicate a significant mass loss of around 70% and 65% at 40 and 60℃ respectively, which suggests the presence of free curcumin with no complete formation of Zn(Cur)O NPs confirming the XRD results. However, at 80 and

95℃, the mass loss is around 15% indicating a better interaction and complexation of curcumin with ZnO NPs, approving by that the results of XRD.
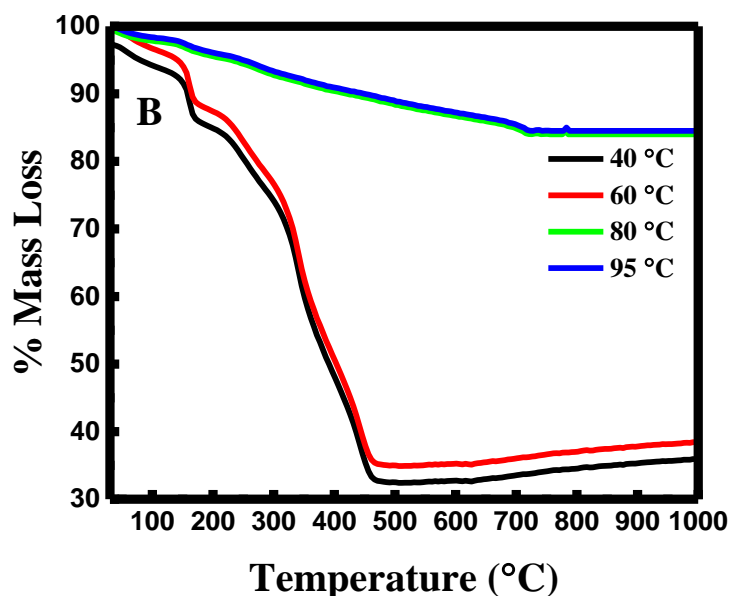
Figure 15 Thermogravimetric analysis of curcumin and Zn(Cur)O NPs prepared at different reflux temperature.

As a result, 80℃ is the most appropriate temperature to be used according to the optimization studies, preventing furthermore the boiling of water during the reflux at higher temperatures.

4. *Effect of polymer addition*

As discussed earlier, coating Zn(Cur)O NPs with a polymer will decrease the toxicity of ZnO nanoparticles keeping their beneficial properties, and preventing the formation of clusters [36-38]. It will be proven that it also increases the stability of

Zn(Cur)O NPs. The addition of chitosan was monitored in 3 different ways, after or before the addition of KOH, or before the start of the reflux.

The UV-Visible measurements and emission spectra are presented in Figure 16A&B. Interestingly, the UV-Visible absorption peak at 360-370 nm became prominent when adding chitosan compared to the Zn(Cur)O NPs prepared without coating suggesting chitosan directly gets involved during the formation of ZnO and creates different defect sites than Zn(Cur)O but similarly to naked ZnO. Though curcumin absorption peak is weak, the fluorescence spectra confirm curcumin conjugation. The highest fluorescence intensity was obtained for the case when adding chitosan after KOH compare to when chitosan was added before KOH suggesting chitosan compete with curcumin for conjugation during the formation of Zn(Cur)O when chitosan is added before KOH by forming particles which are similar to naked ZnO, whereas when chitosan is added after KOH some curcumin are already conjugated with Zn(Cur)O.
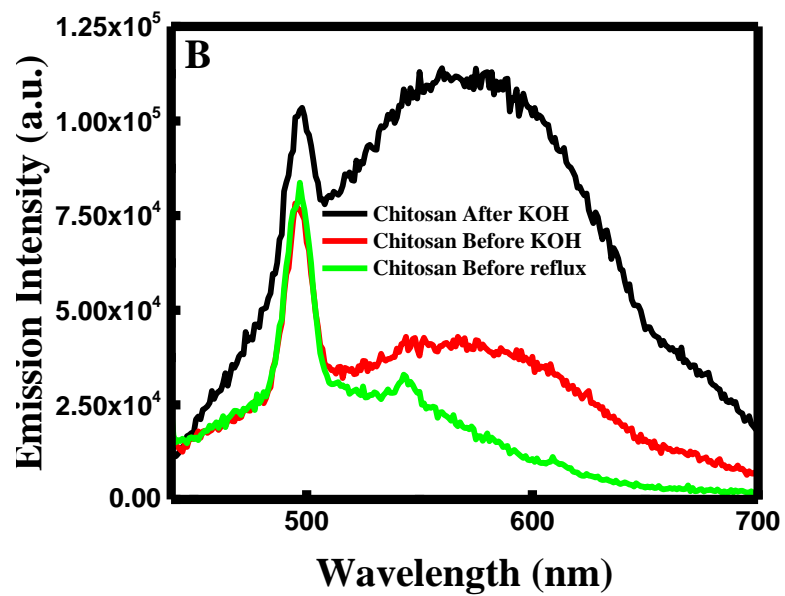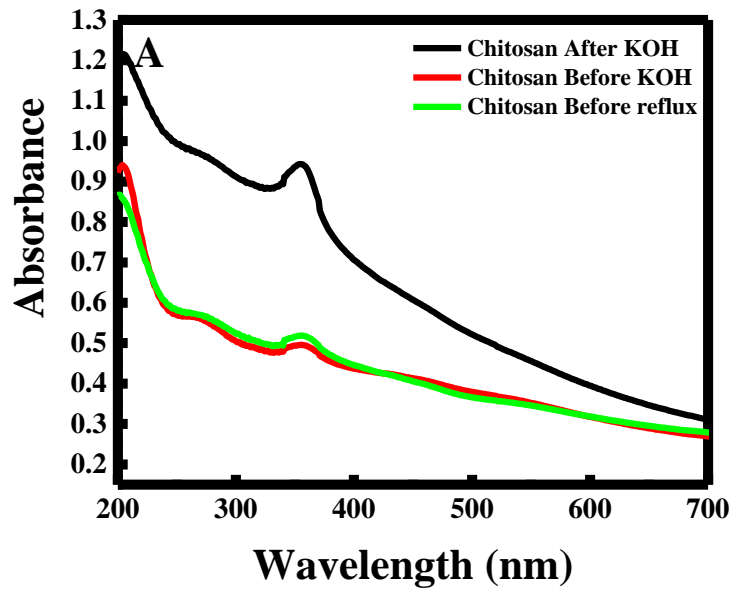
Figure 16 (A) UV-Visible and (B) fluorescence of Zn(Cur)O without chitosan and Zn(Cur)O coated with chitosan in 3 different ways.

Furthermore, as it is noticed from the XRD same characteristic peaks were obtained in all cases compared to the Zn(Cur)O prepared without chitosan (See Figure 17). The relative characteristics peak are 31.63°, 34.45°, 36.32°, 47.45°, 56.66°, 63.02°, 67.87° and 69.25°. This means that the addition of chitosan did not alter the crystallinity of Zn(Cur)O NPs.
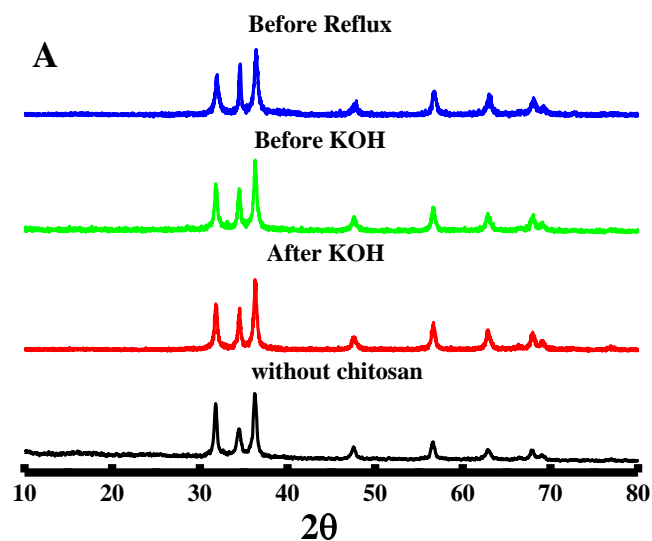
Figure 17 X-Ray diffractogram of curcumin and Zn(Cur)O NPs prepared in the absence and presence of chitosan polymer.

As for TGA, it is well noticed that less than 10% of mass loss was occurred when adding chitosan, compared to the NPs prepared without chitosan. This confirms the role of chitosan as a coating layer increasing the stability of the formed nanoparticles (See Figure 18).
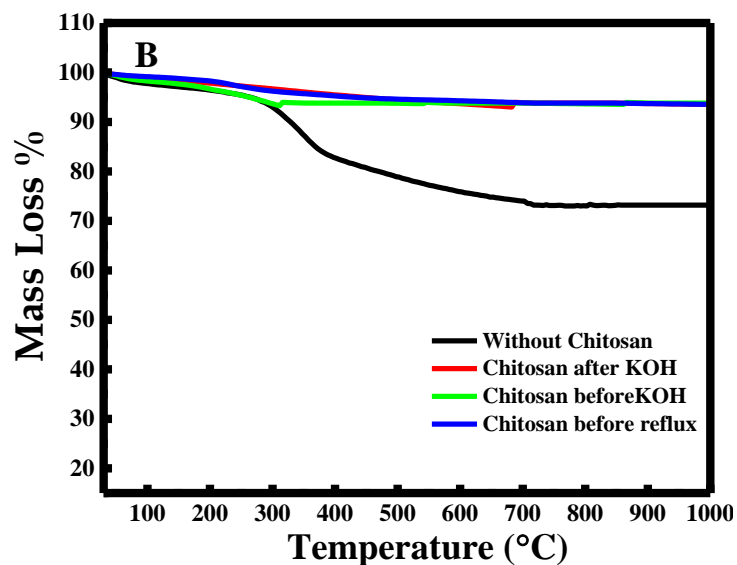
Figure 18 TGA analysis of curcumin and Zn(Cur)O NPs prepared in the absence and presence of chitosan polymer.

To sum up, since no remarkable difference was obtained in XRD and UV-Visible absorption between the three different ways of adding the polymer, chitosan added after KOH will be considered in the applications since it has greater amount of curcumin conjugation (highest fluorescence intensity was obtained).

The final zinc curcumin oxide nanoparticles in absence and presence of chitosan were characterized through SEM to identify their shape. The SEM images are presented in Figure 19A&B.
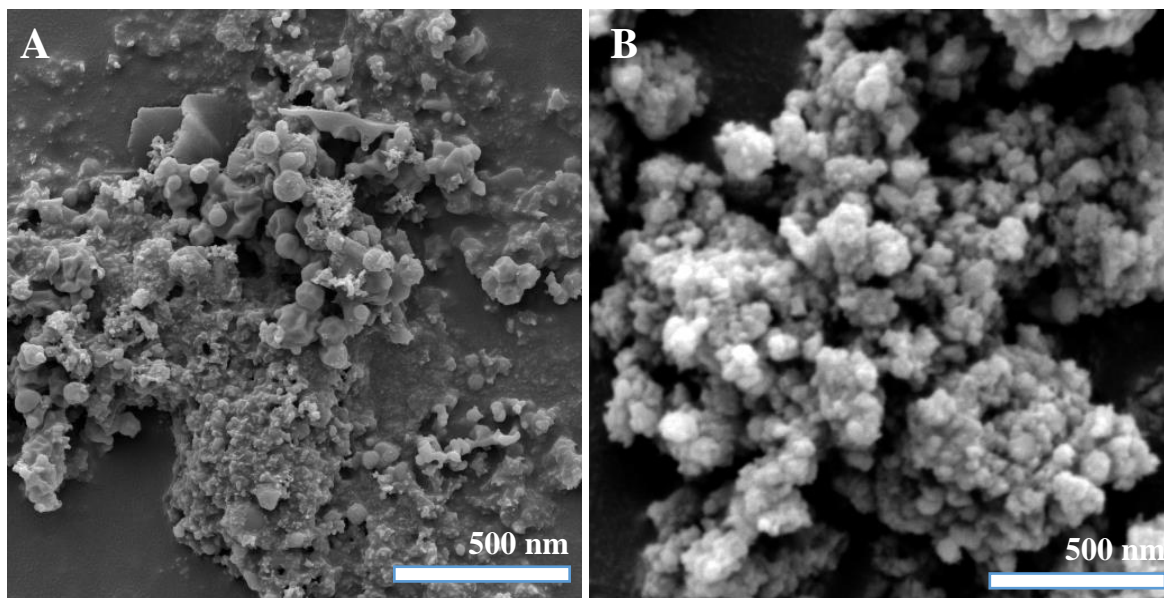
Figure 19 (A) SEM image of Zn(Cur)O NPs and (B) SEM image of Zn(Cur)O NPs coated with chitosan.

Interestingly, spheres NPs were obtained in both cases verifying the role of chitosan as a stabilizing agent and does not affect the composition and the shape of Zn(Cur)O NPs.

D. Conclusion

In conclusion, Zn(Cur)O NPs were synthesized through a simple method in the presence of curcumin. It was found that the flow rate of KOH has a significant effect on the formation of Zn(Cur)O NPs. In addition, the use of curcumin has induced the formation of Zn(Cur)O NPs at pH=13 and at 80℃. Furthermore, the stability of these NPs was increased when coating the formed NPs with chitosan.

CHAPTER IV

ANTI-CANCER ACTIVITY OF ZINC CURCUMIN OXIDE NANOPARTICLES: INHIBITION OF BREAST AND PANCREATIC CANCER CELLS PROLIFERATION

A. Introduction

Cancer is a disease that represents an extremely heterogeneous complex. It involves a variety of disorders accompanied by uncontrolled and abnormal cell growth and proliferation [91], [92]. Additionally, 200 types of cancer are present all around the world [93].

Breast cancer is extremely heterogeneous surrounding a group of genetically and epigenetically distinct infections showing various medical features [94].

Many human breast cancer cell lines, recognized from metastatic breast cancer specimens, are accessible through the American Type Culture Collection (ATCC). MCF-7 cancer cell line is the most studied. MCF-7 are an estrogen receptor (ER)-positive cell line derived from a pleural effusion in a patient with breast cancer [95].

Pancreatic adenocarcinoma (PA) is an aggressive disease that develops in a relatively symptom-free manner and is usually advanced at the time of diagnosis. Capan-1 is a human pancreatic ductal adenocarcinoma cell line. These cells grow in adherent tissue culture and display epithelial morphology [96].

Usually, the treatment of cancer could take place in four ways. First, cancer could be removed by surgery if it is present in one area, chemotherapy could be applied as well, radiation is the third way, and the last one refers to therapy using hormones [97]. Several side effects could be observed when anticancer agents are utilized due to the lack of specific targets, causing poor drug delivery.

Accordingly, nanotechnology has been taken into consideration because of the excessive progress of the drug delivery systems [98], [99].

Generally, nanotechnologies are spread in the market. Nanoscale particle size are synthesized such as coatings, fibers, and so on [100].

Curcumin has been widely used as anticancer agent in various studies against melanoma [101] for example, colon [102], breast [103]–[105], pancreatic [106], head [107], prostate [108], ovarian and neck [109] cancer cells.

Unfortunately, curcumin has low bioavailability and water solubility, so it is quickly metabolized and excreted out of the body [60]. That is why, curcumin will be complexed with ZnO NPs in order to correct these limitations and enhance its anticancer activity.

Zn(Cur)O NPs are widely investigated because of their photo-oxidizing and photocatalytic capabilities against chemical and biological species. Additionally, the US Food and Drug Administration pointed out the safety of ZnO NPs [110].

The purpose of our study is to evaluate and prove the efficiency of Zn(Cur)O NPs with and without chitosan as anti-cancer agent. The study was done on two different type of cancer cells: Capan-1 (pancreatic cancer cell) and MCF-7 (breast cancer cell).

B. Methods of preparation

1. Culture of MCF-7 and Capan-1 cancer cells

MCF-7 and Capan-1 cells were cultured in a completed DMEM high glucose media, where 10% FBS, 1% penicillin/streptomycin were added to free DMEM high glucose. MCF-7 and Capan-1 cells were cultured in a 10 mm petri dish and kept at 37°C in an incubator with a humidified atmosphere containing 95% O_2 and 5% CO_2 until they reached 80-90% confluency.

2. Cytotoxicity study by MTT proliferation assay

After treating the cells with curcumin, ZnO, chitosan, Zn(Cur)O and Zn(cur)O-Chi; MTT assay was used to measure the cell activity. MCF-7 and Capan-1 cells were seeded at a density of 5000 cells per well in 96-well plates. At 30% confluence, cells were subject to a concentration equal to 22 μM for the different treatment. After 24, 48 and 72, hours, 1mg/mL of MTT was added to the cells and kept for 1 hour incubated at 37°C. Later on, the media with the MTT were eliminating from the 96-well plate and DMSO was added in order to solubilize the formazan crystals. ELISA microplate reader, Thermo/LabSystems 352 Multiskan MS, was used to read the plates at a wavelength of 595 nm.

An example of the MTT assay is illustrated in Figure 20.

Cell treated with different C of curcumin
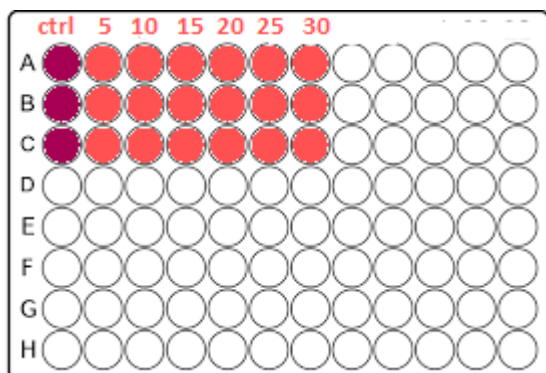
Addition of MTT after 48 hours
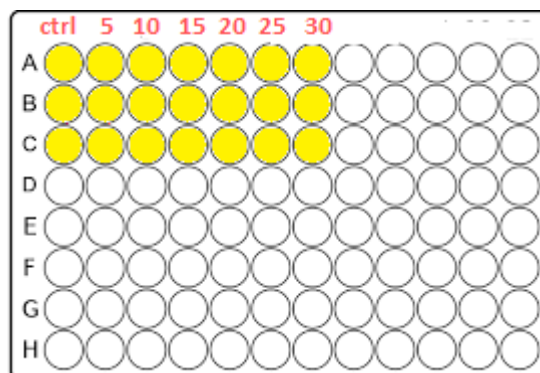
Formation of formazan crystals
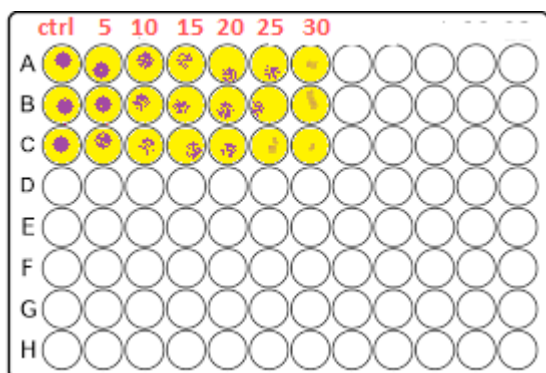
Addition of DMSO and ELISA reading
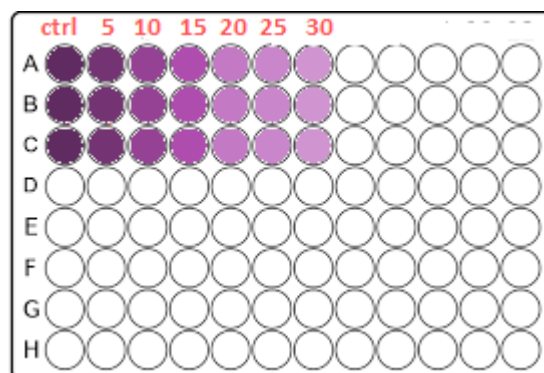
Figure 20 MTT assay for cell analysis.

C. Results and discussion

1. *Cytotoxicity of curcumin against MCF-7 and Capan-1 cells*

MTT proliferation assay was used to measure cytotoxicity of curcumin on MCF-7 and Capan-1 cells.

The half maximal inhibitory concentration (IC_{50}) is a measure of the potency of a matter in preventing a specific biological or biochemical function. IC_{50} is a numerical

measure that specifies how much of a particular inhibitory substance, as a drug, is needed to inhibit a specified biological development or biological element by 50% [111].

The cancerous cell lines were exposed to different concentration of curcumin for 48 hours. As shown in Figure 21, curcumin inhibits the proliferation of MCF-7 and Capan-1 cells up to 50% after 48 hours treatment. Hence, the IC_{50} of curcumin was found to be equal to ~22 µM and ~20 µM for MCF-7 and Capan-1 respectively.

These values were similar to the values obtained in the literature. The IC_{50} of curcumin was estimated to be equal to 21.32 µM and 19.6 µM after treatment for 48 hours for MCF-7 [112] and Capan-1 cells lines [113].
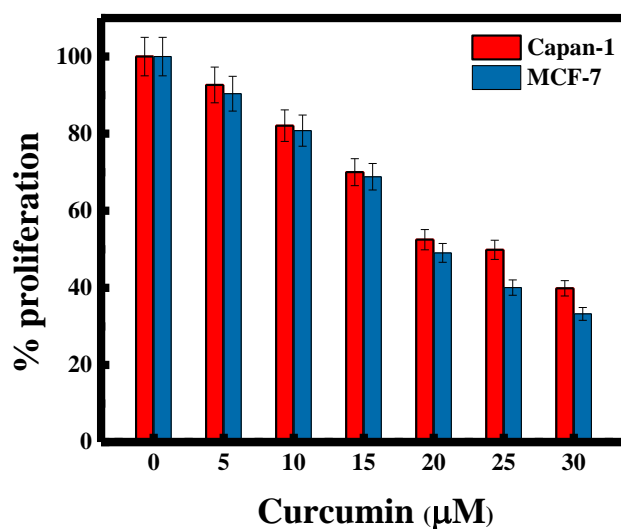
Figure 21 Curcumin cytotoxicity effect against MCF-7 and Capan-1 cell lines.

2. *Cytotoxicity of Chitosan, ZnO, Curcumin, Zn(Cur)O, and Zn(Cur)O-Chi against MCF-7 and Capan-1 cells*

Based on the IC_{50} concentration of curcumin that inhibits 50% of the cell proliferation, the cancerous cells were treated with the same concentration using ZnO, Zn(Cur)O, Zn(Cur)O-Chi and chitosan alone. The treatment was done for 48 and 72 hours. As presented in Figure 22, chitosan had no significant effect on the cell inhibition of MCF-7 cancer cells for a concentration equal to 22 μM (2 μg/mL) after 48 and 72 hours. When treated with zinc oxide nanoparticles, ~40 % inhibition was observed, after 72 hours. Compared to a study done by Kavithaa et al. [114] that has shown 50% inhibition when using 10 μg/mL of zinc oxide nanorods, verifies in the first place the efficiency of our ZnO NPs when using small amount for treatment.

Thus, the use of Zn(Cur)O NPs and Zn(Cur)O-Chi NPs enhances strongly the inhibition of MCF-7 cancer cells. Hence, when treated with 22 μM (2 μg/mL) of Zn(Cur)O NPs and Zn(cur)O-Chi NPs, the inhibition proliferation was up to 60% after 48 hours.

Therefore, a remarkable inhibition proliferation was observed after 72 hours when treated with Zn(Cur)O-Chi NPs, where ~90% inhibition was obtained. Yet, after the same treatment duration using Zn(Cur)O NPs alone, ~82% inhibition was determined. This difference in the value is related to the presence of chitosan, where chitosan helps curcumin in specifying its target.
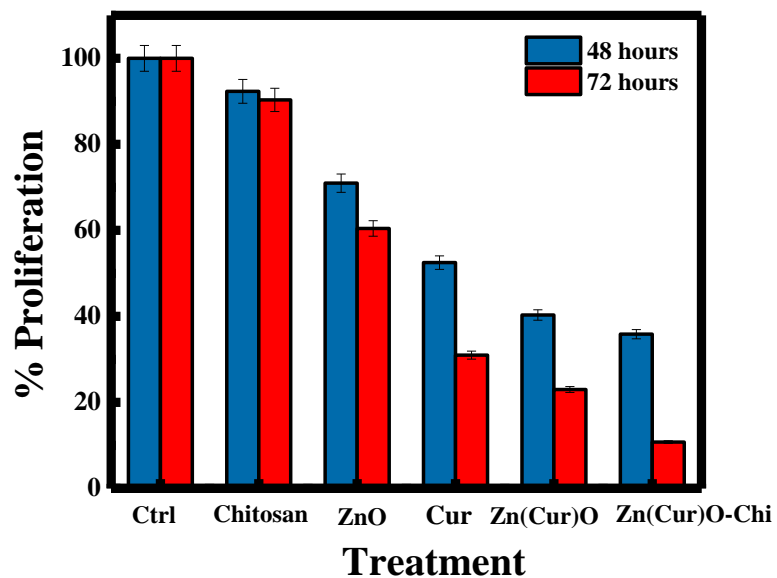
Figure 22 Cytotoxicity effect of different treatment against MCF-7 cell lines.

Similarly, Zn(Cur)O-Chi NPs have shown a good potential against Capan-1 cancerous cells (See Figure 23). More than 85% of the cancerous cells were inhibited when using 2 µg/mL of Zn(Cur)O-Chi NPs after 48 hours. Furthermore, 95% where inhibited after 72 hours.
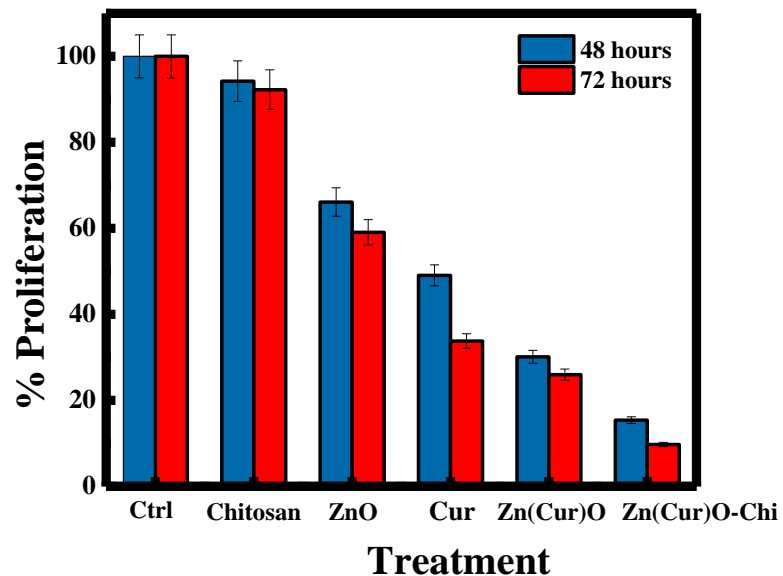
Figure 23 Cytotoxicity effect of different treatment against Capan-1 cell lines.

Thus, Zn(Cur)O NPs have acted also as a suitable anti-cancer agent, where after 72 hours the % of inhibition proliferation was equal to ~80%.

As seen in both graphs, Zn(Cur)O-Chi NPs have shown a high efficiency towards the cancerous cell line. Meaning that, the complexation of curcumin with zinc oxide nanoparticles, in the presence of chitosan, could be used as a potential anticancer agent against various cancer types.

The efficacy of our nanoparticles compared to other anti-cancer agent is depicted in Table 2.

Cell Type	Anti-cancer agent	Concentration	% proliferation	Reference
MCF-7	FA-MTX conjugated Au@SiO$_2$ NPs	25 μg/mL	45 %	[115]
	Liposomal curcumin	10 μg/mL	30 %	[116]
	Zn(Cur)O-Chi NPs	2 μg/mL	60 %	Our work
Capan-1	GA-MNP-Fe$_3$O$_4$ NPs	20 μg/mL	55 %	[117]
	Liposomal curcumin	10 μg/mL	60 %	[118]
	Zn(Cur)O-Chi NPs	2 μg/mL	80 %	Our work

Table 2 Anti-cancer activity of different agent on MCF-7 and Capan-1 cancer cell lines.

D. Conclusion

Curcumin alone has shown ~50% inhibition of MCF-7 and Capan-1 cancer cells proliferation, after 48 hours when treated with 22 μM. As for zinc oxide nanoparticles only ~40% were inhibited. Therefore, the combination of zinc oxide nanoparticles and curcumin enhanced the cytotoxicity of curcumin against both cancerous cells. Moreover, adding chitosan to the system increases the % of proliferation inhibition and therefore it could be used as vehicles system for the potential treatment of cancer.

CHAPTER V

CHITOSAN COATED ZINC CURCUMIN OXIDE NANOPARTICLES FOR THE DETERMINATION OF ASCORBIC ACID

A. Introduction

Ascorbic acid (AA), an essential food supplement, is present significantly in fresh fruits and vegetables, like broccoli for example, in the form of vitamin C. In addition, it is found in beverages because of its nutritional importance and antioxidant activity.

Unfortunately, degradation of ascorbic acid could occur quickly due to many environmental factors such as the solvent used, the pH, the temperature of the environment, the pressure, the light, and the presence of oxygen or metal ions [119], [120]. This might lead to an obvious change in the color or in the quality of the drinks [119].

Ascorbic acid is water-soluble and is used extensively in pharmaceutical and cosmetic products, as well as in human diet. Therefore, its detection in food and pharmaceutical products through simple methods has gained an increased importance.

Up till now, several techniques have been applied including electrochemistry, chromatography, enzymology, titration with an oxidizing agent, spectrophotometry, colorimetry, capillary electrophoresis, and chemiluminescence.

However, these methods are high cost, time-consuming, and suffer from complex sample handling, thus making it problematic to use them [121]–[123]. Spectrophotometry,

for example, is limited by other substances that may possibly interfere when this technique is applied to tissues or food [123]. Even though the electrochemical technique is easy, selective, and sensitive for the quantification of ascorbic acid, the electro-oxidation of AA and the adsorption onto the bare electrode surface requires overvoltage, leading to a poor selectivity and reproducibility due to electrode fooling.

Consequently, nanomaterials are used as electrode modifiers in order to enhance the signal of the electrochemical biosensors and to increase the range of detection. In a recent study, copper sulfide/Prussian blue core-shell nanostructures drop-coated on a glassy carbon electrode were used as a sensor for the detection of ascorbic acid in beverages [122]. In another study, ascorbic acid was sensed and quantified in a colorimetric manner. It can reduce the oxidized form of TMB, 3,3',5,5'-tetramethylbenzidine, thus making the blue color present initially, meaning in the absence of AA, fade gradually [124].

Despite the presence of numerous methods for the detection of vitamin C, developing a low-cost, easy, rapid and sensitive technique is essential in both pharmaceutical and nutritional fields. Accordingly, fluorescence spectroscopy was an ideal choice for sensing due to its easiness, simplicity, and high accuracy in detection even at low concentrations with high sensitivity as well as high selectivity [125].

Hence, metallic nanoparticles, such as gold [126], silver [127], and copper nanoparticles [128], were recently used to detect AA. However, it was necessary to adapt cheaper, and feasible new nanoparticles for this purpose.

In this study, Zn(Cur)O NPs were established as nanoprobe in order to detect ascorbic acid using fluorescence technique. Finally, a comparison of the efficiency in

79

detecting AA between ZnO alone, Zn(Cur)O, and Zn(Cur)O coated with chitosan
Zn(Cur)O-Chi will be performed.

B. Methods of preparation

1. *Sample for ascorbic acid detection*

A stock solution of 25 mmol.L^{-1} (mM) ascorbic acid was prepared by dissolving it in 10 mL of double distilled water. Several solutions were prepared with concentrations in the range of 0 to 10 mM (See Figure 24).

A stock solution of Zn(cur)O-Chi NPs was prepared by dissolving 1 mg in 5 mL of double distilled water. 0.2 mL of Zn(Cur)O-Chi NPs were added to the different concentration of AA and completed with double distilled water to get a final volume equal to 3 mL.
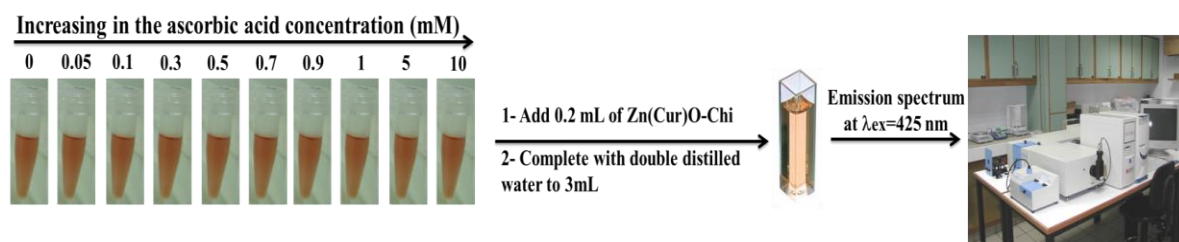
Figure 24 Scheme illustrating the preparation of AA samples.

2. *Selectivity towards nanoprobe*

Two stock of ZnO and Zn(Cur)O nanoparticles were prepared by dissolving 1 mg in 5 mL of double distilled water. The samples were prepared exactly the same way prepared when using Zn(Cur)O-Chi mixed with ascorbic acid.

3. *Selectivity towards interference*

As per investigating the interference, several analytes as L-ascorbic acid, uric acid, glucose, cholesterol and glutathione were measured at a concentration equal to 10 mM and mixed with 0.2 mL of Zn(Cur)O-Chi NPs.

4. *Recovery of the method*

To test the applicability, the present method was used to estimate the analytical recovery of three unknown samples by using the obtained fitted calibration curves.

5. *Photostability of Zn(Cur)O-Chi NPs*

Two distinctive solutions were prepared to test their stability. At the beginning, 0.2 mL of Zn(Cur)O-Chi NPs were dropped into a vial and completed with double distilled water till 3 mL. In a second vial same volume of Zn(Cur)O-Chi NPs was mixed with ascorbic acid and finalized with double distilled water. The two solutions were kept undisturbed for 5 hours and then the emission intensity was measured for 1 hour in interval of 10 minutes.

C. Results and discussion

1. *Interaction of ascorbic acid with Zn(Cur)O-Chi NPs*

Zinc oxide nanoparticles are very useful as chemical and biological sensors for a diverse and widespread range of compounds due to their thermal stability, high surface area, wide band gap, biocompatible nature, and superior response as well [129].

For this purpose, the prepared Zn(Cur)O and Zn(Cur)O-Chi were used as nanoprobe to detect ascorbic acid. The efficiency of those nanoparticles was compared to the activity of ZnO NPs alone without any modifications.

The sensing of AA was done for a concentration range going from 0 to 10 mM. As shown in Figure 25, the emission intensity of Zn(Cur)O-Chi increases with the addition of ascorbic acid. This enhancement is also conducted with a blue shift from 567 nm to 552 nm. This boost in the intensity is due to the ionic interactions between the amino groups of chitosan with the hydroxyl functional group of ascorbic acid. Hence, the complex formed Zn(Cur)O-Chi-AA becomes more soluble based on the enhancement of the hydrophilic properties.
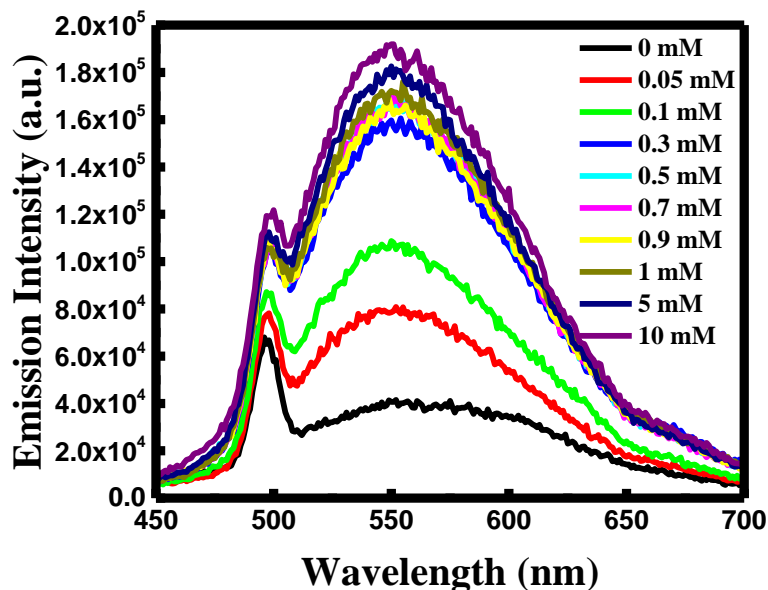
Figure 25 Change in the emission intensity of Zn(Cur)O-Chi NPs with the increase of ascorbic acid concentration.

According to Tian et al., ascorbic acid molecule contains different electrophilic groups. It contains four hydroxyl groups with different acidity allowing in consequence different acid-base reaction. Therefore, the acidic hydroxyl in position 3 of AA is expected to react with the amino group of chitosan, inducing the formation of ammonium ions (See Figure 26). Thus, ammonium ions increase the solubility of the complex and thereby cause the enhancement of the emission intensity [130].
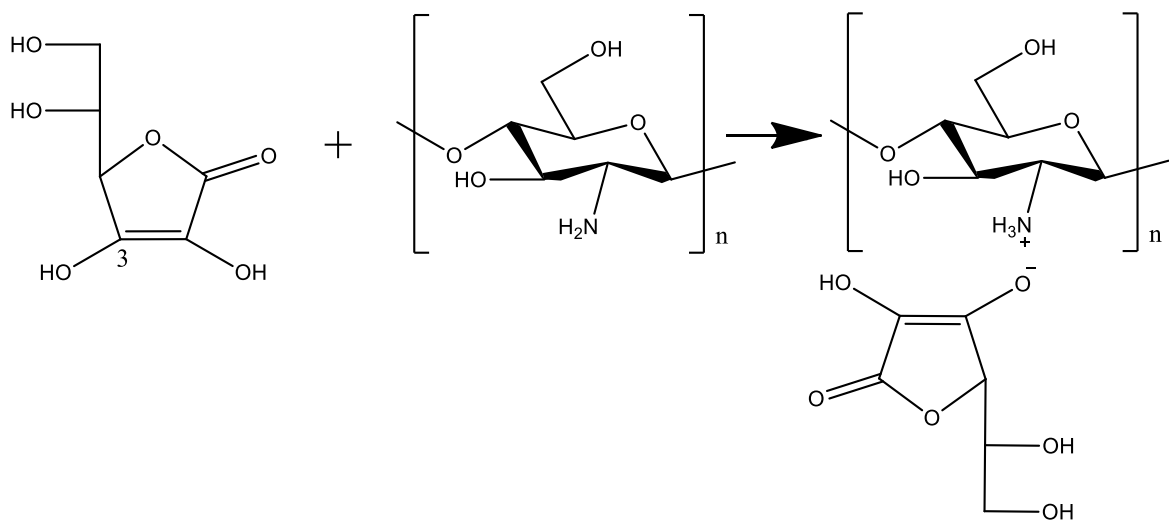
Figure 26 Scheme illustrating the interaction between chitosan and ascorbic acid.

The enhancement of the intensity ratio ($Log(I/I_0)$) versus the concentration of ascorbic acid was depicted in Figure 27A&B, for 2 concentration ranges, from 0 to 0.3 mM and from 0.5 to 10 mM. The linear equations for the two concentration ranges are $\Delta I= 0.42034[AA] + 0.769944$ with a correlation coefficient of 0.99753 and $\Delta I= 0.02737[AA] + 0.58123$ with a correlation coefficient of 0.99187.
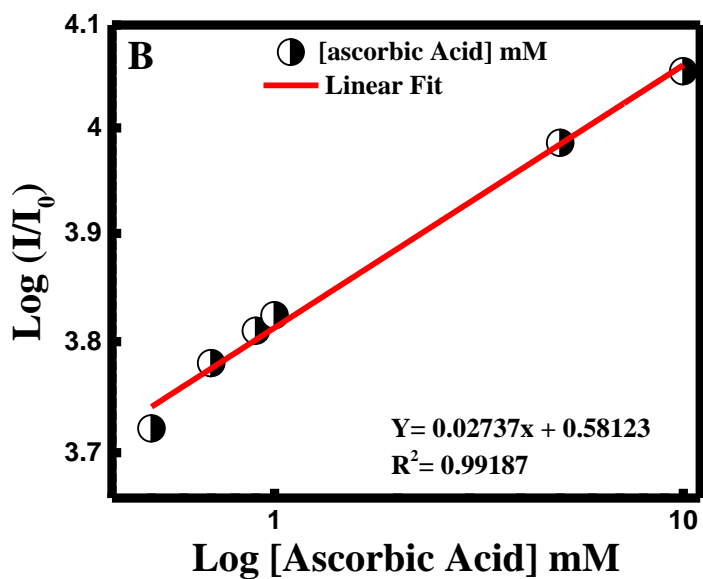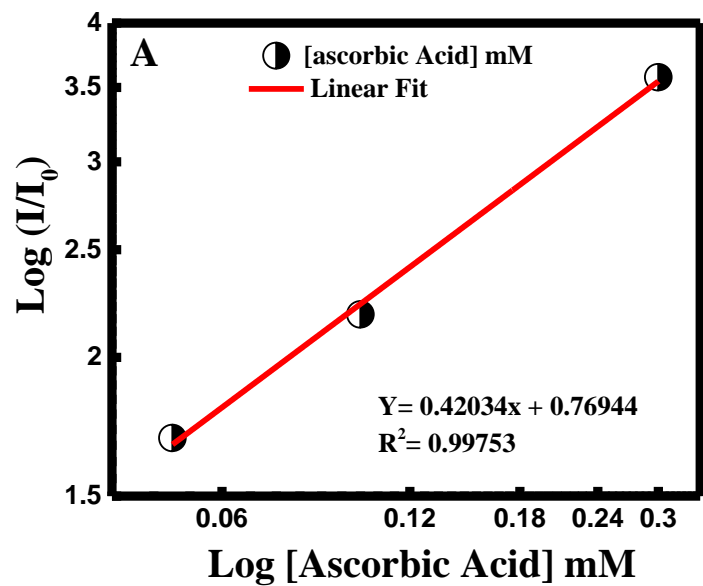
Figure 27 (A) and (B) Linear fit of the proposed method in the range 0-0.3 and 0.5-10 mM respectively.

The limit of detection is found to be 36 μM referring to 3σ/s, where σ is the standard deviation of the measurements and s is the slope of the calibration curve.

The interaction of Zn(Cur)O-Chi NPs with ascorbic acid was also verified through zeta potential analysis. In fact, the surface charge of the NPs in the absence of ascorbic acid was equal to -5.1 mV. The charge of the surface increases to -1.61 mV upon the addition of ascorbic acid. This change in the surface charge reveals the presence of more positive species, which are related to ammonium ions (See Figure 28A&B).
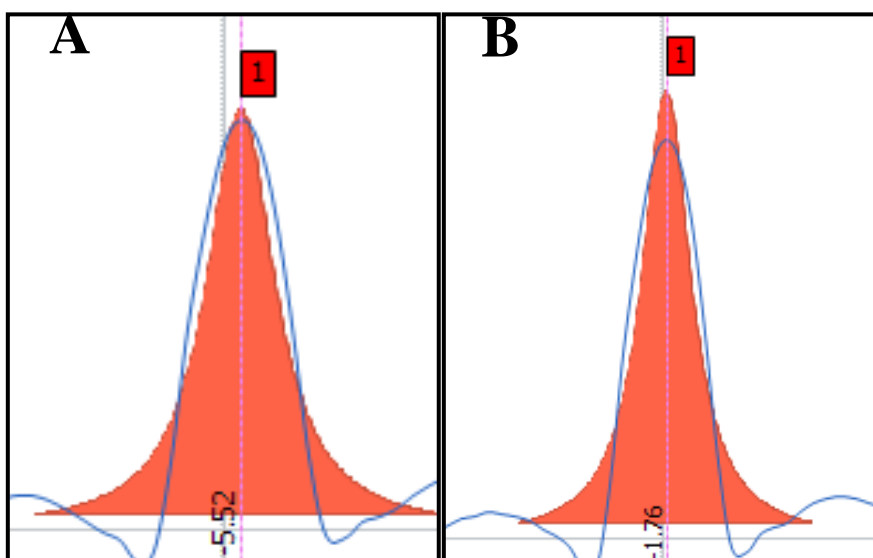
Figure 28 (A) zeta potential value of Zn(Cur)O NPs and (B) zeta potential value of Zn(Cur)O-Chi NPs.

Our fluorescence method resulted in a comparable linear range and limit of detection to those previously reported methods. Several linear ranges and detection limits of different techniques used by other researchers for the detection of ascorbic acid were established in Table 3.

Sensing technique	Range	LOD	Interference	Reference
Chemiluminescence method using Mg-Al-CO_3 LDHs-catalyzed ONOOH	5 nM – 5000 nM	0.5 nM	malic acid, tartaric acid, succinic acid, malonic acid, glucose, sucrose, fructose	[131]
Colorimetric method based on Metal-Organic Framework-Derived copper Nanoparticle@Carbon Nanocomposites as Peroxidase Mimics	10 μM – 1 mM	1.41 μM	starch, fructose, glucose, sucrose, tartaric acid, lysine, tyrosine, phenylamine, aspartic acid, alanine, glutamic acid	[128]
Colorimetric method based on carbon quantum dots as peroxidase mimetic enzyme	1 μM – 105 μM	0.14 μM	sodium acetate, acetic acid, glycine, threonine, lysine, histidine, alanine, tartaric acid, benzoic acid.	[132]
Electrochemical technique using a CdO nanoparticle/ionic liquid modified carbon paste electrode as sensor	0.07 μM – 480 μM	0.03 μM	fructose, lactose, glucose, sucrose, glutamic acid, alanine, phenylalanine, methionine, glycine, valine, histidine, cysteine.	[133]
Fluorescence emission using zinc curcumin oxide nanoparticles coated with chitosan	0 mM - 0.3 mM 0.5 mM - 10 mM	36 μM	L-ascorbic acid, glucose, uric acid, cholesterol, glutathione, lysine, alanine, guanine, tyrosine	Our work

Table 3 Different techniques used for the detection of Ascorbic acid.

2. *Selectivity towards nanoprobe*

Moreover, The selectivity of Zn(Cur)O-Chi towards the sensing of ascorbic acid

was established in the first place by using ZnO and Zn(Cur)O instead of Zn(Cur)O-Chi.

Figure 29 shows the ratio of the emission intensity I/I_0 when using ZnO and Zn(Cur)O as nanoprobe versus the concentration of ascorbic acid.
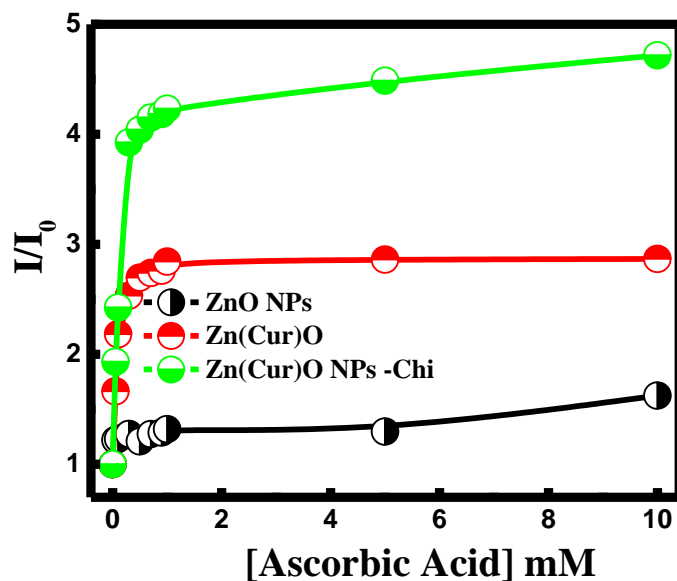
Figure 29 Selectivity of Zn(Cur)O-Chi NPs towards the detection of ascorbic acid compared to ZnO NPs and Zn(Cur)O NPs.

It is clear that ZnO NPs did not show any obvious change in the emission intensity while increasing gradually the concentration of ascorbic acid at 425 nm excitation wavelength. However, Zn(Cur)O and Zn(Cur)O-Chi showed an increase in the emission intensity spectrum upon the addition of ascorbic acid. Thus, the enhancement of the emission intensity using Zn(Cur)O-Chi was about ~ 5 fold, although it was ~ 2.8 fold when using Zn(Cur)O alone.

These results confirm the direct interaction of chitosan layer with ascorbic acid molecule resulting in the formation of a highly soluble complex.

3. *Selectivity towards interference*

The selectivity of Zn(Cur)O-Chi towards the detection of ascorbic acid was also investigated while detecting different analogues of AA that could interfere. For this purpose, different analytes at a concentration equal to 10 mM were analyzed using Zn(Cur)O-Chi.
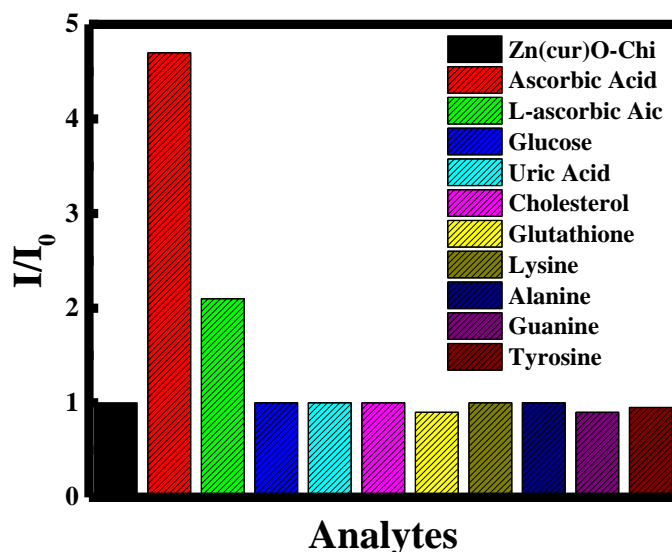
Figure 30 I/I_0 of Zn(Cur)O-Chi NPs alone and of Zn(Cur)O-Chi NPs with different analogues at C= 10 mM.

It is remarkable from Figure 30 that none of the tested analytes (glucose, uric acid, cholesterol, glutathione, lysine, alanine, guanine, and tyrosine) had altered the emission intensity of Zn(Cur)O-Chi where the ratio of I/I_0 was equal to 1. As for L-ascorbic acid, the ratio of the emission intensity I/I_0 was almost equal to 2. This is due to the fact that L-ascorbic acid is an ester formed from ascorbic acid and palmitic acid creating a fat soluble form of vitamin C. Consequently, L-ascorbic acid is slightly soluble in water, thereby

making its interaction with chitosan difficult. These selectivity results confirm the direct interaction between Zn(Cur)O-Chi and ascorbic acid molecule.

4. *Recovery of the method*

The recovery of the proposed method was studied by testing 3 unknown samples. The results obtained are summarized in Table 4. The percent of ascorbic acid recovery of our method was found to be between 94-100% ± 2.5 (mean ± S.D) which is quite acceptable.

	Theoretical Concentration (mM)	Experimental concentration (µM)	Recovery (%)
Unknown 1	0.2	0.0188	94
Unknown 2	0.8	0.805	100.6
Unknown 3	9	8.85	98.3

Table 4 Recovery results of the proposed method.

5. *Photostability of Zn(Cur)O-Chi NPs*

Finally, the photostability of Zn(Cur)O-Chi in the presence and absence of ascorbic acid is illustrated in Figure 31.
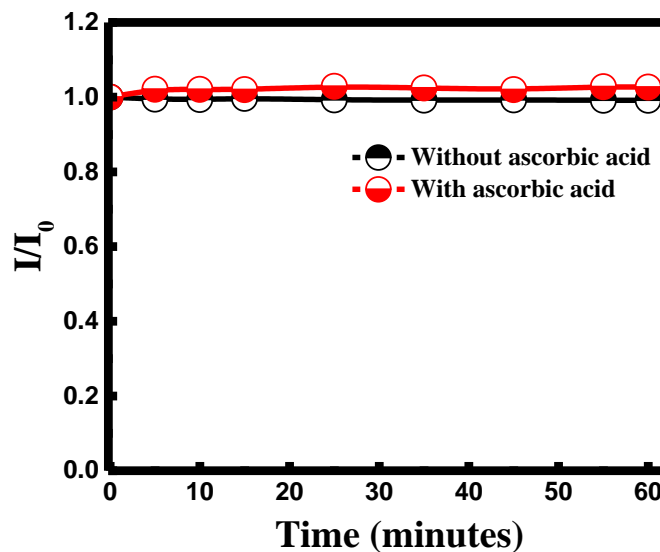
Figure 31 Plot of I/I_0 of Zn(Cur)O-Chi NPs with time in the absence and presence of AA.

It was found that when the emission intensity of Zn(Cur)O-Chi was recorded in the absence and presence of ascorbic acid for one hour, the signal was found to be remarkably stable indicating that the current sensor is relatively stable during measurement time.

D. Conclusion

Zinc curcumin oxide nanoparticles have shown a great nanoprobe for the detection of ascorbic acid in the presence of chitosan. The presence of chitosan encourages the direct interaction of the hydroxyl group of AA with the amino group of chitosan. Although no change in the emission intensity was observed using ZnO NPs alone, Zn(Cur)O NPs were able to detect AA but not as efficiently as Zn(Cur)O-Chi NPs. The method used was

selective and sensitive towards the detection of AA using Zn(Cur)O-Chi NPs as nanoprobe.

The recovery of the method was found to be between 94 and 100% and the limit of

detection was 36 µM.

CHAPTER VI

KINETICS AND ISOTHERMS STUDY OF CONGO RED ADSORPTION: ZINC CURCUMIN OXIDE NANOPARTICLES AS AN EFFICIENT ADSORBENT COMPLEX

A. Introduction

Synthetic dyes present in wastewater have the potential to threaten the natural environment. During the dyeing process, they can be released as wastes. They could be eliminated from paper, printing, plastic, cosmetic, or leather industries. Due to their complex structures, these dyes effluents are not susceptible for biological wastewater treatment. Thus, they are not biodegradable [134]. One of these toxic organic dyes is congo red. Congo red is one of the relevant organic dyes that is found in water. It is a secondary diazo dye with a complex aromatic structure that makes it non-biodegradable and fairly stable. Congo red can be easily dissolved in water, inducing several difficulties when removing from contaminated water. It is as well toxic and carcinogenic, and it affects the eyes, skin, respiratory, and reproductive systems [135]. It is an anionic dye with a pka of 4.5. It can cause allergies and metabolize into benzidine that is mutagenic to aquatic creatures and carcinogenic at the same time [136]. Consequently, several methods such as oxidation, ion exchange, coagulation, adsorption, precipitation, and liquid–liquid extraction

have been used to take out the toxic organic dyes from wastewater. Among these methods, adsorption is considered as a successful separation technique.

Zinc curcumin oxide nanoparticles were applicable in different field. For example in 2016, Moussawi et al. have produced Zn(Cur)O NPs and have studied their adsorption and fluorescence sensing potential on arsenite [87], and its effect of the removal of Perylene, Fluoranthene, and Chrysene [44]. In addition, Nasrallah et al. have established the Scavenging Activity of Zn(Cur)O NPs based on DPPH molecule [46].

Usually curcumin helps in the reduction of organic dyes when combined to metal oxide nanoparticles [73], [137]. We assume that curcumin could have same effects when it is conjugated to zinc oxide nanoparticles and leads to an enhancement in its adsorption activity. To the best of our knowledge, the efficiency of zinc curcumin oxide nanoparticles is not yet elaborated as a suitable adsorbent for the removal of organic dye.

In our work, the adsorption of congo red was established and conducted at different concentrations of Zn(Cur)O NPs and different concentrations of congo red. The effectiveness of Zn(Cur)O NPs as adsorbent was compared by analyzing the effect of ZnO NPs and Zn(Cur)O-Chi NPs.

B. Methods of preparation

For each adsorption experiment, 1 mg of ZnO NPs, Zn(Cur)O NPs, Zn(Cur)O-Chi NPs was dissolved in 1 mL heated double distilled water and sonicated for one minute to assure complete dissociation of Zn(Cur)O NPs. Congo red solution (C=1 mM) was prepared by dissolving 3.48 mg of this dye in 5 mL double distilled water (See Figure 32).

94
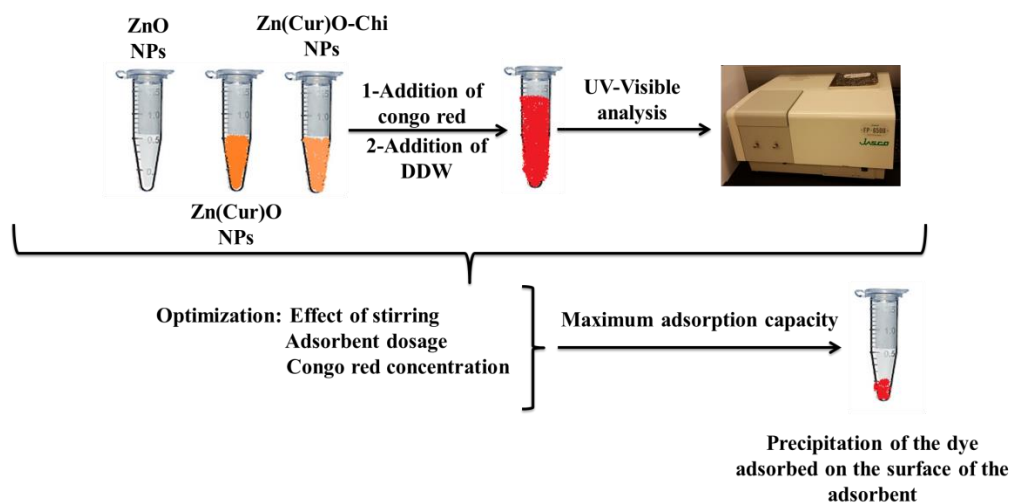
Figure 32 Scheme illustrating the preparation of adsorption sample.

In order to make sure that maximum adsorption of the dye onto the surface of the nanoparticles is attained; stirring effect, the adsorbent dose and congo red concentration were varied.

- In the first place, the experiment was carried out in the absence of stirring, then with stirring at 400 rpm and finally using shaker under 400 rpm.

- In the second place, a fixed amount of congo red (45 μL, 15 μM) was added to different mass of Zn(Cur)O NPs adsorbent (0.05-0.9 mg).

- In the 3rd place, the concentration of congo red was varied from 5 to 100 μM while the adsorbent dose remained fixed (0.9 mg).

In all the experiments the total volume was kept constant and equal to 3 mL. The analysis and the adsorption kinetics was monitored through UV-Visible spectrophotometer at different time intervals (t=0, 5, 10, 20, 30, 40, 60, 80, 110 mins, and after 24 hours).

C. Results and discussion

1. *Adsorption of congo red*

After mixing 150 μL of ZnO, Zn(Cur)O, and Zn(Cur)O-Chitosan NPs, with 45 μL (15 μM) of congo red organic dye and 2.8 mL of double distilled water, the absorbance was measured using UV-Visible spectrophotometer. The experiment was done at different intervals of time (t=0, 5, 10, 20, 30, 40, 60, 80, 110 mins, and 24 hours).

Figure 33 presents the UV-Visible spectrum of Zn(Cur)O with congo red within time.
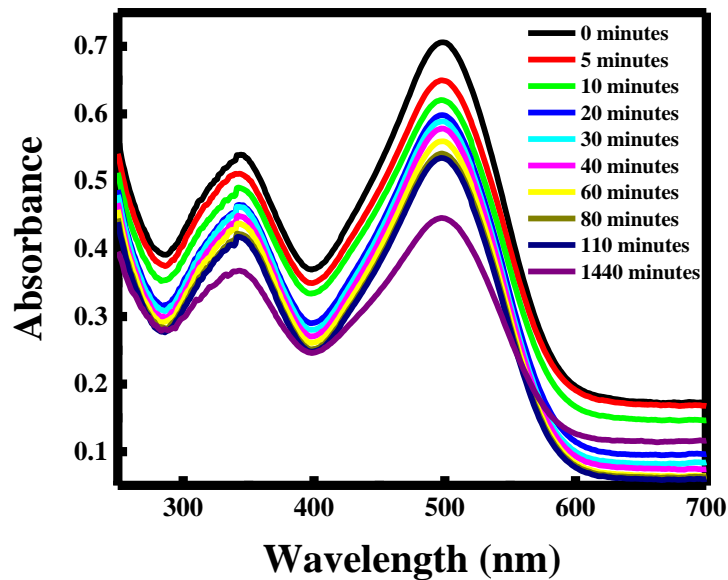
Figure 33 UV-Visible spectra of Zn(Cur)O with congo red within time.

As observed in Figure 33, a decrease in the absorbance was obtained within time. The adsorption capacity was calculated based on the equation below:

$$q_e = \frac{(C_0 - C_e)V}{m} \qquad (1)$$

96

where C_0 and C_e are the initial concentration and the equilibrium concentration of congo red respectively (mg/L), V is the volume of the solution (mL) and m is the mass of Zn(Cur)O NPs (g). It was found that the q_e in this case was equal to 89.85 mg/g which is relatively high compared to previous method used in the literature (See Table 5).

Adsorbent	Concentration of adsorbent (g/L)	Concentration of Congo Red (mg/L)	Kinetic order	q_e (exp) (mg/g)	R^2	Reference
Mesoporous α-Fe$_2$O$_3$ nanorods	1	20	Pseudo-second order	18.7	0.99	[138]
Porous soybean curd xerogels	1.25	40	Pseudo-second order	27.46	0.99	[139]
Activated carbon coffee waste	4	20	Pseudo-second order	9.41	0.99	[140]
Zn(Cur)O	0.15	11.15	Pseudo-second order	89.85	0.99	Our work

Table 5 Different methods used in the removal of congo red.

The high adsorption capacity was also confirmed visually. After 24 hours, the solution color turned from dark red to almost transparent, where the congo red and the zinc curcumin oxide nanoparticles settled down. This precipitation indicates that all the congo red molecules have been adsorbed.

2. *Effect of stirring*

Furthermore, the effect of stirring was also investigated. For this purpose, in a first place the experiment was done without stirring, and in a second place the mixtures were kept under stirring during measurement at 400 rpm and using water bath shaker at 400 rpm also. As depicted in Figure 34, A/A_0 ratio decreases faster in the absence of stirring. Meaning that, the high adsorption was obtained when the reaction occurred without stirring.
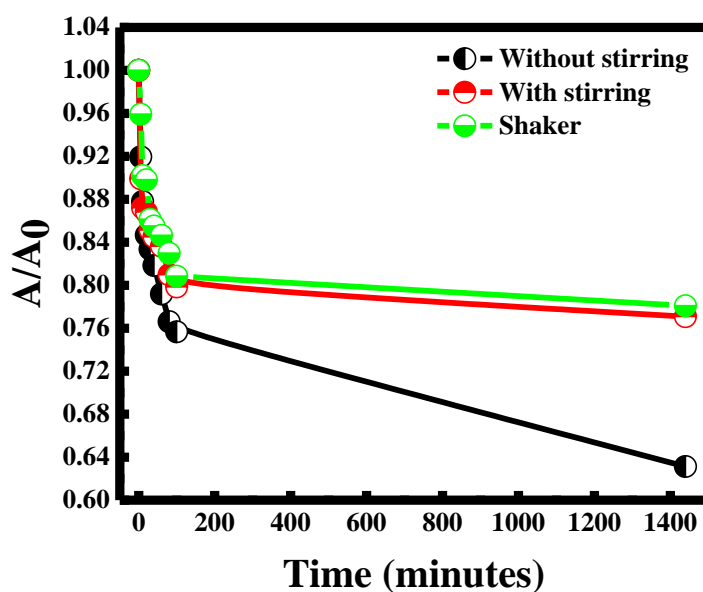
Figure 34 A/A_0 for Zn(Cur)O with congo red without/with stirring and using shaker.

The q_e value in the three cases was equal to 89.85 mg/g, 8.66 mg/g, 5.30 mg/g without stirring, with stirring and using shaker respectively. Hence, the adsorption capacity was found to be higher when keeping the solution undisturbed, meaning that congo red molecule can be easily adsorbed on the surface of Zn(Cur)O.

3. *Efficiency of Zn(Cur)O NPs in the adsorption process*

Moreover to establish the efficiency of Zn(Cur)O NPs as adsorbent of congo red, the adsorption study was done using ZnO NPs and Zn(Cur)O-Chitosan.

In order to understand the adsorption kinetics of the three adsorbents, the pseudo-first order and pseudo-second order kinetic models were plotted using the following equations respectively:

$$\ln(q_e - q_t) = \ln(q_e) - k_1 t \qquad (2)$$

$$\frac{t}{q_t} = \frac{1}{k_2 q_e^2} + \frac{1}{q_e} t \qquad (3)$$

where q_t and q_e are the adsorption capacity at time t and at equilibrium respectively (mg/g), t is the time (min), k_1 is the rate constant of the pseudo-first order model (min^{-1}), and k_2 is the rate constant of the pseudo-second order model (g.mg^{-1}.min^{-1}).

Congo red adsorption was presented for the pseudo-first order and pseudo-second order in Figure 35A&B respectively.
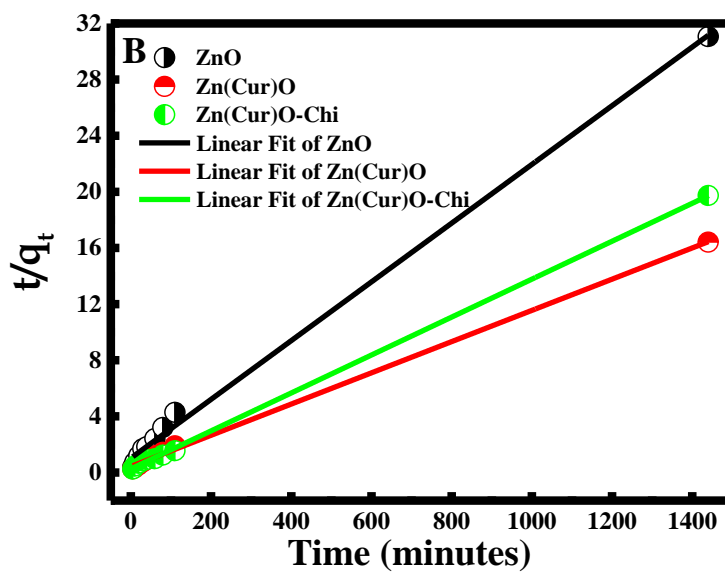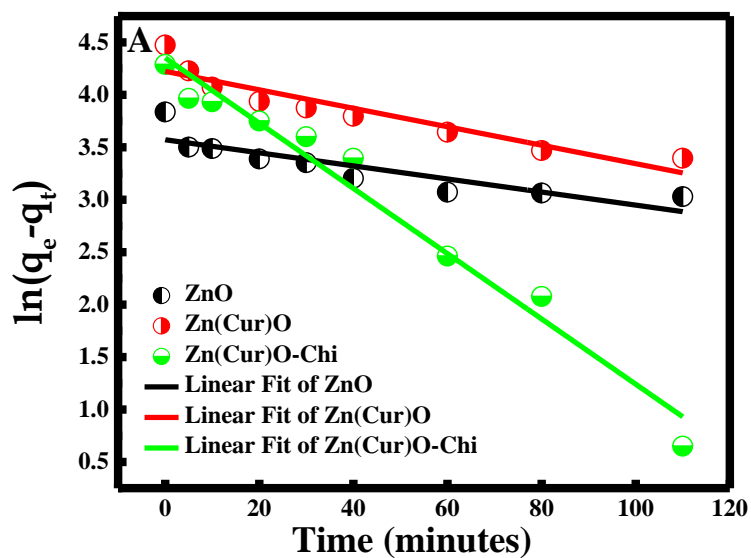
Figure 35 (A) pseudo first order kinetic model and (B) pseudo second order kinetic model for Zn(Cur)O in the presence of congo red.

A linear curve was obtained for the pseudo-first order model where the values of q_e and k_1 are calculated from the intercept and slope, respectively. Similarly, a linear curve was obtained for the pseudo-second order model where q_e is calculated from the slope and k_2 from the intercept (See Table 6).

Adsorbent	Pseudo-first order			Pseudo-second order			q_e (calc)
	q_e (exp)	k1	R^2	q_e (exp)	k2	R^2	
ZnO	35.56	$6.23*10^{-3}$	0.74	47.78	$4.27*10^{-4}$	0.99	46.35
Zn(Cur)O	68.26	$8.80*10^{-3}$	0.86	89.85	$2.91*10^{-4}$	0.99	87.70
Zn(Cur)O-Chi	77.60	$3.11*10^{-2}$	0.96	73.96	$6.99*10^{-4}$	0.99	72.94

Table 6 Kinetic parameters of the pseudo-first order and pseudo-second order models.

Based on the collected information, a remarkable difference in the R^2 values was obtained for the R^2 value, where it was higher when fitting with the pseudo second order. Furthermore, the experimental adsorption capacity values of the pseudo-second order kinetic model were closer to the calculated value of q_e for the three types of adsorbents, confirming that the process follows second order kinetics. Same results were obtained with Madan et al. and Pratiwi et al. [135], [141].

Comparing the values of q_e, it could be noticed that the highest adsorption was obtained when using Zn(Cur)O. This could be explained by the interaction between congo red and curcumin which is masked by chitosan polymer in Zn(Cur)O-Chitosan NPs, and not present at all in ZnO NPs.

4. *Optimization of the adsorption process*

The adsorption study was done at 2 initial stages: first of all, the dose of the adsorbent was optimized and secondly the concentration of congo red was varied. As a general overview, after 24 hours the solution color went from red to almost transparent, and

the congo red molecule adsorbed on the surface of the zinc curcumin oxide nanoparticles settled down, verifying by this the successful adsorption of congo red.

i.   Effect of adsorbent dosage

The adsorption process of Congo red organic dye was studied by varying the Zn(Cur)O NPs dosage from 0.05 to 0.9 mg. In fact, increasing the amount of the adsorbent will increase the number of available adsorption sites on its surface, thus leading to an increase in the adsorption capacity.

As illustrated in Figure 36, the increase in the adsorbent amount improves the adsorption of congo red and enhances the adsorption capacity q_e.
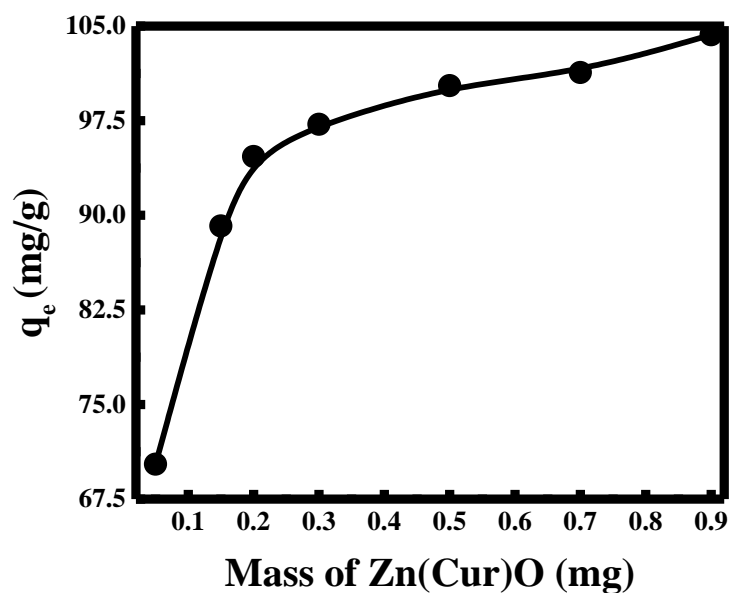
Figure 36 Adsorption capacity q_e for different dose of Zn(Cur)O NPs.

The adsorption capacity was found to be between 70.27 and 104.31 mg/g when varying the Zn(Cur)O NPs dose from 0.05 to 0.9 mg. Thus, the adsorbent dose and the adsorption capacity are directly proportional with a q_e equal to 104.31 mg/g when the dose used was 0.9 mg. This is due to the enhancement in the number of available sites for adsorption on the surface of Zn(Cur)O NPs.

ii.   Effect of dye concentration

The concentration of congo red was varied in order to determine its effect on the adsorption capacity. At a fixed adsorbent amount of 0.9 mg, the dye concentration was changed in a range of 5-100 μM. This was established to determine the maximum adsorption capacity of the synthesized nanoparticles. As shown in Figure 37, the adsorption capacity decreases with the increase of the dye concentration. The adsorption capacity q_e clearly decreases from 110.13 to 67.07 mg/g when the dye concentration increases from 5 to 100 μM.
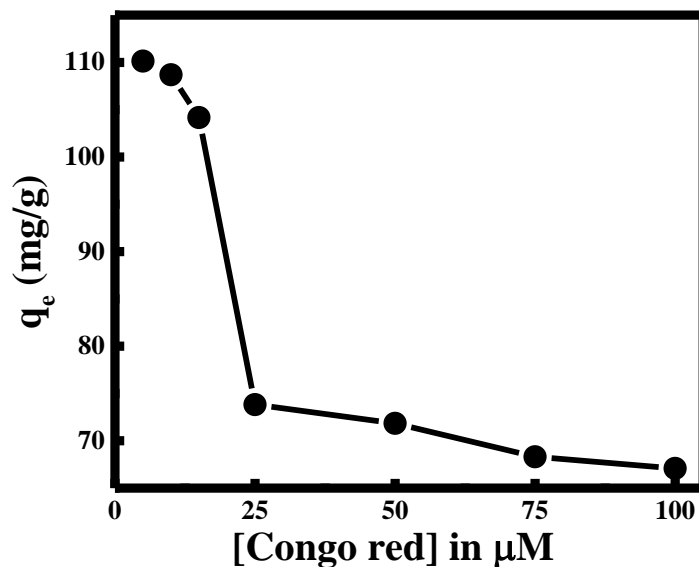
Figure 37 Adsorption capacity q_e for different concentrations of congo red.

This is due to the fact that at low concentration of congo red (below 25 µM), the dye molecules have the ability to get adsorbed easier onto the surface of Zn(Cur)O NPs, leading to higher adsorption capacity, until equilibrium is reached. It is also remarkable that at high concentration of the organic dye, the adsorption capacity is high enough, proving the efficiency of Zn(Cur)O NPs as adsorbent.

In other words, after adsorbing a particular amount of the organic dye, the adsorption sites on the surface of the adsorbent will become saturated. Accordingly, 5 µM of congo red is completely adsorbed onto the surface of the created nanoparticles, with a maximum adsorption capacity q_m of 110.13 mg/g.

5. Kinetic study

The study of adsorption kinetics of congo red dye onto the surface of Zn(Cur)O NPs was established at a congo red concentration of 15 μM and adsorbent dose of 0.9 mg.

The kinetic studies of the adsorption process for the pseudo-first and pseudo-second orders are shown in Figure 38A&B respectively.
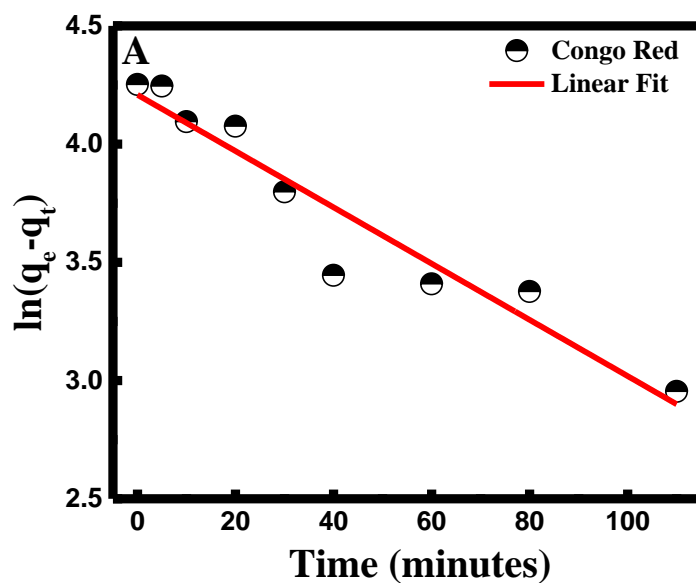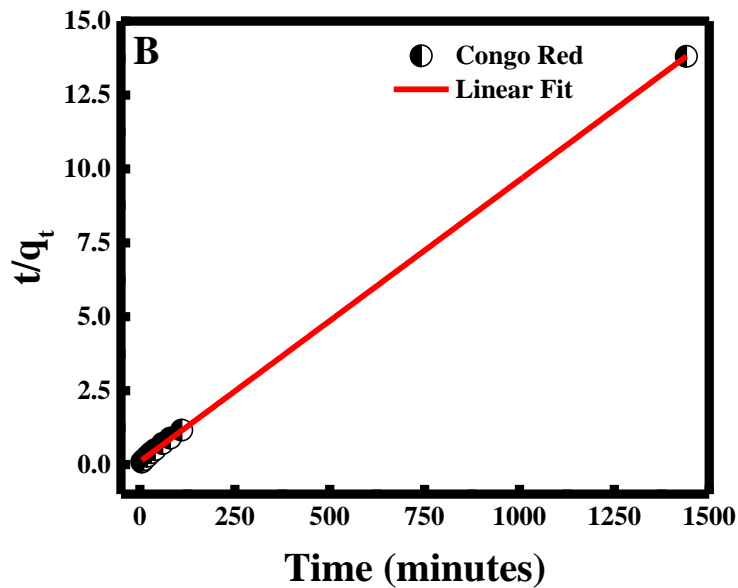
Figure 38 Congo red adsorption in (A) pseudo first order kinetic model and (B) pseudo second order kinetic model.

For the pseudo-first order kinetic model, a linear curve was obtained where the values of k_1 and q_e are calculated from the slope and the intercept, respectively. Likewise, for the pseudo-second order kinetic model, a linear curve was gotten where k_2 is calculated from the intercept and q_e from the slope (See Table 7). According to the computed data, a notable difference was remarked in the R^2 values for the two kinetic models, with the pseudo-second order having the greater value ($R^2=0.99993>R^2=0.91122$).

Besides, the adsorption capacity that was found experimentally (104.31 mg/g) was closer to the calculated adsorption capacity in the pseudo-second order kinetic model (104.91 mg/g), ensuring by that the pseudo-second order kinetics followed by the adsorption process. By pseudo-second order we mean that the adsorption is done by

chemisorption process including sharing of electrons between the dye sorbate and nanoparticles adsorbent. This was also proven by Zhu et al. and Madan et al. [135], [142].

Adsorbent	Pseudo-first order			Pseudo-second order			q_e (calc) (mg/g)
	q_e (exp) (mg/g)	k1 (min^{-1})	R^2	q_e (exp) (mg/g)	k2 (g.mg^{-1}. min^{-1})	R^2	
Zn(Cur)O NPs	67.25	$1.19*10^{-2}$	0.91122	104.31	$9.10*10^{-4}$	0.99993	104.91

Table 7 Fitting results for pseudo first and pseudo second order kinetics analysis.

6. *Adsorption isotherms study*

The adsorption capacity is demonstrated in the isothermal study for several congo red organic dye concentrations at a fixed dosage of Zn(Cur)O NPs adsorbent equal to 0.9 mg. Freundlich and Langmuir models are the two most commonly used isotherms.

Freundlich isotherm proposes that the adsorption happens in a multi-layer manner. Meaning that the adsorbent has unlimited number of adsorption sites on its surface with dissimilar energies, and the mechanism is heterogeneous. It is represented by the following equation:

$$\ln(q_e) = \ln(K_f) + \frac{1}{n}\ln(C_f) \quad (4)$$

where K_f is the Freundlich constant that signifies the adsorption capacity (amount of dye adsorbed), $\frac{1}{n}$ is also a Freundlich constant that represents the intensity of adsorption. It is

plotted linearly, $\ln(q_e)$ vs. $\ln(C_f)$, as presented in Figure 39A. K_f and $\frac{1}{n}$ can be calculated from the intercept and slope, respectively.
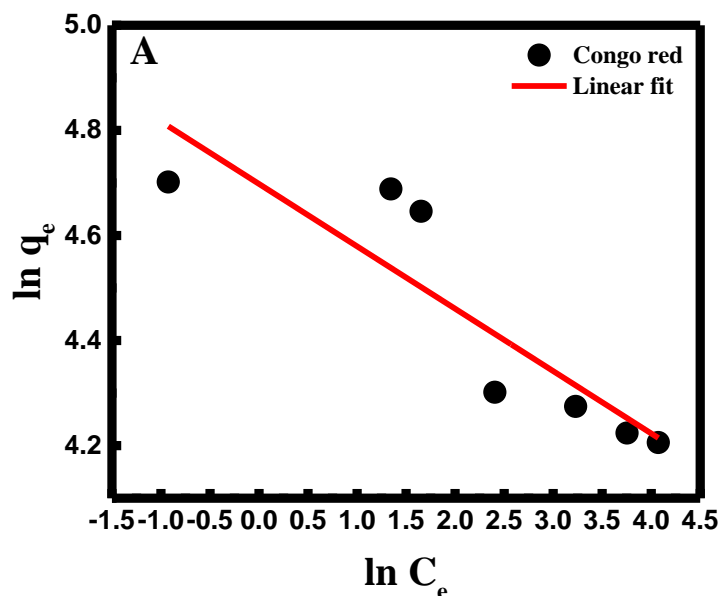
Figure 39A The Freundlich isotherm model.

As for Langmuir isotherm, the surface of the adsorbent contains limited adsorption sites with equal energies, where only one dye could be adsorbed on each site. Monolayer adsorption is carried out with a homogenous mechanism. It is illustrated using the following equation:

$$\frac{C_e}{q_e} = \frac{1}{q_m} K_L + \frac{C_e}{q_m} \quad (5)$$

where q_m is the maximum adsorption capacity (mg/g) and K_L is the Langmuir constant that corresponds to the energy of adsorption. They could be obtained from slope and the intercept respectively when $\frac{C_e}{q_e}$ is plotted against C_e (See Figure 39B).
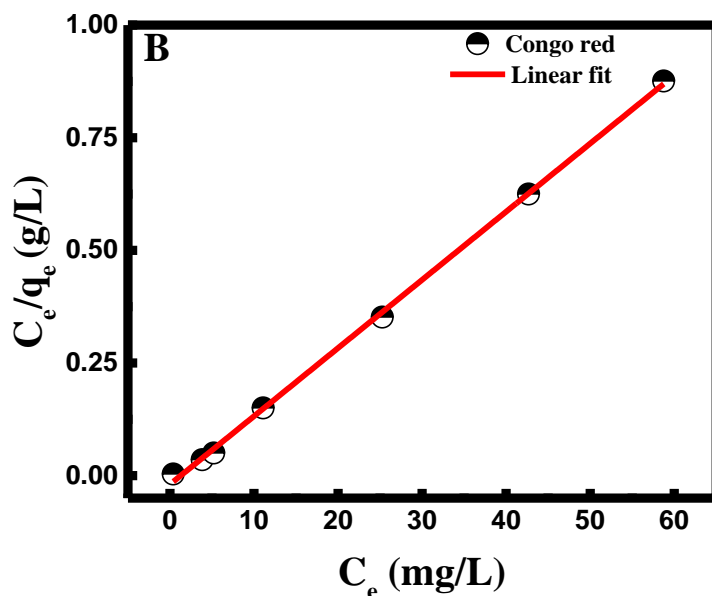
Figure 39B The Langmuir isotherm model.

According to the results obtained, it could be confirmed that congo red adsorption on Zn(Cur)O NPs follows the Langmuir isotherm. It has a much higher R^2 value than that of the Freundlich isotherm (0.99901>0.74025), approving by that the monolayer adsorption onto a homogenous surface (See Table 8).

Adsorbent	Langmuir isotherm			Freundlich isotherm		
	q_m (mg/g)	K_L	R^2	$\dfrac{1}{n}$	K_f	R^2
Zn(Cur)O NPs	66.09	-1.29	0.99901	-0.1187	109.73	0.74025

Table 8 Isotherm study for congo red organic dye.

The obtained results were similar to the ones acquired by Madan et al. [135] verifying the efficacy of Zn(Cur)O NPs as adsorbent for congo red dye.

D. Conclusion

Zinc curcumin oxide nanoparticles were proven to have high efficiency in the adsorption process compared to ZnO NPs alone. In addition, a satisfied adsorption capacity of congo red onto their surface at high concentration was observed. The adsorption capacity increases with increasing the adsorbent dose with a q_e value equal to 110.31 mg/g. In contrary, q_e decreases with increasing the organic dye concentration but remains relatively high (q_e=67.07 mg/g). In addition, the best kinetic model was the pseudo-second order, meaning chemisorption is taking place. Finally, isothermal study was performed to point out that the experimental data fits the Langmuir isotherm.

CHAPTER VII

EFFECT OF PH ON THE REMOVAL OF ANIONIC AND CATIONIC DYES USING ZINC CURCUMIN OXIDE AS ADSORBENT

A. Introduction

Nowadays, organic dyes have gained much importance due to their usage in different types of industries such as leather, plastic, textile, paints, cosmetics, paper, and food production [143], [144]. These dyes are significantly present in wastewater and can cause a danger to human beings [143]. They are considered as pollutants that can bring out a risk to the environment. By breakdown and decomposition, they are prone to form carcinogenic and mutagenic compounds due to their high toxicity [144]. Numerous techniques have been applied until now, such as photo-catalysis, advanced oxidation, coagulation, membrane filtration; flocculation-solidification, electrochemical practices, and adsorption. Among them all, adsorption is the most suitable one in terms of cost, simplicity, ecofriendliness, and efficiency [143], [145].

Congo red (CR) is one of the anionic dyes with a pka equal to 4.5. When it breaks down, it develops carcinogenic properties and mutagenic activities in aquatic ecosystems [136]. Methyl orange (MO) is a different anionic azo dye. It is also carcinogenic, toxic and mutagenic, and it lasts for a long time in the environment [146].

Moving on to another type of dyes, the cationic organic dyes, methylene blue (MB) is highly important because it can initiate vomiting, diarrhea, nausea, and breathing difficulties. It blocks the passage of solar radiations into water affecting by that the amount of oxygen necessary for the aquatic life [147]. Rhodamine 6G (Rh6G) is one more toxic cationic organic dye that has bad consequences related to the eyes and respiratory system. If rhodamine 6G contaminated water is drunk, it can provoke skin irradiation as well as cancer [148]. Likewise, rhodamine B (RhB) is a basic cationic dye utilized as a water tracer fluorescent molecule. It can cause irritation of skin and eyes as well as respiratory problems [149].

Further, the pH of the medium affects significantly the adsorption process due to the fact that the surface charge of the adsorbent will vary with the pH. Because of this variation, the interaction between the adsorbent and the organic dyes will also vary depending on the nature of the dye being anionic or cationic.

Therefore, developing an efficient complex for the adsorption process was taken into consideration.

In this study, zinc oxide nanoparticles (ZnO NPs) were selected because of their varied biomedical applications. Curcumin was used as a conjugated agent with zinc oxide nanoparticles to form a complex in order to obtain zinc curcumin oxide nanoparticles (Zn(Cur)O NPs) that will be used as adsorbent with a large and efficient surface area for the adsorption process of organic dyes. The pH of the solution will be varied to study its effect on the adsorption of different dyes onto the surface of the adsorbent nanoparticles.

112

B. Methods of preparation

Organic dyes solutions (C=1 mM) were prepared as follows:

Different amounts of 3.48 mg congo red, 1.64 mg methyl orange, 1.6 mg methylene blue, 2.36 mg rhodamine 6G, and 2.4 mg rhodamine B were dissolved each in 5 mL double distilled water.

For each adsorption experiment, 1 mL of double distilled water was heated and 1 mg of Zn(Cur)O NPs was dissolved in it using a sonicator to guarantee a complete dissociation of Zn(Cur)O NPs.

The organic dyes concentrations and the adsorbent dose were fixed to be 50 µM (150 µL) and 900 mg/L (900 µL) respectively (See Figure 40).
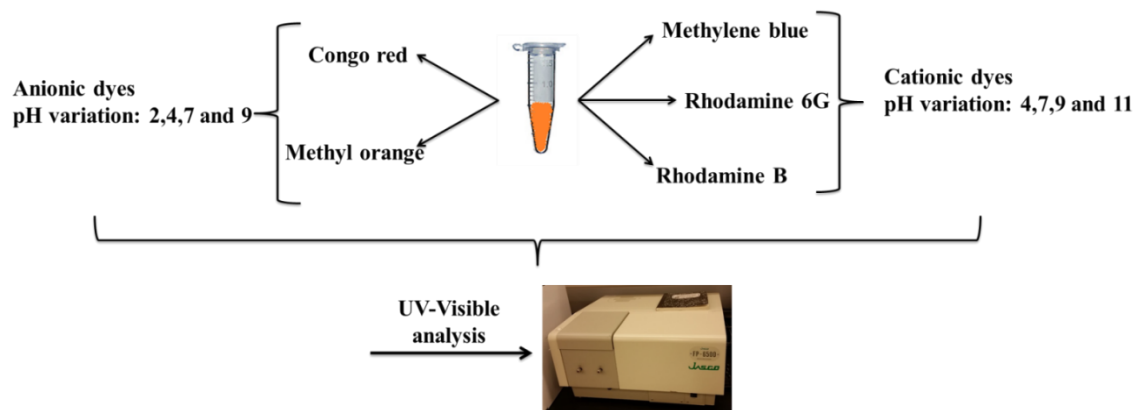
Figure 40 Scheme illustrating the different dues used for the adsorption experiment.

The solutions of different pH were prepared using 0.1 M NaOH and 0.1 M HCl solutions. For each dye, the experiments were performed at four different pH. For the

anionic dyes, pH=2, 4, 7, and 9 were considered. As for the cationic dyes, the adsorption study was done at pH=4, 7, 9, and 11.

C. Results and discussion

1. Effect of pH on the adsorption

The pH of the solution is an important parameter that affects the whole adsorption process. It can modify the surface charge of the adsorbent. By doing that, the interactions between the organic dye and the adsorbent nanoparticles will vary between attraction and repulsion. Consequently, the adsorption capacity will decrease or increase with increasing the pH, depending on the nature of the organic dye, being anionic or cationic, and its interaction with Zn(Cur)O NPs.

a. Anionic dyes

i. Congo red

Anionic congo red is a di-azo organic dye, containing two N=N groups, having a molecular weight of 696.68 g/mol and a chemical formula of $C_{32}H_{22}N_6Na_2O_6S_2$. The two UV-Visible peaks obtained at 344 nm and 497 nm correspond to the naphthalene ring and azo groups respectively [150].

The structure of congo red is characterized by the presence of two sulfonate functional groups $R\text{-}SO_3^-$. At highly acidic pH (pH=2), the color of the solution turns from dark red into dark blue. In addition, the surface charge of Zn(Cur)O NPs becomes positively charged. Therefore, the negatively charged sulfonate group of congo red could be

complexed with the positively charged adsorbent molecule by the zinc due to the high electrostatic attraction forces between them. This will make the adsorption capacity high. It will decrease with increasing the pH because of the repulsive interactions between the negative sulfonate groups and the negatively charged nanoparticles at high basic pH.

This was proven in Figure 41 where the adsorption capacity decreases with the increasing of the pH from q_e=94.54 mg/g at pH=2 to q_e=70.86 mg/g at pH=9. This was verified by zeta potential were the values were equal to -84.8 mV and 23.6 mV congo red and the Zn(Cur)O NPs respectively.

Figure 41 Adsorption capacity of zinc curcumin oxide nanoparticles for congo red removal at different pH.

ii.   Methyl orange

Another anionic organic dye is methyl orange. Its chemical formula is $C_{14}H_{14}N_3NaO_3S$ and molecular weight 327.33 g/mol. It is a part of the azo dyes family due

to the presence of an azo group N=N in its chemical structure. Since it is an anionic dye also, it should be expected to behave like congo red organic dye at acidic and basic pH. From the structure of MO, there is a sulfonate group $R\text{-}SO_3^-$ in addition to an amine group $R\text{-}N(CH_3)_2$. Logically, the negatively charged sulfonate should be attracted to the positively charged Zn(Cur)O NPs at acidic pH, and this attraction should decrease gradually at higher pH, leading to a decrease in the adsorption capacity.

Surprisingly, this was not determined experimentally in that case. As we can notice in Figure 42A, the adsorption capacity interestingly increases with the pH from 16.41 mg/g at pH=2 to 44.38 mg/g at pH=9.
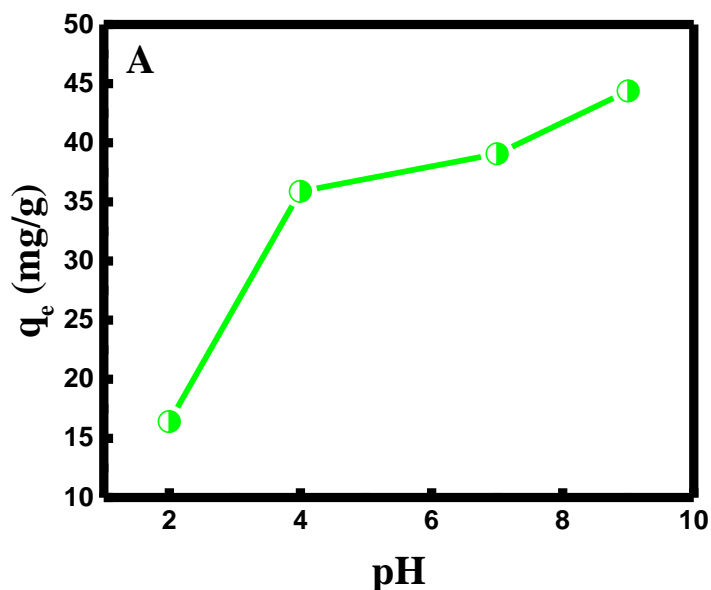
Figure 42A Adsorption capacity of zinc curcumin oxide nanoparticles for methyl orange removal at different pH.

This difference is due to the presence of the amine group having a lone pair on the nitrogen atom that is able to be delocalized at basic pH on two N atoms as shown in the in

Figure 42B, hence increasing the probability of binding between the lone pair on the two

nitrogen atoms and the zinc of the nanoparticles adsorbent.

B
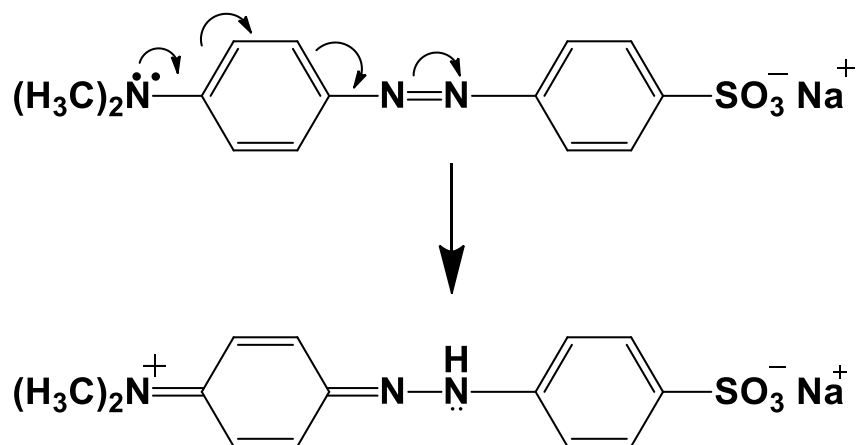
Figure 42B Aspects of methyl orange in basic media.

Further, Na^+ is present in methyl orange. In acidic medium, it competes with H^+

ions and the positively charged surface of the adsorbent, leading to a decrease in the

adsorption capacity [151].

b. Cationic dyes

    i. Methylene blue

Moving on to the cationic organic dyes, methylene blue having a chemical formula

of $C_{16}H_{18}CIN_3S$, its molecular weight is 319.86 g/mol. It absorbs at $\lambda_{max}=664$ nm. Since

methylene blue is a cationic dye, it is predictable that the adsorption capacity should

increase with increasing the pH. The results obtained prove the presence of higher

interactions between the positively charged dye and the negatively charged adsorbent at

basic pH. This was also confirmed from the zeta analysis where MB possesses a positively surface charge equal to +30.23 mV and Zn(Cur)O NPs is negatively charged with zeta value equal to -19.70 mV.

The adsorption capacity q_e improved from 18.02 to 34.71 mg/g when the pH changed from 4 to 11 as depicted in Figure 43. This is explained by the fact that the attraction forces increases between the two opposing charges of the dye and the adsorbent, enhancing by that the adsorption.
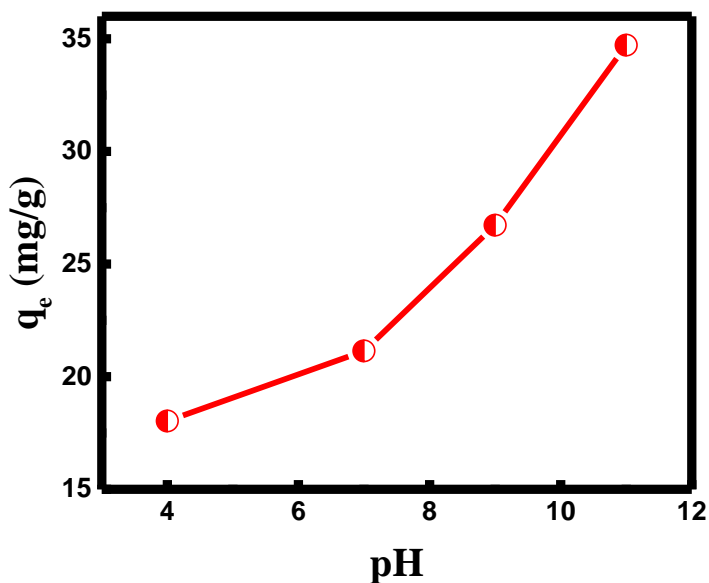
Figure 43 Adsorption capacity of zinc curcumin oxide nanoparticles for methylene blue removal at different pH.

In fact, another factor should also be taken into consideration, which is the presence of the π-π interactions between the nanoparticles and the aromatic ring of the organic dye. At acidic pH, there is less adsorption only due to the π-π interactions with the

118

absence of the attraction and the presence of repulsion between two positively charged species [152].

ii.   Rhodamine 6G

Furthermore, rhodamine 6G is also a cationic dye. It is called also "rhodamine 590" and has a chemical formula of $C_{28}H_{31}N_2O_3Cl$ with a molecular weight of 479.02 g/mol. The maximum absorption peak is located at a maximum wavelength of around 530 nm [153]. The adsorption capacity increased from 23.99 mg/g to 38.184 mg/g when the pH varied from 4 to 11 (Figure 44).
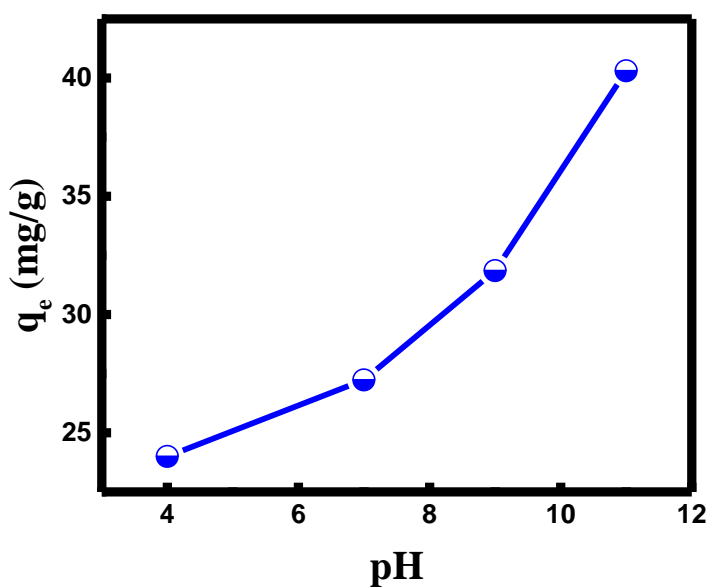
Figure 44 Adsorption capacity of zinc curcumin oxide nanoparticles for rhodamine 6G removal at different pH.

This is true due to the fact that the electrostatic attractions increased between the negative surface charge of zinc curcumin oxide nanoparticles and the cationic dye, allowing more adsorption onto the surface of the adsorbent. Similarly, Rh6G have given a positive

surface charge with zeta value equal to +25.87, inducing electrostatic interaction with the negatively charged Zn(Cur)O NPs (-19.70 mV).

iii. Rhodamine B

The chemical formula of Rhodamine B is $C_{28}H_{31}CIN_2O_3$. Its molecular weight is 479.02 g/mol. The absorbance peak is attained at λ_{max} around 543 nm [154]. Being as well cationic, it is expected to achieve higher adsorption at basic pH. This was demonstrated experimentally where the adsorption capacity q_e increased from 22.4 mg/g at pH=4 to 28.34 mg/g at pH=11 (Figure 45). This is not a very noticeable difference in the adsorption capacity between acidic and basic pH media compared to the previous organic dyes but it could be considered fine.
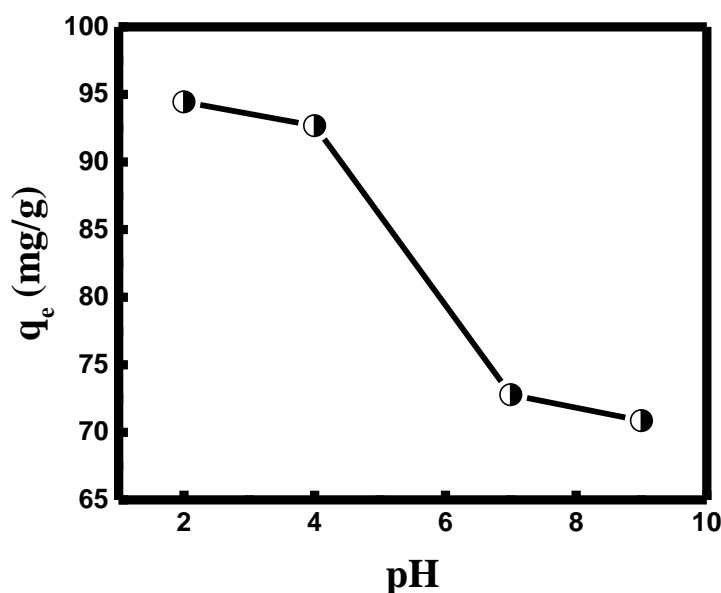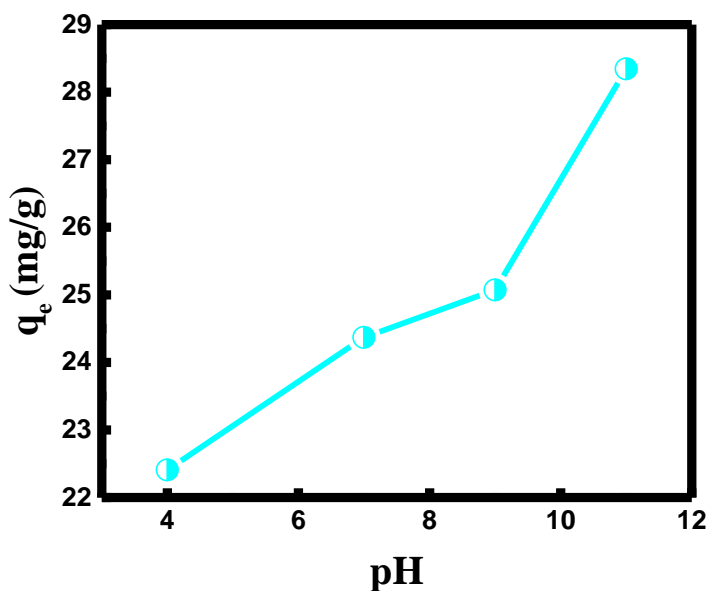
Figure 45 Adsorption capacity of zinc curcumin oxide nanoparticles for rhodamine B removal at different pH.

Same as the other cationic organic dyes, the adsorption increases because of the attractive interactions between the negative surface charge of the adsorbent (-19.70 mV) and the positive organic dye rhodamine B (+10.28 mV).

2. *Kinetic studies*

Kinetic studies of the adsorption of the different organic dyes onto the surface of zinc curcumin oxide nanoparticles were conducted. The results were plotted using the pseudo-first order and pseudo-second order kinetic model equations at a constant dye concentration of 50 μM and nanoparticles adsorbent amount of 0.9 mg.

The plots of the pseudo-first and pseudo-second kinetic models that are used to study the adsorption process of the various dyes are demonstrated in Figure 46A&B.
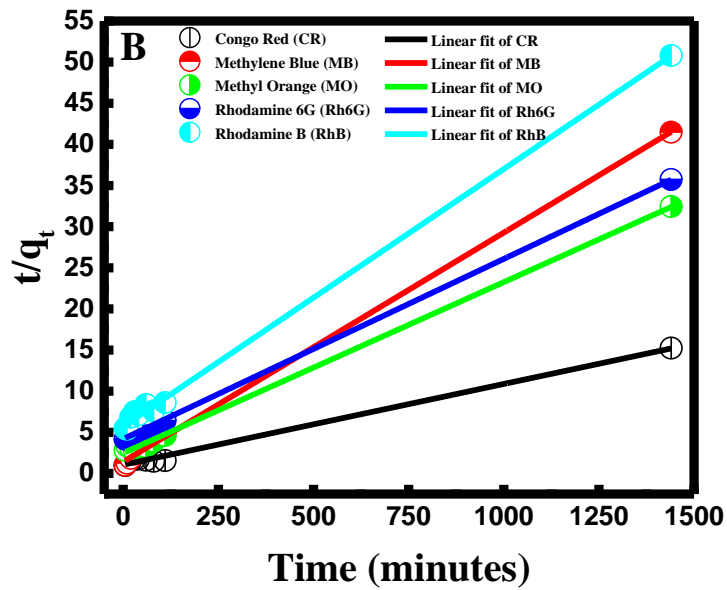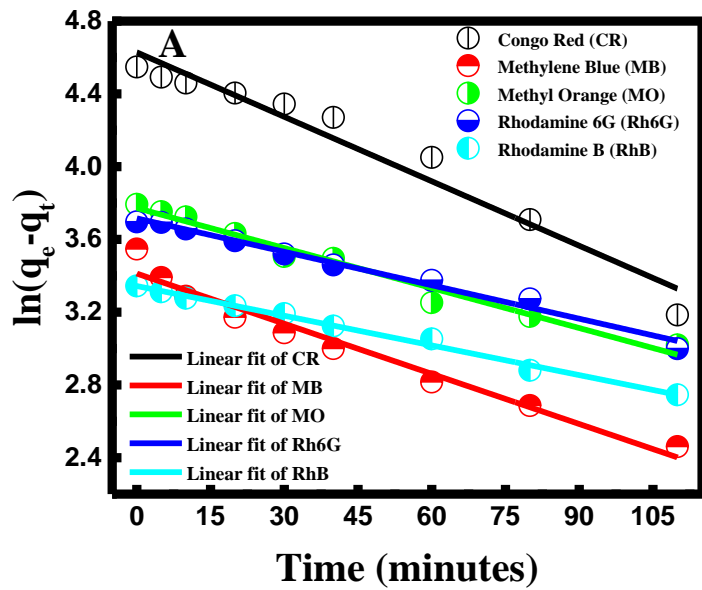
Figure 46 Kinetics study (A) pseudo-first order and (B) pseudo-second order models.

For the pseudo-first order, the values of the rate constant k_1 and the adsorption capacity at equilibrium q_e are calculated from the slope and the intercept, respectively (See Table 9).

Organic Dye	Pseudo-first order			
	q_e (exp) (mg/g)	k_1 (min^{-1})	R^2	q_e (calc) (mg/g)
Congo Red	102.33	$1.18*10^{-2}$	0.9495	94.44
Methyl Orange	43.49	$7.33*10^{-3}$	0.9752	44.38
Methylene Blue	30.33	$9.19*10^{-3}$	0.9660	34.72
Rhodamine 6G	37.18	$6.13*10^{-3}$	0.9851	40.30
Rhodamine B	25.63	$5.44*10^{-3}$	0.9890	28.34

Table 9 Pseudo first order kinetics and the relative k_1 and adsorption capacity value.

Similarly, for the pseudo-second order, the rate constant k_2 is calculated from the intercept while the adsorption capacity at equilibrium q_e is calculated from the slope (See Table 10).

Organic Dye	Pseudo-second order			
	q_e (exp) (mg/g)	k_2 (g.mg^{-1}. min^{-1})	R^2	q_e (calc) (mg/g)
Congo Red	94.52	$1.05237*10^{-4}$	0.99517	94.44
Methyl Orange	44.66	$2.02129*10^{-4}$	0.99863	44.38
Methylene Blue	35.89	$5.47555*10^{-4}$	0.99928	34.72
Rhodamine 6G	40.82	$1.43262*10^{-4}$	0.99986	40.30
Rhodamine B	28.58	$2.13981*10^{-4}$	0.99832	28.34

Table 10 Pseudo second order kinetics and the relative k_2 and adsorption capacity value.

According to the obtained data, a remarkable difference was observed in the R^2 values of the two kinetic models of all the dyes, with the pseudo-second order having the greater values. This was also proven by Zhu et al. and Madan et al. [135], [142].

Moreover, the experimental adsorption capacity values of the different organic dyes were approximately similar to the calculated adsorption capacity values in the pseudo-second order kinetic model with higher value of R^2, proving that the adsorption process of these dyes follows a pseudo-second order kinetic model. This means that the adsorption is done by chemisorption that requires the share of electrons between the zinc curcumin oxide nanoparticles adsorbent and the organic dyes. The efficiency of zinc curcumin oxide nanoparticles compared to different type of adsorbent is summarized in Table 11.

Organic dye	Type and amount of adsorbent	Concentration of the dye (mg/mL)	q_e (mg/g)	References
Congo red	10 g/L of Pinus Pinaster Bark	5	0.47	[155]
	0.015 g of $Fe_{2.95}La_{0.05}O_4$	100	79.11	[156]
	0.9 mg of Zn(cur)O NPs	16	94.54	Our work
Methyl orange	50 mg of the β-CD/Fe_3O_4@PVP microspheres	13	47.62	[157]
	2g of chitosan/diatomite complex	50	35.12	[158]
	0.9 mg of Zn(cur)O NPs	16	44.38	Our work
Methylene blue	0.1 g of carbonized peanut shell	2.5	5.34	[159]
	0.2 g/L of biochar	50	20	[160]
	0.9 mg of Zn(cur)O NPs	16	34.71	Our work
Rhodamine 6G	10 mg/L of Fe_3O_4	6	150	[161]
	1g/L of activated carbon	50	44.7	[162]
	0.9 mg of Zn(cur)O NPs	16	38.184	Our work
Rhodamine B	50 mg of **seeds of** *Aleurites Moluccana*	50	101	[163]
	0.9 mg of Zn(cur)O NPs	16	28.34	Our work

Table 11 Different adsorbent use for the removal of the organic dyes.

It is obvious that in the majority of the adsorption experiments, a minimum dose of 10 mg of the adsorbent is needed. Fortunately, only 0.9 mg of Zn(Cur)O NPs were efficient to enhance the adsorption capacity of the dyes.

D. Conclusion

In conclusion, zinc curcumin oxide nanoparticles were used as adsorbent for the removal of organic dyes. Anionic dyes like congo red and methyl orange, in addition to cationic dyes such as methylene blue, rhodamine 6G and rhodamine B, were found to exhibit a successful adsorption process onto the surface of Zn(Cur)O NPs when using only 0.9 mg. The pH of the medium affected primarily the results due to the change in the surface charge of the nanoparticles based on the acidity and basicity. Consequently, the interactions between the organic dyes and the adsorbent were varied accordingly. Congo red was the only dye that has the highest adsorption capacity at an acidic pH, while the other dyes were better adsorbed in a basic medium. Finally, the adsorption process of all the dyes was found to follow a pseudo-second order kinetic model.

CHAPTER VIII

CONCLUSION

In brief, curcumin was complexed to zinc oxide nanoparticles via a simple green synthesis by adding KOH drop by drop using a burette, under basic conditions of pH=13 at 80℃, to generate Zn(Cur)O NPs. In basic media, curcumin reacts completely and helps in the generation of Zn(Cur)O NPs. The surface of these obtained nanoparticles was coated with chitosan polymer layer in order to increase their stability. The importance of chitosan was remarkable through TGA analysis where the mass loss was less than 10%.

The importance of Zn(Cur)O-Chi NPs in biomedical application was in the first place verified by testing them as anti-cancer reagent. A great anticancer activity was observed due to the inhibition of MCF-7 and Capan-1 cancer cells proliferation. It was found that 2 μg/mL of Zn(Cur)O-Chi NPs were sufficient to inhibit the proliferation of 90% and 95% of the MCF-7 and Capan-1 cancerous cells.

Staying in the biomedical field, Zn(Cur)O-Chi NPs were used as nanoprobe to detect ascorbic acid. The detection of AA was done based on the fluorescence emission technique, which was found easy to handle, feasible and with low cost. The proposed nanoparticles have shown a linear relationship in the range of 0-19 mM. The detection of AA molecule was completed based on the interaction of the amino group of chitosan with the hydroxyl group of ascorbic acid. The selectivity of the nanoparticles was also investigated towards ZnO NPs and Zn(Cur)O NPs nanoprobe. It was found that the presence of chitosan boost the interaction between AA and the nanoparticles. In addition,

the proposed NPs were selective towards the analytes that could interfere with ascorbic acid. The percent recovery was between 94 and 100% and the limit of detection (LOD) was 36 μM.

Zinc curcumin oxide could also be applied in the environmental field. For this reason, the efficiency of Zn(Cur)O NPs as adsorbent for the removal of organic dye was established. In the first place, the adsorption process of congo red using Zn(Cur)O NPs was optimized by varying the stirring effect, the adsorbent type, adsorbent dose, and dye concentration. Hence, it was found that the stirring inhibits the deposition of congo red on the surface of Zn(Cur)O NPs. So on, the presence of chitosan decreases also the adsorption capacity of the nanoparticles. Moreover, the adsorption capacity q_e of congo red rises with increasing the dosage of adsorbent with a q_e of 110.31 mg/g. In contrary, q_e declines with increasing the concentration of congo red organic dye but remains reasonable with q_e=67.07 mg/g. The data were found to fit the pseudo-second order and Langmuir model.

After confirming the effectiveness of Zn(Cur)O NPs as adsorbent, several organic dye were investigated. Since organic dyes are present in the form of anionic and cationic dyes, the pH of the adsorption experiments was modified accordingly. It was found that for congo red (anionic dye), the highest adsorption capacity (94.54 mg/g) was obtained in acidic media. The adsorption of methyl orange (anionic dye) was also preceded. It was remarkable that the highest adsorption capacity was obtained in basic media (44.38 mg/g). These results are in contradiction with the results obtained for congo red. This difference is due to the presence of the amine group having a lone pair on the nitrogen atom that has the ability to be delocalized at basic pH on two N atoms. Furthermore, 3 cationic dyes have

undergone the adsorption process; methylene blue, rhodamine 6G and rhodamine B. Interestingly, a boost in the adsorption capacity was obtained in basic media due to the electrostatic interaction between the positively charged dye and the negatively charged adsorbent. The adsorption capacity was equal to 34.71, 38.184, and 28.34 for MB, Rh6G and RhB respectively. The difference in the adsorption capacity is due to the difference in the zeta potential value of the dye surface, where MB owns the high surface charge +30.23 mV.

In summary, zinc curcumin oxide in the presence and absence of chitosan; has shown a great interest in the biomedical and environmental domain.

REFERENCES

[1]   M. A. Willard, L. K. Kurihara, E. E. Carpenter, S. Calvin, and V. G. Harris, "Chemically prepared magnetic nanoparticles," *Int. Mater. Rev.*, vol. 49, no. 3–4, pp. 125–170, 2004, doi: 10.1179/095066004225021882.

[2]   M. Ates, J. Daniels, Z. Arslan, and I. O. Farah, "Effects of aqueous suspensions of titanium dioxide nanoparticles on Artemia salina: Assessment of nanoparticle aggregation, accumulation, and toxicity," *Environ. Monit. Assess.*, vol. 185, no. 4, pp. 3339–3348, 2013, doi: 10.1007/s10661-012-2794-7.

[3]   S. F. Larner, J. Wang, J. Goodman, M. B. O'Donoghue Altman, M. Xin, and K. K. W. Wang, "In vitro neurotoxicity resulting from exposure of cultured neural cells to several types of nanoparticles," *J. Cell Death*, vol. 10, no. 11, pp. 1–7, 2017, doi: 10.1177/1179670717694523.

[4]   M. U. Khalid, S. R. Khan, and S. Jamil, "Morphologically Controlled Synthesis of Cubes like Tin Oxide Nanoparticles and Study of its Application as Photocatalyst for Congo Red Degradation and as Fuel Additive," *J. Inorg. Organomet. Polym. Mater.*, vol. 28, no. 1, pp. 168–176, 2018, doi: 10.1007/s10904-017-0687-5.

[5]   S. Sabir, M. Arshad, and S. K. Chaudhari, "Zinc oxide nanoparticles for revolutionizing agriculture: Synthesis and applications," *Sci. World J.*, vol. 2014, pp. 1–8, 2014, doi: 10.1155/2014/925494.

[6]   K. A. Razak, N. M. Nor, and N. S. Ridhuan, "Metal Oxide Nanostructure-modified Electrode for Glucose Biosensor," *Adv. Mater. their Appl. Micro to nano scale*, pp. 31–68, 2017.

[7]   P. J. P. Espitia, N. de F. F. Soares, J. S. dos R. Coimbra, N. J. de Andrade, R. S. Cruz, and E. A. A. Medeiros, "Zinc Oxide Nanoparticles: Synthesis, Antimicrobial Activity and Food Packaging Applications," *Food Bioprocess Technol.*, vol. 5, no. 5, pp. 1447–1464, 2012, doi: 10.1007/s11947-012-0797-6.

[8]   S. Chaudhary, A. Umar, K. K. Bhasin, and S. Baskoutas, "Chemical sensing

applications of ZnO nanomaterials," *Materials (Basel).*, vol. 11, no. 2, pp. 1–38, 2018, doi: 10.3390/ma11020287.

[9]   J. Duraimurugan, G. S. Kumar, P. Maadeswaran, S. Shanavas, P. M. Anbarasan, and V. Vasudevan, "Structural, optical and photocatlytic properties of zinc oxide nanoparticles obtained by simple plant extract mediated synthesis," *J. Mater. Sci. Mater. Electron.*, vol. 30, no. 2, pp. 1927–1935, 2019, doi: 10.1007/s10854-018-0466-2.

[10]   H. Mittal, P. P. Morajkar, A. Al Alili, and S. M. Alhassan, "In-Situ Synthesis of ZnO Nanoparticles using Gum Arabic Based Hydrogels as a Self-template for Effective Malachite Green Dye Adsorption," *J. Polym. Environ.*, vol. 28, no. 6, pp. 1637–1653, 2020, doi: 10.1007/s10924-020-01713-y.

[11]   M. N. Zafar, Q. Dar, F. Nawaz, M. N. Zafar, M. Iqbal, and M. F. Nazar, "Effective adsorptive removal of azo dyes over spherical ZnO nanoparticles," *J. Mater. Res. Technol.*, vol. 8, no. 1, pp. 713–725, 2019, doi: 10.1016/j.jmrt.2018.06.002.

[12]   G. Yuvaraja, C. Prasad, Y. Vijaya, and M. V. Subbaiah, "Application of ZnO nanorods as an adsorbent material for the removal of As(III) from aqueous solution: kinetics, isotherms and thermodynamic studies," *Int. J. Ind. Chem.*, vol. 9, no. 1, pp. 17–25, 2018, doi: 10.1007/s40090-018-0136-5.

[13]   K. Nalwa, "Synthesis of ZnO nanoparticles and its application in adsorption," *Adv. Mater. Proc.*, vol. 2, no. 11, pp. 697–703, 2017, doi: 10.5185/amp/2017/696.

[14]   I. Ghiloufi, J. El Ghoul, A. Modwi, and L. El Mir, "Ga-doped ZnO for adsorption of heavy metals from aqueous solution," *Mater. Sci. Semicond. Process.*, vol. 42, pp. 102–106, 2016, doi: 10.1016/j.mssp.2015.08.047.

[15]   D. Medina Cruz *et al.*, "Green nanotechnology-based zinc oxide (ZnO) nanomaterials for biomedical applications: a review," *J. Phys. Mater.*, vol. 3, no. 3, pp. 1–25, 2020, doi: 10.1088/2515-7639/ab8186.

[16]   T. Dayakar., K. Venkateswara Rao., K. Bikshalu., V. Rajendar., and S. H. Park, "Novel synthesis and structural analysis of zinc oxide nanoparticles for the non enzymatic glucose biosensor," *Mater. Sci. Eng. C*, vol. 75, pp. 1472–1479, 2017,

doi: 10.1016/j.msec.2017.02.032.

[17] Y. Zheng, Z. Wang, F. Peng, and L. Fu, "Application of biosynthesized ZnO nanoparticles on an electrochemical H2O2 biosensor," *Brazilian J. Pharm. Sci.*, vol. 52, no. 4, pp. 781–786, 2016, doi: 10.3724/sp.j.1096.2012.20015.

[18] D. Sharma, M. I. Sabela, S. Kanchi, K. Bisetty, A. A. Skelton, and B. Honarparvar, "Green synthesis, characterization and electrochemical sensing of silymarin by ZnO nanoparticles: Experimental and DFT studies," *J. Electroanal. Chem.*, vol. 808, pp. 160–172, 2018, doi: 10.1016/j.jelechem.2017.11.039.

[19] P. J. Cao *et al.*, "Down to ppb level NO2 detection by ZnO/rGO heterojunction based chemiresistive sensors," *Chem. Eng. J.*, vol. 401, p. 125491, 2020, doi: 10.1016/j.cej.2020.125491.

[20] M. J. Akhtar, M. Ahamed, S. Kumar, M. A. Majeed Khan, J. Ahmad, and S. A. Alrokayan, "Zinc oxide nanoparticles selectively induce apoptosis in human cancer cells through reactive oxygen species," *Int. J. Nanomedicine*, vol. 7, pp. 845–857, 2012, doi: 10.2147/IJN.S29129.

[21] A. Becheri, M. Dürr, P. Lo Nostro, and P. Baglioni, "Synthesis and characterization of zinc oxide nanoparticles: Application to textiles as UV-absorbers," *J. Nanoparticle Res.*, vol. 10, no. 4, pp. 679–689, 2008, doi: 10.1007/s11051-007-9318-3.

[22] M. Ul-Islam, W. A. Khattak, M. W. Ullah, S. Khan, and J. K. Park, "Synthesis of regenerated bacterial cellulose-zinc oxide nanocomposite films for biomedical applications," *Cellulose*, vol. 21, no. 1, pp. 433–447, 2014, doi: 10.1007/s10570-013-0109-y.

[23] O. A. Shalygina, I. V. Nazarov, A. V. Baranov, and V. Y. Timoshenko, "Structure and photoluminescence properties of zinc oxide/ytterbium oxide nanocomposites," *J. Sol-Gel Sci. Technol.*, vol. 81, no. 2, pp. 333–337, 2017, doi: 10.1007/s10971-016-4258-y.

[24] R. A. Zargar, M. Arora, and R. A. Bhat, "Study of nanosized copper-doped ZnO dilute magnetic semiconductor thick films for spintronic device applications," *Appl.*

Phys. A Mater. Sci. Process., vol. 124, no. 1, pp. 1–9, 2018, doi: 10.1007/s00339-017-1457-5.

[25] J. Wang *et al.*, "High-efficiency polymer solar cells employing solution-processible and thickness-independent gallium-doped zinc oxide nanoparticles as cathode buffer layers†," *J. Mater. Chem. C*, vol. 4, no. 46, pp. 10820–10826, 2016, doi: 10.1039/c6tc04366f.

[26] R. C. De Souza, L. U. Haberbeck, H. G. Riella, D. H. B. Ribeiro, and B. A. M. Carciofi, "Antibacterial activity of zinc oxide nanoparticles synthesized by solochemical process," *Brazilian J. Chem. Eng.*, vol. 36, no. 2, pp. 885–893, 2019, doi: 10.1590/0104-6632.20190362s20180027.

[27] P. Sivakumar, M. Lee, Y. S. Kim, and M. S. Shim, "Photo-triggered antibacterial and anticancer activities of zinc oxide nanoparticles," *J. Mater. Chem. B*, vol. 6, no. 30, pp. 4852–4871, 2018, doi: 10.1039/c8tb00948a.

[28] S. Dhobale *et al.*, "Zinc oxide nanoparticles as novel alpha-amylase inhibitors," *J. Appl. Phys.*, vol. 104, no. 9, pp. 1–5, 2008, doi: 10.1063/1.3009317.

[29] S. H. Soytaş, O. Oğuz, and Y. Z. Menceloğlu, *Polymer Nanocomposites With Decorated Metal Oxides*. 2019.

[30] P. G. Devi and A. S. Velu, "Synthesis, structural and optical properties of pure ZnO and Co doped ZnO nanoparticles prepared by the co-precipitation method," *J. Theor. Appl. Phys.*, vol. 10, no. 3, pp. 233–240, 2016, doi: 10.1007/s40094-016-0221-0.

[31] T. Santhaveesuk, K. Siwawongkasem, S. Pommek, and S. Choopun, "High Performance Humidity Sensor Based on ZnO Nanoparticles Synthesized by Co-Precipitation Method," *Appl. Mech. Mater.*, vol. 848, pp. 99–102, 2016, doi: 10.4028/www.scientific.net/amm.848.99.

[32] M. Parashar, V. K. Shukla, and R. Singh, "Metal oxides nanoparticles via sol–gel method: a review on synthesis, characterization and applications," *J. Mater. Sci. Mater. Electron.*, vol. 31, no. 5, pp. 3729–3749, 2020, doi: 10.1007/s10854-020-02994-8.

[33] S. M. Gupta and M. Tripathi, "A review on the synthesis of TiO 2 nanoparticles by

solution route," *Cent. Eur. J. Chem.*, vol. 10, no. 2, pp. 279–294, 2012, doi: 10.2478/s11532-011-0155-y.

[34] C. B. Ong, A. W. Mohammad, R. Rohani, M. M. Ba-Abbad, and N. H. H. Hairom, "Solar photocatalytic degradation of hazardous Congo red using low-temperature synthesis of zinc oxide nanoparticles," *Process Saf. Environ. Prot.*, vol. 104, pp. 549–557, 2016, doi: 10.1016/j.psep.2016.04.006.

[35] J. N. Hasnidawani, H. N. Azlina, H. Norita, N. N. Bonnia, S. Ratim, and E. S. Ali, "Synthesis of ZnO Nanostructures Using Sol-Gel Method," *Procedia Chem.*, vol. 19, pp. 211–216, 2016, doi: 10.1016/j.proche.2016.03.095.

[36] M. A. Malik, M. Y. Wani, and M. A. Hashim, "Microemulsion method: A novel route to synthesize organic and inorganic nanomaterials. 1st Nano Update," *Arab. J. Chem.*, vol. 5, no. 4, pp. 397–417, 2012, doi: 10.1016/j.arabjc.2010.09.027.

[37] J. C. Lin, C. P. Lee, and K. C. Ho, "Zinc oxide synthesis via a microemulsion technique: Morphology control with application to dye-sensitized solar cells," *J. Mater. Chem.*, vol. 22, no. 4, pp. 1270–1273, 2012, doi: 10.1039/c1jm15227k.

[38] H. Kumar and R. Rani, "Structural and Optical Characterization of ZnO Nanoparticles Synthesized by Microemulsion Route," *Int. Lett. Chem. Phys. Astron.*, vol. 19, pp. 26–36, 2013, doi: 10.18052/www.scipress.com/ilcpa.19.26.

[39] Y. X. Gan, A. H. Jayatissa, Z. Yu, X. Chen, and M. Li, "Hydrothermal Synthesis of Nanomaterials," *J. Nanomater.*, vol. 2020, pp. 1–3, 2020, doi: 10.1155/2020/8917013.

[40] H. S. Wasly, M. S. A. El-Sadek, and M. Henini, "Influence of reaction time and synthesis temperature on the physical properties of ZnO nanoparticles synthesized by the hydrothermal method," *Appl. Phys. A Mater. Sci. Process.*, vol. 124, no. 1, pp. 1–12, 2018, doi: 10.1007/s00339-017-1482-4.

[41] J. Singh, T. Dutta, K. H. Kim, M. Rawat, P. Samddar, and P. Kumar, "'Green' synthesis of metals and their oxide nanoparticles: Applications for environmental remediation," *J. Nanobiotechnology*, vol. 16, no. 1, pp. 1–24, 2018, doi: 10.1186/s12951-018-0408-4.

[42] K. Lingaraju *et al.*, "Biogenic synthesis of zinc oxide nanoparticles using Ruta graveolens (L.) and their antibacterial and antioxidant activities," *Appl. Nanosci.*, vol. 6, no. 5, pp. 703–710, 2016, doi: 10.1007/s13204-015-0487-6.

[43] W. P. T. D. Perera *et al.*, "Curcumin loaded zinc oxide nanoparticles for activity-enhanced antibacterial and anticancer applications," *RSC Adv.*, vol. 10, no. 51, pp. 30785–30795, 2020, doi: 10.1039/d0ra05755j.

[44] R. N. Moussawi and D. Patra, "Nanoparticle Self-Assembled Grain Like Curcumin Conjugated ZnO: Curcumin Conjugation Enhances Removal of Perylene, Fluoranthene, and Chrysene by ZnO," *Sci. Rep.*, vol. 6, no. 1, pp. 1–13, 2016, doi: 10.1038/srep24565.

[45] C. H. Lee, L. P. Nalluri, and S. R. Popuri, "Optimization studies for encapsulation and controlled release of curcumin drug using Zn+2 cross-linked alginate and carboxy methylcellulose blend," *J. Polym. Res.*, vol. 26, no. 13, pp. 1–17, 2019, doi: 10.1007/s10965-018-1667-3.

[46] O. Nasrallah, R. El Kurdi, M. Mouslmani, and D. Patra, "Doping of ZnO Nanoparticles with Curcumin: pH Dependent Release and DPPH Scavenging Activity of Curcumin in the Nanocomposites," *Curr. Nanomater.*, vol. 3, no. 3, pp. 147–152, 2018, doi: 10.2174/2405461503666181116115755.

[47] R. Epelbaum, M. Schaffer, B. Vizel, V. Badmaev, and G. Bar-Sela, "Curcumin and gemcitabine in patients with advanced pancreatic cancer," *Nutr. Cancer*, vol. 62, no. 8, pp. 1137–1141, 2010, doi: 10.1080/01635581.2010.513802.

[48] S. Prasad, A. K. Tyagi, and B. B. Aggarwal, "Recent developments in delivery, bioavailability, absorption and metabolism of curcumin: The golden pigment from golden spice," *Cancer Res. Treat.*, vol. 46, no. 1, pp. 2–18, 2014, doi: 10.4143/crt.2014.46.1.2.

[49] X. Xie *et al.*, "PLGA nanoparticles improve the oral bioavailability of curcumin in rats: Characterizations and mechanisms," *J. Agric. Food Chem.*, vol. 59, no. 17, pp. 9280–9289, 2011, doi: 10.1021/jf202135j.

[50] B. B. Aggarwal and B. Sung, "Pharmacological basis for the role of curcumin in

chronic diseases: an age-old spice with modern targets," *Trends Pharmacol. Sci.*, vol. 30, no. 2, pp. 85–94, 2009, doi: 10.1016/j.tips.2008.11.002.

[51] S. M. Nabavi *et al.*, "Curcumin and Melanoma: From Chemistry to Medicine," *Nutr. Cancer*, vol. 70, no. 2, pp. 164–175, 2018, doi: 10.1080/01635581.2018.1412485.

[52] P. Basnet and N. Skalko-Basnet, "Curcumin: An anti-inflammatory molecule from a curry spice on the path to cancer treatment," *Molecules*, vol. 16, no. 6, pp. 4567–4598, 2011, doi: 10.3390/molecules16064567.

[53] M. H. Farzaei *et al.*, "Curcumin in liver diseases: A systematic review of the cellular mechanisms of oxidative stress and clinical perspective," *Nutrients*, vol. 10, no. 7, pp. 1–28, 2018, doi: 10.3390/nu10070855.

[54] W. H. Lee, C. Y. Loo, P. M. Young, D. Traini, R. S. Mason, and R. Rohanizadeh, "Recent advances in curcumin nanoformulation for cancer therapy," *Expert Opin. Drug Deliv.*, vol. 11, no. 8, pp. 1183–1201, 2014, doi: 10.1517/17425247.2014.916686.

[55] K. I. Priyadarsini, "The chemistry of curcumin: From extraction to therapeutic agent," *Molecules*, vol. 19, no. 12, pp. 20091–20112, 2014, doi: 10.3390/molecules191220091.

[56] M. Li, M. O. Ngadi, and Y. Ma, "Optimisation of pulsed ultrasonic and microwave-assisted extraction for curcuminoids by response surface methodology and kinetic study," *Food Chem.*, vol. 165, pp. 29–34, 2014, doi: 10.1016/j.foodchem.2014.03.115.

[57] A. Noorafshan and S. Ashkani-Esfahani, "A Review of Therapeutic Effects of Curcumin," *Curr. Pharm. Des.*, vol. 19, no. 11, pp. 2032–2046, 2013, doi: 10.2174/138161213805289273.

[58] D. W. Zhang, M. Fu, S. H. Gao, and J. L. Liu, "Curcumin and diabetes: A systematic review," *Evidence-based Complement. Altern. Med.*, vol. 2013, pp. 1–16, 2013, doi: 10.1155/2013/636053.

[59] H. J. J. Pabon, "A synthesis of curcumin and related compounds," *Recl. des Trav. Chim. des Pays-Bas*, vol. 83, no. 4, pp. 379–386, 1964, doi:

10.1002/recl.19640830407.

[60] P. Anand, A. B. Kunnumakkara, R. A. Newman, and B. B. Aggarwal, "Bioavailability of curcumin: Problems and promises," *Mol. Pharm.*, vol. 4, no. 6, pp. 807–818, 2007, doi: 10.1021/mp700113r.

[61] S. S. Patel, A. Acharya, R. S. Ray, R. Agrawal, R. Raghuwanshi, and P. Jain, "Cellular and molecular mechanisms of curcumin in prevention and treatment of disease," *Crit. Rev. Food Sci. Nutr.*, vol. 60, no. 6, pp. 887–939, 2020, doi: 10.1080/10408398.2018.1552244.

[62] V. Laura *et al.*, "Potential of curcumin in skin disorders," *Nutrients*, vol. 11, no. 9, pp. 1–25, 2019, doi: 10.3390/nu11092184.

[63] C. Yang *et al.*, "Advances in Clinical Study of Curcumin," *Curr. Pharm. Des.*, vol. 19, no. 11, pp. 1966–1973, 2013, doi: 10.2174/1381612811319110002.

[64] Y. Sunagawa *et al.*, "Colloidal submicron-particle curcumin exhibits high absorption efficiency—a double-blind, 3-way crossover study," *J. Nutr. Sci. Vitaminol. (Tokyo).*, vol. 61, no. 1, pp. 37–44, 2015, doi: 10.3177/jnsv.61.37.

[65] D. J. McClements, F. Li, and H. Xiao, "The nutraceutical bioavailability classification scheme: Classifying nutraceuticals according to factors limiting their oral bioavailability," *Annu. Rev. Food Sci. Technol.*, vol. 6, pp. 299–327, 2015, doi: 10.1146/annurev-food-032814-014043.

[66] S. Bimonte *et al.*, "Curcumin anticancer studies in pancreatic cancer," *Nutrients*, vol. 8, no. 7, pp. 1–12, 2016, doi: 10.3390/nu8070433.

[67] A. R. Vaughn, A. Branum, and R. K. Sivamani, "Effects of Turmeric (Curcuma longa) on Skin Health: A Systematic Review of the Clinical Evidence," *Phyther. Res.*, vol. 30, no. 8, pp. 1243–1264, 2016, doi: 10.1002/ptr.5640.

[68] C. Daruich De Souza, B. Ribeiro Nogueira, and M. E. C. M. Rostelato, "Review of the methodologies used in the synthesis gold nanoparticles by chemical reduction," *J. Alloys Compd.*, vol. 798, pp. 714–740, 2019, doi: 10.1016/j.jallcom.2019.05.153.

[69] R. El Kurdi and D. Patra, "Tuning the surface of Au nanoparticles using poly(ethylene glycol)- block -poly(propylene glycol)- block -poly(ethylene glycol):

Enzyme free and label free sugar sensing in serum samples using resonance Rayleigh scattering spectroscopy," *Phys. Chem. Chem. Phys.*, vol. 2, no. 14, pp. 9616–9629, 2018, doi: 10.1039/c8cp01147h.

[70] R. El Kurdi and D. Patra, "The role of OH- in the formation of highly selective gold nanowires at extreme pH: Multi-fold enhancement in the rate of the catalytic reduction reaction by gold nanowires," *Phys. Chem. Chem. Phys.*, vol. 19, no. 7, pp. 5077–5090, 2017, doi: 10.1039/c6cp08607a.

[71] M. J. Khan, K. Shameli, A. Q. Sazili, J. Selamat, and S. Kumari, "Rapid green synthesis and characterization of silver nanoparticles arbitrated by curcumin in an alkaline medium," *Molecules*, vol. 24, no. 4, pp. 1–12, 2019, doi: 10.3390/molecules24040719.

[72] R. Sankar *et al.*, "Facile synthesis of Curcuma longa tuber powder engineered metal nanoparticles for bioimaging applications," *J. Mol. Struct.*, vol. 1129, pp. 8–16, 2017, doi: 10.1016/j.molstruc.2016.09.054.

[73] M. Qasem, R. El Kurdi, and D. Patra, "Green Synthesis of Curcumin Conjugated CuO Nanoparticles for Catalytic Reduction of Methylene Blue," *ChemistrySelect*, vol. 5, no. 5, pp. 1694–1704, 2020, doi: 10.1002/slct.201904135.

[74] S. Kamble *et al.*, "Evaluation of Curcumin Capped Copper Nanoparticles as Possible Inhibitors of Human Breast Cancer Cells and Angiogenesis: a Comparative Study with Native Curcumin," *AAPS PharmSciTech*, vol. 17, no. 5, pp. 1030–1041, 2016, doi: 10.1208/s12249-015-0435-5.

[75] A. P. Ranjan *et al.*, "Curcumin-ER prolonged subcutaneous delivery for the treatment of non-small cell lung cancer," *J. Biomed. Nanotechnol.*, vol. 12, no. 4, pp. 679–688, 2016, doi: 10.1166/jbn.2016.2207.

[76] N. Dhillon *et al.*, "Phase II trial of curcumin in patients with advanced pancreatic cancer," *Clin. Cancer Res.*, vol. 14, no. 14, pp. 4491–4499, 2008, doi: 10.1158/1078-0432.CCR-08-0024.

[77] A. M. Ealias and M. P. Saravanakumar, "A review on the classification, characterisation, synthesis of nanoparticles and their application," *IOP Conf. Ser.*

Mater. Sci. Eng., vol. 263, pp. 1–15, 2017, doi: 10.1088/1757-899X/263/3/032019.

[78]   A. Czyżowska and A. Barbasz, "A review: zinc oxide nanoparticles–friends or enemies?," *Int. J. Environ. Health Res.*, pp. 1–17, 2020, doi: 10.1080/09603123.2020.1805415.

[79]   A. Król, P. Pomastowski, K. Rafińska, V. Railean-Plugaru, and B. Buszewski, "Zinc oxide nanoparticles: Synthesis, antiseptic activity and toxicity mechanism," *Adv. Colloid Interface Sci.*, vol. 249, pp. 37–52, 2017, doi: 10.1016/j.cis.2017.07.033.

[80]   K. S. Siddiqi, A. ur Rahman, Tajuddin, and A. Husen, "Properties of Zinc Oxide Nanoparticles and Their Activity Against Microbes," *Nanoscale Res. Lett.*, vol. 13, no. 1, pp. 1–13, 2018, doi: 10.1186/s11671-018-2532-3.

[81]   T. X. Wang and T. J. Lou, "Solvothermal synthesis and photoluminescence properties of ZnO nanorods and nanorod assemblies from ZnO2 nanoparticles," *Mater. Lett.*, vol. 62, no. 15, pp. 2329–2331, 2008, doi: 10.1016/j.matlet.2007.11.083.

[82]   J. S. Jang, C. J. Yu, S. H. Choi, S. M. Ji, E. S. Kim, and J. S. Lee, "Topotactic synthesis of mesoporous ZnS and ZnO nanoplates and their photocatalytic activity," *J. Catal.*, vol. 254, no. 1, pp. 144–155, 2008, doi: 10.1016/j.jcat.2007.12.010.

[83]   K. Kakiuchi, E. Hosono, T. Kimura, H. Imai, and S. Fujihara, "Fabrication of mesoporous ZnO nanosheets from precursor templates grown in aqueous solutions," *J. Sol-Gel Sci. Technol.*, vol. 39, no. 1, pp. 63–72, 2006, doi: 10.1007/s10971-006-6321-6.

[84]   Y. Ding and Z. L. Wang, "Structures of planar defects in ZnO nanobelts and nanowires," *Micron*, vol. 40, no. 3, pp. 335–342, 2009, doi: 10.1016/j.micron.2008.10.008.

[85]   C. Sreelakshmi, N. Goel, K. K. R. Datta, A. Addlagatta, R. Ummanni, and B. V. S. Reddy, "Green Synthesis of Curcumin Capped Gold Nanoparticles and Evaluation of Their Cytotoxicity," *Nanosci. Nanotechnol. Lett.*, vol. 5, pp. 1–8, 2013, doi: 10.1166/nnl.2013.1678.

[86]   R. El Kurdi and D. Patra, "Tuning the surface of Au nanoparticles using

poly(ethylene glycol)- block -poly(propylene glycol)- block -poly(ethylene glycol): Enzyme free and label free sugar sensing in serum samples using resonance Rayleigh scattering spectroscopy," *Phys. Chem. Chem. Phys.*, vol. 20, no. 14, pp. 9616–9629, 2018, doi: 10.1039/c8cp01147h.

[87] R. N. Moussawi and D. Patra, "Modification of nanostructured ZnO surfaces with curcumin: Fluorescence-based sensing for arsenic and improving arsenic removal by ZnO," *RSC Adv.*, vol. 6, no. 21, pp. 17256–17268, 2016, doi: 10.1039/c5ra20221c.

[88] M. M. Haneefa, M. Jayandran, and V. Balasubramanian, "Evaluation of antimicrobial activity of green-synthesized manganese oxide nanoparticles and comparative studies with curcuminaniline functionalized nanoform," *Asian J. Pharm. Clin. Res.*, vol. 10, no. 3, pp. 347–352, 2017, doi: 10.22159/ajpcr.2017.v10i3.16246.

[89] S. Peng, Z. Li, L. Zou, W. Liu, C. Liu, and D. J. McClements, "Improving curcumin solubility and bioavailability by encapsulation in saponin-coated curcumin nanoparticles prepared using a simple pH-driven loading method," *Food Funct.*, pp. 1829–1839, 2018, doi: 10.1039/c7fo01814b.

[90] K. R. Soumya, S. Snigdha, S. Sugathan, J. Mathew, and E. K. Radhakrishnan, "Zinc oxide–curcumin nanocomposite loaded collagen membrane as an effective material against methicillin-resistant coagulase-negative Staphylococci," *3 Biotech*, vol. 7, no. 238, pp. 1–10, 2017, doi: 10.1007/s13205-017-0861-z.

[91] N. R. Jabir, S. Tabrez, G. M. Ashraf, S. Shakil, G. A. Damanhouri, and M. A. Kamal, "Nanotechnology-based approaches in anticancer research," *Int. J. Nanomedicine*, vol. 7, pp. 4391–4408, 2012, doi: 10.2147/IJN.S33838.

[92] A. P. Feinberg, R. Ohlsson, and S. Henikoff, "The epigenetic progenitor origin of human cancer," *Nat. Rev. Genet.*, vol. 7, no. 1, pp. 21–33, 2006, doi: 10.1038/nrg1748.

[93] S. Y. Madani, N. Naderi, O. Dissanayake, A. Tan, and A. M Seifalian, "A new era of cancer treatment: carbon nanotubes as drug delivery tools," *Int. J. Nanomedicine*, vol. 6, pp. 2963–2979, 2011.

[94] X. Dai, H. Cheng, Z. Bai, and J. Li, "Breast cancer cell line classification and Its relevance with breast tumor subtyping," *J. Cancer*, vol. 8, no. 16, pp. 3131–3141, 2017, doi: 10.7150/jca.18457.

[95] R. Reilly, *Breast Cancer*. 2007.

[96] E. L. Deer *et al.*, "Phenotype and genotype of pancreatic cancer cell lines," *Pancreas*, vol. 39, no. 4, pp. 425–435, 2010, doi: 10.1097/MPA.0b013e3181c15963.

[97] K. B. Sutradhar and M. L. Amin, "Nanotechnology in Cancer Drug Delivery and Selective Targeting," *ISRN Nanotechnol.*, vol. 2014, pp. 1–12, 2014, doi: 10.1155/2014/939378.

[98] K. B. Sutradhar and L. Amin, "Nanoemulsions: Increasing possibilities in drug delivery," *Eur. J. Nanomedicine*, vol. 5, no. 2, pp. 97–110, 2013, doi: 10.1515/ejnm-2013-0001.

[99] N. Praetorius and T. Mandal, "Engineered Nanoparticles in Cancer Therapy," *Recent Pat. Drug Deliv. Formul.*, vol. 1, no. 1, pp. 37–51, 2007, doi: 10.2174/187221107779814104.

[100] E. A. J. Bleeker *et al.*, "Considerations on the EU definition of a nanomaterial: Science to support policy making," *Regul. Toxicol. Pharmacol.*, vol. 65, no. 1, pp. 119–125, 2013, doi: 10.1016/j.yrtph.2012.11.007.

[101] Y. E. Marín *et al.*, "Curcumin downregulates the constitutive activity of NF-κB and induces apoptosis in novel mouse melanoma cells," *Melanoma Res.*, vol. 17, no. 5, pp. 274–283, 2007, doi: 10.1097/CMR.0b013e3282ed3d0e.

[102] R. Hanif, L. Qiao, S. J. Shiff, and B. Rigas, "Curcumin, a natural plant phenolic food additive, inhibits cell proliferation and induces cell cycle changes in colon adenocarcinoma cell lines by a prostaglandin-independent pathway," *J. Lab. Clin. Med.*, vol. 130, no. 6, pp. 576–584, 1997, doi: 10.1016/S0022-2143(97)90107-4.

[103] B. B. Aggarwal *et al.*, "Curcumin suppresses the paclitaxel-induced nuclear factor-κB pathway in breast cancer cells and inhibits lung metastasis of human breast cancer in nude mice," *Clin. Cancer Res.*, vol. 11, no. 20, pp. 7490–7498, 2005, doi: 10.1158/1078-0432.CCR-05-1192.

[104] H. J. Kang, S. H. Lee, J. E. Price, and L. S. Kim, "Curcumin suppresses the paclitaxel-induced nuclear factor-B in breast cancer cells and potentiates the growth inhibitory effect of paclitaxel in a breast cancer nude mice model," *Breast J.*, vol. 15, no. 3, pp. 223–229, 2009, doi: 10.1111/j.1524-4741.2009.00709.x.

[105] B. E. Bachmeier *et al.*, "Curcumin downregulates the inflammatory cytokines CXCL1 and -2 in breast cancer cells via NFκB," *Carcinogenesis*, vol. 29, no. 4, pp. 779–789, 2008, doi: 10.1093/carcin/bgm248.

[106] C. M. Mach, L. Mathew, S. A. Mosley, R. Kurzrock, and J. A. Smith, "Determination of minimum effective dose and optimal dosing schedule for liposomal curcumin in a xenograft human pancreatic cancer model," *Anticancer Res.*, vol. 29, no. 6, pp. 1895–1899, 2009.

[107] S. Aggarwal, Y. Takada, S. Singh, J. N. Myers, and B. B. Aggarwal, "Inhibition of growth and survival of human head and neck squamous cell carcinoma cells by curcumin via modulation of nuclear factor-κB signaling," *Int. J. Cancer*, vol. 111, no. 5, pp. 679–692, 2004, doi: 10.1002/ijc.20333.

[108] K. Nakamura *et al.*, "Curcumin down-regulates AR gene expression and activation in prostate cancer cell lines.," *Int. J. Oncol.*, vol. 21, no. 4, pp. 825–830, 2002, doi: 10.3892/ijo.21.4.825.

[109] M. M. Lotempio *et al.*, "Curcumin suppresses growth of head and neck squamous cell carcinoma," *Clin. Cancer Res.*, vol. 11, no. 19, pp. 6994–7002, 2005, doi: 10.1158/1078-0432.CCR-05-0301.

[110] G. Rahimi Kalateh Shah Mohammad, E. Karimi, E. Oskoueian, and M. Homayouni-Tabrizi, "Anticancer properties of green-synthesised zinc oxide nanoparticles using Hyssopus officinalis extract on prostate carcinoma cells and its effects on testicular damage and spermatogenesis in Balb/C mice," *Andrologia*, vol. 52, no. 1, pp. 1–10, 2020, doi: 10.1111/and.13450.

[111] N. M. Ali *et al.*, "Synthetic curcumin derivative DK1 possessed G2 / M arrest and induced apoptosis through accumulation of intracellular ROS in MCF - 7 breast cancer cells," *Cancer Cell Int.*, vol. 17, no. 1, pp. 1–12, 2017, doi: 10.1186/s12935-

017-0400-3.

[112] F. Sadat *et al.*, "A Comparison between the cytotoxic effects of pure curcumin and curcumin-loaded PLGA-PEG nanoparticles on the MCF-7 human breast cancer cell line," *Artif. Cells, Nanomedicine, Biotechnol.*, vol. 44, no. 1, pp. 423–430, 2016, doi: 10.3109/21691401.2014.955108.

[113] D. Sutaria, B. K. Grandhi, A. Thakkar, J. Wang, and S. Prabhu, "Chemoprevention of pancreatic cancer using solid-lipid nanoparticulate delivery of a novel aspirin , curcumin and sulforaphane drug combination regimen," *Int. J. Oncol.*, vol. 41, no. 6, pp. 2260–2268, 2012, doi: 10.3892/ijo.2012.1636.

[114] K. Kavithaa, M. Paulpandi, T. Ponraj, K. Murugan, and S. Sumathi, "Induction of intrinsic apoptotic pathway in human breast cancer (MCF-7) cells through facile biosynthesized zinc oxide nanorods," *Karbala Int. J. Mod. Sci.*, vol. 2, no. 1, pp. 46–55, 2016, doi: 10.1016/j.kijoms.2016.01.002.

[115] R. Agabeigi, S. H. Rasta, M. Rahmati-Yamchi, R. Salehi, and E. Alizadeh, "Novel Chemo-Photothermal Therapy in Breast Cancer Using Methotrexate-Loaded Folic Acid Conjugated Au@SiO2 Nanoparticles," *Nanoscale Res. Lett.*, vol. 15, no. 1, pp. 1–14, 2020, doi: 10.1186/s11671-020-3295-1.

[116] H. B. Ruttala and Y. T. Ko, "Liposomal co-delivery of curcumin and albumin/paclitaxel nanoparticle for enhanced synergistic antitumor efficacy," *Colloids Surfaces B Biointerfaces*, vol. 128, pp. 419–426, 2015, doi: 10.1016/j.colsurfb.2015.02.040.

[117] C. Wang, H. Zhang, B. Chen, H. Yin, and W. Wang, "Study of the enhanced anticancer efficacy of gambogic acid on Capan-1 pancreatic cancer cells when mediated via magnetic Fe3O4 nanoparticles.," *Int. J. Nanomedicine*, vol. 6, pp. 1929–1935, 2011, doi: 10.2147/ijn.s24707.

[118] A. P. Ranjan, A. Mukerjee, L. Helson, R. Gupta, and J. K. Vishwanatha, "Efficacy of liposomal curcumin in a human pancreatic tumor xenograft model: Inhibition of tumor growth and angiogenesis," *Anticancer Res.*, vol. 33, no. 9, pp. 3603–3610, 2013.

[119] V. Gérard *et al.*, "Ascorbic Acid Derivatives as Potential Substitutes for Ascorbic Acid to Reduce Color Degradation of Drinks Containing Ascorbic Acid and Anthocyanins from Natural Extracts," *J. Agric. Food Chem.*, vol. 67, no. 43, pp. 12061–12071, 2019, doi: 10.1021/acs.jafc.9b05049.

[120] A. W. Munyaka, E. E. Makule, I. Oey, A. Van Loey, and M. Hendrickx, "Thermal Stability of l-ascorbic acid and ascorbic acid oxidase in broccoli (Brassica oleracea var. italica)," *J. Food Sci.*, vol. 75, no. 4, pp. 336–340, 2010, doi: 10.1111/j.1750-3841.2010.01573.x.

[121] X. Gong, Y. Liu, Z. Yang, S. Shuang, Z. Zhang, and C. Dong, "An 'on-off-on' fluorescent nanoprobe for recognition of chromium(VI) and ascorbic acid based on phosphorus/nitrogen dual-doped carbon quantum dot," *Anal. Chim. Acta*, vol. 968, pp. 85–96, 2017, doi: 10.1016/j.aca.2017.02.038.

[122] L. Li *et al.*, "CuS/Prussian blue core-shell nanohybrid as an electrochemical sensor for ascorbic acid detection," *Nanotechnology*, vol. 30, no. 32, pp. 1–12, 2019, doi: 10.1088/1361-6528/ab1613.

[123] Y. Cen *et al.*, "A cobalt oxyhydroxide-modified upconversion nanosystem for sensitive fluorescence sensing of ascorbic acid in human plasma," *Nanoscale*, vol. 7, pp. 13951–13957, 2015, doi: 10.1039/c5nr03588k.

[124] T. Wu *et al.*, "Colorimetric detection of ascorbic acid and alkaline phosphatase activity based on the novel oxidase mimetic of Fe–Co bimetallic alloy encapsulated porous carbon nanocages," *Talanta*, vol. 202, pp. 354–361, 2019, doi: 10.1016/j.talanta.2019.05.034.

[125] S. R. Ankireddy and J. Kim, "Selective detection of dopamine in the presence of ascorbic acid via fluorescence quenching of inp/zns quantum dots," *Int. J. Nanomedicine*, vol. 10, pp. 113–119, 2015, doi: 10.2147/IJN.S88388.

[126] P. Kannan and S. A. John, "Determination of nanomolar uric and ascorbic acids using enlarged gold nanoparticles modified electrode," *Anal. Biochem.*, vol. 386, no. 1, pp. 65–72, 2009, doi: 10.1016/j.ab.2008.11.043.

[127] M. A. Khalilzadeh and M. Borzoo, "Green synthesis of silver nanoparticles using

onion extract and their application for the preparation of a modified electrode for determination of ascorbic acid," *J. Food Drug Anal.*, vol. 24, no. 4, pp. 796–803, 2016, doi: 10.1016/j.jfda.2016.05.004.

[128] H. Tan *et al.*, "Metal-organic framework-derived copper nanoparticle@carbon nanocomposites as peroxidase mimics for colorimetric sensing of ascorbic acid," *Chem. - A Eur. J.*, vol. 20, no. 49, pp. 16377–16383, 2014, doi: 10.1002/chem.201404960.

[129] S. Chaudhary, A. Umar, K. K. Bhasin, and S. Baskoutas, "Chemical sensing applications of ZnO nanomaterials," *Materials (Basel).*, vol. 11, no. 287, pp. 1–38, 2018, doi: 10.3390/ma11020287.

[130] X. L. Tian, D. F. Tian, Z. Y. Wang, and F. K. Mo, "Synthesis and evaluation of chitosan-Vitamin C complex," *Indian J. Pharm. Sci.*, vol. 71, no. 4, pp. 371–376, 2009, doi: 10.4103/0250-474X.57284.

[131] Z. Wang, X. Teng, and C. Lu, "Carbonate interlayered hydrotalcites-enhanced peroxynitrous acid chemiluminescence for high selectivity sensing of ascorbic acid," *Analyst*, vol. 137, no. 8, pp. 1876–1881, 2012, doi: 10.1039/c2an00030j.

[132] X. Shu, Y. Chang, H. Wen, X. Yao, and Y. Wang, "Colorimetric determination of ascorbic acid based on carbon quantum dots as peroxidase mimetic enzyme," *RSC Adv.*, vol. 10, no. 25, pp. 14953–14957, 2020, doi: 10.1039/d0ra02105a.

[133] V. Arabali *et al.*, "Electrochemical determination of vitamin C in the presence of NADH using a CdO nanoparticle/ionic liquid modified carbon paste electrode as a sensor," *J. Mol. Liq.*, vol. 213, pp. 312–316, 2016, doi: 10.1016/j.molliq.2015.10.001.

[134] S. Dawood, T. K. Sen, and C. Phan, "Synthesis and characterisation of novel-activated carbon from waste biomass pine cone and its application in the removal of congo red dye from aqueous solution by adsorption," *Water. Air. Soil Pollut.*, vol. 225, no. 1, pp. 1–16, 2014, doi: 10.1007/s11270-013-1818-4.

[135] S. Madan, R. Shaw, S. Tiwari, and S. K. Tiwari, "Adsorption dynamics of Congo red dye removal using ZnO functionalized high silica zeolitic particles," *Appl. Surf. Sci.*,

vol. 487, pp. 907–917, 2019, doi: 10.1016/j.apsusc.2019.04.273.

[136] N. B. Swan and M. A. A. Zaini, "Adsorption of Malachite Green and Congo Red Dyes from Water: Recent Progress and Future Outlook," *Ecol. Chem. Eng. S*, vol. 26, no. 1, pp. 119–132, 2019, doi: 10.1515/eces-2019-0009.

[137] Z. M. Abou-Gamra and M. A. Ahmed, "Synthesis of mesoporous TiO2-curcumin nanoparticles for photocatalytic degradation of methylene blue dye," *J. Photochem. Photobiol. B Biol.*, vol. 160, pp. 134–141, 2016, doi: 10.1016/j.jphotobiol.2016.03.054.

[138] D. Maiti, S. Mukhopadhyay, and P. S. Devi, "Evaluation of Mechanism on Selective, Rapid, and Superior Adsorption of Congo Red by Reusable Mesoporous α-Fe2O3 Nanorods," *ACS Sustain. Chem. Eng.*, vol. 5, no. 12, pp. 11255–11267, 2017, doi: 10.1021/acssuschemeng.7b01684.

[139] Z. Zhang, Y. Li, Q. Du, and Q. Li, "Adsorption of Congo Red from Aqueous Solutions by Porous Soybean Curd Xerogels," *Polish J. Chem. Technol.*, vol. 20, no. 3, pp. 95–102, 2018, doi: 10.2478/pjct-2018-0044.

[140] R. Lafi, I. Montasser, and A. Hafiane, "Adsorption of congo red dye from aqueous solutions by prepared activated carbon with oxygen-containing functional groups and its regeneration," *Adsorpt. Sci. Technol.*, vol. 37, no. 1–2, pp. 160–181, 2019, doi: 10.1177/0263617418819227.

[141] M. I. Pratiwi, N. Afifah, and R. Saleh, "Adsorption of organic cationic dye into Fe-doped ZnO nanoparticle coupled with montmorillonite adsorbent," *AIP Conf. Proc.*, vol. 2023, no. 1, pp. 1–5, 2018, doi: 10.1063/1.5064020.

[142] H. Y. Zhu, R. Jiang, J. Yao, F. Q. Fu, and J. B. Li, "Novel ZnO/Zn–Cr hydrotalcite-like anionic clay as a high-performance and recyclable material for efficient photocatalytic removal of organic dye under simulated solar irradiation," *Res. Chem. Intermed.*, vol. 42, no. 5, pp. 4359–4372, 2016, doi: 10.1007/s11164-015-2280-2.

[143] Y. Li *et al.*, "Facile synthesis of a triptycene-based porous organic polymer with a high efficiency and recyclable adsorption for organic dyes," *J. Appl. Polym. Sci.*, vol. 136, no. 39, pp. 1–10, 2019, doi: 10.1002/app.47987.

[144] N. Chaukura, E. C. Murimba, and W. Gwenzi, "Synthesis, characterisation and methyl orange adsorption capacity of ferric oxide–biochar nano-composites derived from pulp and paper sludge," *Appl. Water Sci.*, vol. 7, no. 5, pp. 2175–2186, 2017, doi: 10.1007/s13201-016-0392-5.

[145] J. Zhao, H. Y. Lin, G. C. Liu, X. Wang, and X. L. Wang, "Two Cu(II) coordination polymers based on a flexible bis(pyridyl-tetrazole): Solvent-ratio induced various structures and distinct adsorption performance for organic dyes," *Inorganica Chim. Acta*, vol. 464, pp. 114–118, 2017, doi: 10.1016/j.ica.2017.05.008.

[146] M. J. Chatterjee, S. T. Ahamed, M. Mitra, C. Kulsi, A. Mondal, and D. Banerjee, "Visible-light influenced photocatalytic activity of polyaniline -bismuth selenide composites for the degradation of methyl orange, rhodamine B and malachite green dyes," *Appl. Surf. Sci.*, vol. 470, pp. 472–483, 2019, doi: 10.1016/j.apsusc.2018.11.085.

[147] M. Mahanthappa, N. Kottam, and S. Yellappa, "Enhanced photocatalytic degradation of methylene blue dye using CuS–CdS nanocomposite under visible light irradiation," *Appl. Surf. Sci.*, vol. 475, pp. 828–838, 2019, doi: 10.1016/j.apsusc.2018.12.178.

[148] U. Pal, A. Sandoval, S. I. U. Madrid, G. Corro, V. Sharma, and P. Mohanty, "Mixed titanium, silicon, and aluminum oxide nanostructures as novel adsorbent for removal of rhodamine 6G and methylene blue as cationic dyes from aqueous solution," *Chemosphere*, vol. 163, pp. 142–152, 2016, doi: 10.1016/j.chemosphere.2016.08.020.

[149] N. Nekouei Marnani and A. Shahbazi, "A novel environmental-friendly nanobiocomposite synthesis by EDTA and chitosan functionalized magnetic graphene oxide for high removal of Rhodamine B: Adsorption mechanism and separation property," *Chemosphere*, vol. 218, pp. 715–725, 2019, doi: 10.1016/j.chemosphere.2018.11.109.

[150] B. T. Gadisa, R. Appiah-Ntiamoah, and H. Kim, "Amorphous iron sulfide nanowires as an efficient adsorbent for toxic dye effluents remediation," *Environ. Sci. Pollut.*

Res., vol. 26, no. 3, pp. 2734–2746, 2019, doi: 10.1007/s11356-018-3811-3.

[151] I. Mantasha, H. A. M. Saleh, K. M. A. Qasem, M. Shahid, M. Mehtab, and M. Ahmad, "Efficient and selective adsorption and separation of methylene blue (MB) from mixture of dyes in aqueous environment employing a Cu(II) based metal organic framework," *Inorganica Chim. Acta*, vol. 511, pp. 1–11, 2020, doi: 10.1016/j.ica.2020.119787.

[152] M. Sharifi-Bonab, S. Aber, D. Salari, and F. Khodam, "Synthesis of CoZnAl-layered double hydroxide / graphene oxide nanocomposite for the removal of methylene blue : Kinetic , thermodynamic , and isotherm studies," *Environ. Prog. Sustain. Energy*, vol. 39, no. 2, pp. 1–12, 2020, doi: 10.1002/ep.13316.

[153] I. T. Sugiarto, Isnaeni, and K. Y. Putri, "Analysis of dual peak emission from Rhodamine 6G organic dyes using photoluminescence," *J. Phys. Conf. Ser.*, vol. 817, pp. 1–6, 2017, doi: 10.1088/1742-6596/755/1/011001.

[154] A. A. Oyekanmi, A. Ahmad, K. Hossain, and M. Rafatullah, "Adsorption of Rhodamine B dye from aqueous solution onto acid treated banana peel: Response surface methodology, kinetics and isotherm studies," *PLoS One*, vol. 14, no. 5, pp. 1–20, 2019, doi: 10.1371/journal.pone.0216878.

[155] K. Litefti, M. S. Freire, M. Stitou, and J. González-Álvarez, "Adsorption of an anionic dye (Congo red) from aqueous solutions by pine bark," *Sci. Rep.*, vol. 9, no. 1, pp. 1–11, 2019, doi: 10.1038/s41598-019-53046-z.

[156] L. Wang, J. Li, Y. Wang, and L. Zhao, "Preparation of nanocrystalline Fe 3-xLa xO 4 ferrite and their adsorption capability for Congo red," *J. Hazard. Mater.*, vol. 196, pp. 342–349, 2011, doi: 10.1016/j.jhazmat.2011.09.032.

[157] Q. Si, Q. Wen, Q. Yang, Y. Song, and Y. Li, "Preparation of β-cyclodextrin/Fe3O4/polyvinylpyrrolidone composite magnetic microspheres for the adsorption of methyl orange," *Chem. Res. Chinese Univ.*, vol. 33, no. 6, pp. 1012–1016, 2017, doi: 10.1007/s40242-017-7083-0.

[158] P. Zhao, R. Zhang, and J. Wang, "Adsorption of methyl orange from aqueous solution using chitosan/diatomite composite," *Water Sci. Technol.*, vol. 75, no. 7, pp.

1633–1642, 2017, doi: 10.2166/wst.2017.034.

[159] J. Gülen and F. Zorbay, "Methylene Blue Adsorption on a Low Cost Adsorbent—Carbonized Peanut Shell," *Water Environ. Res.*, vol. 89, no. 9, pp. 805–816, 2017, doi: 10.2175/106143017x14902968254836.

[160] S. H. Kong *et al.*, "Self-purging microwave pyrolysis: an innovative approach to convert oil palm shell into carbon-rich biochar for methylene blue adsorption," *J. Chem. Technol. Biotechnol.*, vol. 94, no. 5, pp. 1397–1405, 2019, doi: 10.1002/jctb.5884.

[161] S. Phoemphoonthanyakit, P. Seeharaj, P. Damrongsak, and K. Locharoenrat, "Effect of Adsorption Characteristics of Rhodamine 6G Dye Solution in Fe3O4 Magnetic Nanoparticles on Fluorescence Quantum Yield," *J. Spectrosc.*, vol. 2019, pp. 1–5, 2019, doi: 10.1155/2019/2853989.

[162] G. Annadurai, R. S. Juang, and D. J. Lee, "Adsorption of rhodamine 6G from aqueous solutions on activated carbon," *J. Environ. Sci. Heal. - Part A Toxic/Hazardous Subst. Environ. Eng.*, vol. 36, no. 5, pp. 715–725, 2001, doi: 10.1081/ESE-100103755.

[163] D. L. Postai, C. A. Demarchi, F. Zanatta, D. C. C. Melo, and C. A. Rodrigues, "Adsorption of rhodamine B and methylene blue dyes using waste of seeds of Aleurites Moluccana, a low cost adsorbent," *Alexandria Eng. J.*, vol. 55, no. 2, pp. 1713–1723, 2016, doi: 10.1016/j.aej.2016.03.017.